Springer Geology

Ekaterina A. Matrosova ·
Andrey V. Bobrov · Luca Bindi

Geochemistry of Chromium in the Earth's Mantle

Springer

Springer Geology

The book series Springer Geology comprises a broad portfolio of scientific books, aiming at researchers, students, and everyone interested in geology. The series includes peer-reviewed monographs, edited volumes, textbooks, and conference proceedings. It covers the entire research area of geology including, but not limited to, economic geology, mineral resources, historical geology, quantitative geology, structural geology, geomorphology, paleontology, and sedimentology.

More information about this series at http://www.springer.com/series/10172

Ekaterina A. Matrosova · Andrey V. Bobrov · Luca Bindi

Geochemistry of Chromium in the Earth's Mantle

Springer

Ekaterina A. Matrosova
Vernadsky Institute of Geochemistry
and Analytical Chemistry RAS
Moscow, Russia

Andrey V. Bobrov
Department of Geology
Moscow State University
Moscow, Russia

Luca Bindi
Dipartimento di Scienze della Terra
Università degli Studi di Firenze
Florence, Italy

ISSN 2197-9545 ISSN 2197-9553 (electronic)
Springer Geology
ISBN 978-3-030-27017-9 ISBN 978-3-030-27018-6 (eBook)
https://doi.org/10.1007/978-3-030-27018-6

This Springer imprint is published by the registered company Springer Nature Switzerland AG
The registered company address is: Gewerbestrasse 11, 6330 Cham, Switzerland

Contents

Abbreviations

Ak	Akimotoite ($MgSiO_3$ with ilmenite-type structure)
Al-*Ak*	Aluminum-rich akimotoite
Al-*Brd*	Aluminum-rich bridgmanite
Al-*Grt*	Al-rich garnet
Al-*Maj*	Al-rich majorite
anhB	Anhydrous phase B
Brd	Bridgmanite ($MgSiO_3$ with perovskite-type structure)
Cf	Phase with calcium ferrite-type structure
Chr	Chromite
CPrv	$CaSiO_3$ perovskite
CPx	Monoclinic pyroxene
Cr-*Ak*	Chromium-rich akimotoite
Cr-*Brd*	Chromium-rich bridgmanite
Cr-*Grt*	Cr-rich garnet
Crn	Corundum
Ct	$MgCr_2O_4$ with calcium titanate-type structure
Du	Dunite
En	Enstatite
Esk	Eskolaite (Cr_2O_3)
Fo	Forsterite
fPer	Ferropericlase
Grt	Garnet
Harz	Harzburgite
Ilm	Ilmenite
Knr	Knorringite ($Mg_3Cr_2Si_3O_{12}$)
Lherz	Lherzolite
Maj	Majorite ($Mg_4Si_4O_{12}$)
M*Chr*	Magnesiochromite
mCt	$Mg(Mg,Cr)(Mg,Si)O_4$ phase with modified calcium titanate-type structure

mLd	$Mg_2Cr_2O_5$ with modified ludwigite-type structure
MPrv	$MgSiO_3$ perovskite
Ol	Olivine
OPx	Orthorhombic pyroxene
Per	Periclase
Prp	Pyrope ($Mg_3Al_2Si_3O_{12}$)
Px	Pyroxene
Rgw	Ringwoodite
Rt	Rutile
Sp	Spinel
Sti	Stishovite
Uv	Uvarovite
Wad	Wadsleyite
Wehr	Wehrlite

Chapter 1
Introduction

A huge amount of data has been accumulated in the field of high-pressure mineralogy to date (Agee 1998; Stachel 2001; Akaogi 2007; Irifune and Tsuchiya 2007; Kaminsky 2012; and others). Direct study of the substance of the Earth's mantle using data on the minerals of mantle xenolith and inclusions in natural diamonds is significantly restricted. According to the geothermobarometric estimates, most of such minerals are formed at a depth of 150–200 km, i.e., their associations characterize the *P*–*T* conditions of the upper mantle (Sobolev 1977; Sobolev et al. 1997; Taylor and Anand 2004). At the same time, there is a continuous replenishment of the database on mineral inclusions in diamonds related to the depths of the Earth's transition zone (410–660 km) (Davies et al. 2004; Stachel et al. 2000a) and lower mantle (>660 km) (Harte et al. 1999; Harte and Harris 1994; Kaminsky et al. 2001; Hayman et al. 2005; Stachel et al. 2000b).

Along with the mineralogical data, the geophysical data and experimental results obtained at high pressures and temperatures are important sources for ideas on the deep structure of the Earth. Deep analysis of mineralogical, geophysical, and experimental information provided evidence for the most important phase transitions in the Earth's mantle, showed their relationships to the jumps in seismic wave velocities, and defined the major phase assemblages typical of the different parts of the upper mantle, transition zone, and lower mantle, which ultimately allowed to clarify the existing models of the structure of the deep geospheres (Harte 2010; Pushcharovsky and Pushcharovsky 2012).

Study of the behavior of minor elements at high pressures and temperatures is very important for understanding of the chemical and phase compositions of the deep parts of the Earth. The solubility of such microelements in high-pressure phases is poorly studied, although even their small concentrations may significantly affect the physical properties of mantle minerals (Panero et al. 2006; Andrault 2007). It is also known that, in some cases, minor components strongly influence on the physicochemical parameters of the most important mantle equilibria, as well as on the crystal chemical

E. A. Matrosova et al., *Geochemistry of Chromium in the Earth's Mantle*,
Springer Geology, https://doi.org/10.1007/978-3-030-27018-6_1

characteristics of the mantle phases. Therefore, recently the behavior of microelements in the deep geospheres of the Earth and their distribution between the mantle phases has attracted considerable interest among researchers (Panero et al. 2006; Andrault 2007; Corgne et al. 2012; Bobrov et al. 2014).

One of such elements is chromium, which is characterized by the low bulk concentrations in the Earth's mantle (0.42 wt% Cr_2O_3) (Ringwood 1966); however, some mantle phases (garnet, chrome-spinel, etc.) show very high contents of chromium (Stachel and Harris 1997; Harte et al. 1999). Until recently, publications on the study of the phase equilibria in multicomponent mantle systems with natural chemistry (pyrolite, pyrope and spinel peridotite) (Hirose 2002; Irifune 1987; Irifune and Ringwood 1987; etc.) contained only limited information on interphase partitioning of chromium component, which is mostly explained by very low concentrations of this element in starting compositions. Study of the phase equilibria in the Cr-rich systems covered only the area of crystallization of knorringitic garnet and its solid solutions (Irifune et al. 1982; Klemme 2004; Turkin and Sobolev 2009).

To fill this gap and to solve the indicated problem of the interphase chromium component partitioning in the Earth's mantle, here we report our data on the experimental study of the SiO_2–MgO–Cr_2O_3 model system and related multicomponent systems at pressures and temperatures corresponding to a wide range of mantle conditions.

Acknowledgements We would like to thank Professor Tetsuo Irifune for collaboration and providing facilities for high-pressure experimental studies at the Geodynamics Research Center, Ehime University. We are grateful to our colleagues A. A. Bendeliani, E. Bykova, L. S. Dubrovinsky, V. K. Garanin, L. S. Ismailova, Yu. A. Litvin, S. Ovsyannikov, D. Yu. Pushcharovsky, O. G. Safonov, A. V. Spivak, and A. P. Tamarova for fruitful discussions, comments, and help in the work.
Preparation of this book was supported by the Russian Science Foundation, project no. 17-17-01169.

References

Agee CB (1998) Phase transformations and seismic structure in the upper mantle and transition zone. In: Hemley RJ (ed) Reviews in mineralogy. Ultrahigh-pressure mineralogy: physics and chemistry of the Earth's interior, Mineralogical Society of America. Washington, DC 37: 165–203

Akaogi M (2007) Phase transitions of minerals in the transition zone and upper part of the lower mantle, vol 421 (Special papers). Geological Society of America, pp 1–13

Andrault D (2007) Properties of lower-mantle Al-(Mg,Fe)SiO_3 perovskite, vol 421 (Special papers). Geological Society of America, pp 5–36

Bobrov AV, Litvin YuA, Kuzyura AV, Dymshits AM, Jeffries T, Bindi L (2014) Partitioning of trace elements between Na-bearing majoritic garnet and melt at 8.5 GPa and 1500–1900 °C. Lithos 189:159–166

Corgne A, Armstrong LS, Keshav S, Fei Y, McDonough WF, Minarik WG, Moreno K (2012) Trace element partitioning between majoritic garnet and silicate melt at 10–17 GPa: Implications for deep mantle processes. Lithos 148:128–141

Davies RM, Griffin WL, O'Reilly SY, McCandless TE (2004) Inclusions in diamond from the K14 and K10 kimberlites, Buffalo Hills, Alberta, Canada: diamond growth in a plume. Lithos 77:99–111

Harte B (2010) Diamond formation in the deep mantle: the record of mineral inclusions and their distribution in relation to mantle dehydration zones. Min Mag 74(2):189–215

Harte B, Harris JW (1994) Lower mantle mineral association preserved in diamonds. Min Mag 58A:384–385

Harte B, Harris JW, Hutchison MT, Watt GR, Wilding MC (1999) Lower mantle mineral associations in diamonds from Sao Luiz, Brazil. Mantle Petrol: Field Observations and High Pressure Experimentation: a tribute to Francis R (Joe) Boyd (The Geochemical Society, Houston) 6: 125–153

Hirose K (2002) Phase transitions in pyrolitic mantle around 670-km depth: implications for upwelling of plumes from the lower mantle. J Geophys Res, vol 107

Hayman PC, Kopylova MG, Kaminsky FV (2005) Lower mantle diamonds from Rio Soriso (Juina area, Mato Grosso, Brazil). Contrib Mineral Petrol 149(4):430–445

Irifune T (1987) An experimental investigation of the pyroxene–garnet transformation in a pyrolite composition and its bearing on the constitution of the mantle. Phys Earth Planet Inter 45:324–336

Irifune T, Ringwood AE (1987) Phase transformations in a harzburgite composition to 26 GPa: implications for dynamical behaviour of the subducting slab. Earth Planet Sci Lett 86:365–376

Irifune T, Tsuchiya T (2007) Mineralogy of the Earth—phase transitions and mineralogy of the lower mantle. Treatise on Geophysics. Elsevier 2:33–62

Irifune T, Ohtani E, Kumazawa M (1982) Stability field of knorringite $Mg_3Cr_2Si_3O_{12}$ at high pressure and its implication to the occurrence of Cr-rich pyrope in the upper mantle. Phys Earth Planet Inter 27:263–272

Kaminsky F (2012) Mineralogy of the lower mantle: a review of super-deep mineral inclusions in diamond. Earth Sci Rev 110:127–147

Kaminsky FV, Zakharchenko OD, Davies R, Griffin WL, Khachatryan-Blinova GK, Shiryaev AA (2001) Superdeep diamonds from the Juina area, Mato Grosso State, Brazil. Contrib Min Petrol 140:734–753

Klemme S (2004) The influence of Cr on the garnet–spinel transition in the Earth's mantle: experiments in the system $MgO–Cr_2O_3–SiO_2$ and thermodynamic modeling. Lithos 77:639–646

Panero WR, Akber-Knutson S, Stixrude L (2006) Al_2O_3 incorporation in $MgSiO_3$ perovskite and ilmenite. Earth Planet Sci Lett 252:152–161

Pushcharovsky DY, Pushcharovsky YuM (2012) The mineralogy and the origin of deep geospheres: a review. Earth Sci Rev 113:94–109

Ringwood AE (1966) The chemical composition and origin of the Earth. In: Hurley PM (ed) Advances in Earth science. M.I.T. Press, Cambridge, pp 287–356

Sobolev NV (1977) Deep-seated inclusions in kimberlites and the problem of the composition of the upper mantle. American Geophysical Union, Washington, DC, p 279

Sobolev NV, Kaminsky FV, Griffin WL, Efimova ES, Win TT, Ryan CG, Botkunov AI (1997) Mineral inclusions in diamonds from the Sputnik kimberlite pipe, Yakutia. Lithos 39:135–157

Stachel T (2001) Diamonds from the asthenosphere and the transition zone. Eur J Mineral 13:883–892

Stachel T, Harris JW (1997) Diamond precipitation and mantle metasomatism-evidence from the trace element chemistry of silicate inclusions in diamonds from Akwatia, Ghana. Contrib Mineral Petrol 129(2–3):143–154

Stachel T, Brey GP, Harris JW (2000a) Kankan diamonds (Guinea) I: from the lithosphere down to the transition zone. Contib Mineral Petrol 140:1–15

Stachel T, Harris JW, Brey GP, Joswig W (2000b) Kankan diamonds (Guinea) II: lower mantle inclusion parageneses. Contib Mineral Petrol 140:16–27

Taylor LA, Anand M (2004) Diamonds: time capsules from the Siberian Mantle. Chem Erde 64:1–7

Turkin AI, Sobolev NV (2009) Pyrope–knorringite garnets: overview of experimental data and natural parageneses. Russian Geol Geophys 50(12):1169–1182

Chapter 2
Basics of Geochemistry and Mineralogy of Chromium

Chromium (Cr) is the chemical element with the atomic number 24. It is the first element in group 6 (VIb) of the periodic table. It is a steely-grey, lustrous, hard, and brittle metal, which takes a high polish, resists tarnishing, and has a high melting point (2130 °C). The name of the element is derived from the Greek word χρῶμα, *chrōma*, meaning color, because of the variety of intense colors of its compounds.

Chromium was discovered as an element in the orange-red crystalline mineral crocoite (Pb(II) chromate) found in 1761 by Johann Gottlob Lehmann (1719–1767) in the Beryozovskoye Mine (Ural Mountains, Russia) and initially used as a pigment. The samples of crocoite ore were studied by Louis Nicolas Vauquelin. In 1797, he produced chromium trioxide (CrO_3) by mixing crocoite with hydrochloric acid and then, in 1798, Vauquelin isolated metallic chromium by heating the oxide in a charcoal oven (Donath 1962). In the same year, chromium was independently extracted from crocoite by Martin Heinrich Klaproth.

E. A. Matrosova et al., *Geochemistry of Chromium in the Earth's Mantle*,
Springer Geology, https://doi.org/10.1007/978-3-030-27018-6_2

Louis Nicolas Vauquelin (1763–1829)

Martin Heinrich Klaproth (1743–1817)

The atomic weight of the most abundant (83.789%) chromium isotope is 51.996. A total of 26 isotopes of chromium from ^{42}Cr to ^{67}Cr are known. Among them, there are three stable isotopes: ^{52}Cr, ^{53}Cr, and ^{54}Cr. ^{53}Cr is the product of ^{53}Mn radiogenic decay (a half-life is 3.74 m.y.). In addition, there are 19 radioisotopes with ^{50}Cr being the most stable (with a half-life of more than 1.8×10^{11} m.y.). The half-life of ^{51}Cr is 27.8 days, and it is applied as an isotope indicator. All other radioactive isotopes have half-lives less than 24 h and most of them have half-lives less than 1 min. The least stable is ^{66}Cr with a half-life of 10 ms.

Chromium is a quite abundant element on the Earth. It is the 22nd most abundant element in Earth's crust with an average concentration of 8.3×10^{-3}%, and is more typical for the mantle, where it is the seventh abundant element after O, Mg, Si, Fe, Ca, and Al (Jagoutz et al. 1979; Hartmann and Wedepohl 1993).

Chromium is mostly mined as chromite $FeCr_2O_4$. The largest deposits of chromium are located in South Africa (first place in the world, ~2/5 of chromite ores and concentrates), Kazakhstan (second place, ~1/3), Russian Federation, Zimbabwe, and Madagascar. Smaller deposits are in Turkey, India, Armenia, Brazil, and Philippines. The deposits are represented by massive and impregnated ores in ultramafic rocks. For this reason, ultrabasic rocks are the most enriched in chromium (2×10^{-1}%). The concentrations of chromium in basic and acid rocks are much lower and reach only 2×10^{-2} and 2.5×10^{-4}%, respectively.

More than 80 minerals with chromium playing an important structural role are known, but among them only Cr-rich spinels (up to 54 wt% Cr_2O_3) have commercial significance. In addition, significant concentrations of chromium are typical of other minerals, which often accompany chromium ores, but do not represent a suitable source for the element (uvarovite, volkonskoite, kammererite, fuchsite, etc.). The production of stainless steel is the main area where the useful properties of chromium are applied. It is used in the chemical, refractory, and foundry industries as well.

Chromium is an element exhibiting variable valences of state. Although this metal forms many chemical compounds, in which it may show a wide range of oxidation states from 0 to +6, the +3 and +6 states are the most common in chromium minerals. Poorly mobile compounds of Cr^{3+} predominate in humid landscapes; its water migration is weak there. Cr^{3+} is inert in eluvial soils of steppes and deserts as well, but under these strongly oxidized alkaline environments, Cr^{3+} may be transformed to Cr^{6+}, which may be accumulated upon salinization. Cr in the hexavalent state is a powerful oxidant at low or neutral pH. Easily soluble potassium chromates and other rare Cr-minerals are known in deserts (Perel'man 1989). Compounds with Cr in states 0, +1, +4, and +5 are rare.

Chromium may form various anionic and cationic complexes: Cr^{3+} occurs in acidic solutions as $[Cr(H_2O)_6]^{3+}$, whereas the major form of Cr^{3+} in basic solutions is $[Cr(OH)_6]^{3+}$. Among the most important Cr^{6+} compounds are chromate $[CrO_4]^{2-}$ and dichromate $[Cr_2O_7]^{2-}$ anions, the formation of which in poorly acidic or alkaline media is controlled by the reaction like $2[CrO_4]^{2-} + 2H^+ \leftrightarrow [Cr_2O_7]^{2-} + H_2O$ (Alekseev 1987). The mobility of chromium in soils increases under the poorly acidic environments. Cr^{3+} in the acidic medium is inert; at pH 5.5, it precipitates almost

completely. Cr^{6+} is very unstable being mobilized easily in acidic and alkaline soils (Lozanovskaya et al. 1998). Highly oxidized forms of Cr^{6+} are less stable than Cr^{3+} (Lozanovskaya et al. 1998; Perel'man 1989).

The different chromium compounds are described below.

Trivalent chromium most often occupies octahedral sites in mineral structures (garnet, akimotoite, bridgmanite, chromite, and high-pressure phases with the calcium titanate-type structure, wadsleyite, ringwoodite, etc.) (Bindi et al. 2014a, b, c and others); rarely Cr occurs in the dodecahedral (bridgmanite) (Bindi et al. 2014a) and tetrahedral (wadsleyite) (Sirotkina et al. 2018) sites. The octahedral radius of Cr^{3+} = 0.615 Å (Shannon and Prewitt 1969) is between $r(^{VI}Al^{3+})$ = 0.53 Å and $r(^{VI}Fe^{3+})$ = 0.645 Å, $r(^{VI}Ti^{4+})$ = 0.68 Å, $r(^{VI}Mg^{2+})$ = 0.72 Å. Because of this, Cr^{3+} may substitute for Al^{3+}, Fe^{3+}, Ti^{4+}, and Mg^{2+} in octahedral sites in different rock-forming minerals. The substitution Al^{3+}–Cr^{3+}, which is typical of the spinel ($MgAl_2O_4$)–chromite ($FeCr_2O_4$) series, is the predominant one. The substitution Fe^{3+}–Cr^{3+} typical of the magnetite (Fe_3O_4)–chromite ($FeCr_2O_4$) solid solution is abundant as well. The heterovalent substitution Ti^{4+}–Cr^{3+} is typical in ulvöspinel ($Fe^{2+}TiO_4$). The limited substitution Mg^{2+}–Cr^{3+} occurs, for example, in high-pressure phases with the structures of wadsleyite or ringwoodite and requires a charge compensation.

Hexavalent chromium occurs in natural chromates, such as crocoite $PbCr^{6+}O_4$ (Donath 1962), vauquelinite $Pb_2Cu(Cr^{6+}O_4)(PO_4)(OH)$ (Fanfani and Zanazzi 1968), and fornacite $Pb_2Cu(Cr^{6+}O_4)(AsO_4)(OH)$ (Fanfani and Zanazzi 1967), which in most cases are very rare. Such minerals are observed in the zone of oxidation of lead ores near the massifs of ultramafic rocks. Weathering accompanied by decomposition of Cr-rich spinels and chromium-bearing silicates may result in the formation of chromic acid (H_2CrO_4). Cr^{6+} in chromates occurs in the tetrahedral coordination with a mean <Cr–O> bond distance of ~1.65 Å. Such value is close to <As–O> (~1.68 Å) tetrahedral bond distance.

In extremely reduced environments, on the contrary, there is the appearance of chromium in the divalent state. In particular, divalent chromium is most likely incorporated in the composition of olivine from lunar basalts. The concentration of Cr_2O_3 in such olivine reaches 0.6 wt% (Haggerty et al. 1970). Sutton et al. (1993) supported entrance of chromium as $Cr^{2+}{}_2SiO_4$ component in olivine from lunar basalts. Increase in the concentration of chromium in lunar olivines is explained by their formation under the conditions of low oxygen fugacity (Haggerty 1978; O'Neill 1991; Sato 1976; Sato et al. 1973) and by the fact that the ionic radius of $^{VI}Cr^{2+}$ (0.82 Å) (Shannon 1976) is close to $r(^{VI}Fe^{2+})$ = 0.77 Å and $r(^{VI}Mg^{2+})$ = 0.72 Å. Despite this, the crystal structure of minerals with Cr^{2+} are highly distorted due to the well-known Jahn-Teller effect on this cation.

Hanson and Jones (1998) studied partitioning of Cr^{2+} and Cr^{3+} between olivine and basaltic melt in the presence of spinel. It was shown that the degree of chromium oxidation depends on the presence of iron in the system. In particular, total chromium occurs in the trivalent state at an oxygen fugacity corresponding to the QFM + 1 buffer, whereas in the iron-free systems, at $\log fO_2 = -3$ (QFM + 3 − QFM + 4). Cr^{2+} enters olivine under an oxygen fugacity of <(IW − 1) in both Fe-bearing and Fe-free systems (Fig. 2.1) (Hanson and Jones 1998; Papike et al. 2004).

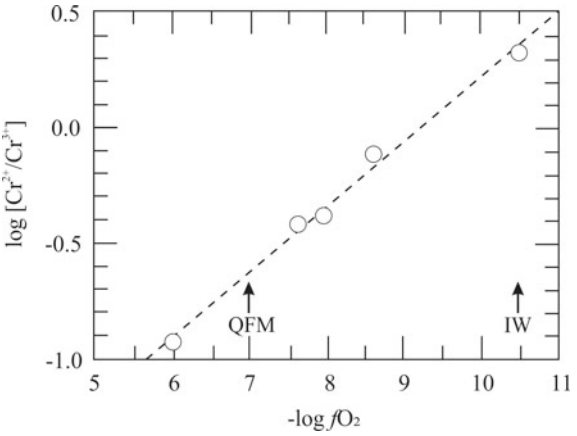

Fig. 2.1 Correlation between log $[Cr^{2+}/Cr^{3+}]$ and $-\log fO_2$ in experiments in the iron-free system. The Cr^{2+}/Cr^{3+} calculation procedure is described by Hanson and Jones (1998)

Table 2.1 Redox conditions and their influence on the degree of chromium oxidation in lunar and terrestrial minerals

Moon: (IW − 2) − IW	Earth: (IW + 2) − (IW + 6)
Basaltic melt	
High concentrations of Cr^{2+}; low concentrations of Cr^{3+}	Mostly Cr^{3+}
Mechanisms of Cr incorporation in olivine	
Almost absent	$^{M2}vac–^{M1}2Cr^{3+}$; $^{M2}Na–^{M1}Cr^{3+}$
Cr^{2+} substitutes for Mg or Fe^{2+}	Absent
Mechanisms of Cr incorporation in pyroxene	
$^{M1}Cr^{3+} – {}^{IV}Al^{3+}$	$^{M1}Cr^{3+}–{}^{IV}Al^{3+}$
Cr^{2+} substitutes for Mg or Fe^{2+}	Absent

Such reduced conditions (close to the (IW − 1) buffer (Papike et al. 2004)) are very rare and may be only typical of central inclusions in deep diamonds (Bulanova et al. 1993), lunar basalts (Table 2.1), and meteorites. The concentration of Cr_2O_3 in olivine from meteorites reaches 0.7 wt% (Fig. 2.2).

High-Mg olivine associated with graphite and pyrrhotite predominates as central inclusions in diamond of ultrabasic assemblages (Bulanova et al. 1993).

There is an assumption (Ryabchikov et al. 1981; Bulanova et al. 1993) that, by the analogy with lunar rocks, chromium in such phases of the Earth's mantle as olivine (or other $(Mg,Fe)_2SiO_4$ polymorphs from inclusions in diamond) occurs in the divalent state as a $Cr^{2+}{}_2SiO_4$ end-member due to the low-oxygen fugacity in the parental diamond-forming medium. However, the concentration of Cr_2O_3 in mantle olivine is not high (in particular for olivine from the central zones of diamond crystals) and reaches 0.2 wt%.

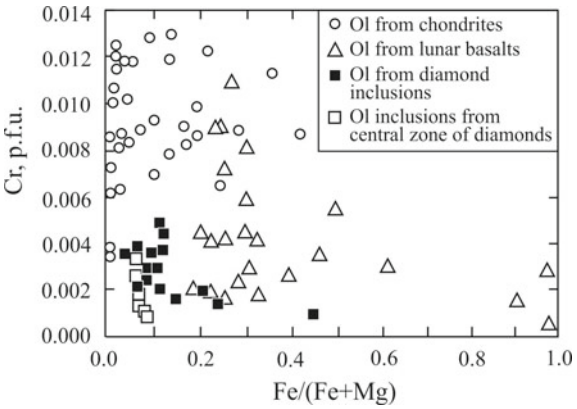

Fig. 2.2 Correlation between the concentrations of Cr and Fe/(Fe + Mg) in olivine from chondrite (Jones and Scott 1989; Jones 1990; McCoy et al. 1991; Weinbruch et al. 1994; Leshin et al. 1997), lunar basalts (Haggerty et al. 1970; Papike 1998), inclusions in diamond (Hutchison et al. 2001; Kaminsky et al. 2001; Stachel et al. 2003; Sobolev et al. 2004; Phillips et al. 2004), and inclusions in the central zones of diamond (Bulanova et al. 1993)

Cr^0 may occur in meteorites (Olsen et al. 1973) as well as in terrestrial rocks, like in association with native Ti, Ni, Fe, and other metals in podiform chromitites from the Luobusa ophiolite complex (South Tibet, China) (Robinson et al. 2004).

Chromium in meteorites is predominantly lithophilic element and enters the composition of chromites, pyroxenes and olivines, but to a lesser degree shows chalcophilic and siderophilic properties. Sometimes chromium in meteorites forms uncommon phases as krinovite ($NaMg_2CrSi_3O_{10}$) (Olsen and Fuchs 1968) and kosmochlor ($NaCrSi_2O_6$) (Frondel and Klein 1965). At a relatively low oxygen fugacity typical of enstatite chondrites and achondrites, chromium acquires chalcophile properties and forms minerals like daubréelite ($FeCr_2S_4$) (Keil 1968) and brezinaite (Cr_3S_4) (Bunch and Fuchs 1969), as well as it can enter significantly the composition of troilite. Daubréelite is the most abundant accessory mineral in many iron meteorites, enstatite chondrites, and achondrites. Brezinaite was registered only in the Tucson iron meteorite (Busch and Fuchs 1969), in which the oxygen activity was rather low for chromium to become chalcophile.

Quite low concentrations of Cr (<0.01 wt%) are typical of metallic phases from stony meteorites of all classes. The concentration of Cr in kamacite from C2 meteorites reaches 1 wt%, whereas the concentration of Cr in taenite from C3 meteorites ranges within 0.01–0.7 wt%.

It was shown by Wänke et al. (1978) and by Dreibus and Wanke (1979) that meteorites were enriched in chromium in relation to the Earth's mantle. These authors concluded that this was explained by predominant redistribution of chromium into the Earth's core. The later experimental studies showed that chromium really became a siderophile element at a temperature above 1500 °C and at redox conditions of the Earth's mantle (Brey and Wanke 1983; Rammensee et al. 1983).

Chromium takes a special place in petrology and geochemistry of the Earth's mantle. According to the bulk concentration in mantle peridotites, chromium is a typical minor element and its influence on parameters of phase transformations and, consequently, on physical and chemical properties of mantle rocks almost has not been studied yet. However, even low concentrations of chromium are sufficient for stabilization of chrome spinel upon partial melting of the mantle material, which is of key importance for the formation of high-chromium associations in the Earth's mantle. The potential value of chromium for thermobarometric purposes has not been fully disclosed as well.

Wijbrans et al. (2016) showed that the concentration of the majoritic component in garnet depends not only on pressure, but on the composition of garnet as well, in particular on the Cr/(Cr + Al) ratio, whereas the temperature has a small influence. This fact is very important for understanding of phase relations in the Earth's upper mantle. It was shown that at the same pressure, garnets with the higher concentration of chromium would have the lower contents of the majoritic component in comparison with varieties depleted in chromium. In this regard, we may conclude that high-chromium majoritic garnets (e.g., see review in Stachel 2001) were formed at very high mantle depths. Based on the concentration of the majoritic component in garnet and the value of the Cr/(Cr + Al) ratio, Wijbrans et al. (2016) worked out a geobarometer for garnets of the peridotitic and eclogitic assemblages.

Reconstruction of the chemical and phase compositions of the deep Earth geospheres is significantly based on the results of the study of mantle xenoliths in kimberlite and inclusions in natural diamonds. The data of geobarometry show that the chemical equilibria in most of deep xenoliths from kimberlite and lamproite pipes were gained at depths of <200 km (e.g., Taylor and Anand 2004). Therefore, to obtain reliable information on mineralogy and geochemistry of the transition zone and lower mantle of the Earth, first of all, we should use the data obtained from inclusions in superdeep diamonds.

A number of ultrahigh-pressure minerals providing the most reliable information on the phase composition and structure of deep zones of the Earth have been described in such inclusions to date (e.g., Stachel 2001; Moore and Gurney 1985). These phase assemblages include majoritic garnet and some phases indicating the *P–T* conditions of the lowermost upper mantle, transition zone, and lower mantle, such as $(Mg,Fe)SiO_4$ with the ringwoodite- and wadsleyite-type structures, $(Mg,Fe,Al)(Al,Si)O_3$ with the ilmenite- (akimotoite) and perovskite-type (bridgmanite) structures, $CaSiO_3$ with the perovskite-type structure, magnesiowüstite (ferropericlase), etc. As it is evident from X-ray diffraction data, most of these minerals were isochemically transformed into the lower pressure minerals (Harte et al. 1999; Joswig et al. 1999; Stachel et al. 2000b; Kaminsky et al. 2001), so that the proof for their primarily ultra-deep origin is often quite problematic.

Among the abovementioned minerals, majoritic garnet is the only direct indicator of the high depth of formation of mineral assemblages in the lowermost upper mantle and transition zone, since this phase may be reliably identified by its chemical composition. It is known that most of these garnets belong to the eclogitic assemblage (Stachel et al. 2000a; Stachel 2001; Gasparik 2002; Taylor and Anand 2004), and

only in rare cases majoritic garnets may be attributed to the peridotite paragenesis, judging from the presence of chromium in them or association with olivine (Taylor and Anand 2004). As a whole, garnets with significant admixture of the knorringite ($Mg_3Cr_2Si_3O_{12}$) end-member are typical of the peridotitic assemblage of inclusions in natural diamonds (Sobolev 1977).

However, the results of experimental studies available, as well as the complex analysis of the *P*–*T* regime in the Earth's mantle provide physicochemical parameters of the major phase transitions (Harte et al. 1999; Stachel et al. 2000a, b; Akaogi 2007; Pushcharovsky and Pushcharovsky 2012). In addition, they illustrate mechanisms and conditions of isomorphism in relation to the major components of mantle phases, and provide evidence for the influence of various minor elements on the major phase transitions (Andrault 2007). It is known that even the lowest concentrations of minor elements in high-pressure phases may affect significantly on parameters of the major phase equilibria and on crystallochemical patterns of mantle phases.

In the next section, we provide a brief description related to the chromium incorporation of the upper mantle minerals, such as olivine, pyroxenes, chrome spinel, and garnet (containing the high-pressure components like majorite and knorringite). The characteristics of some chromium-bearing phases, most likely stable in the transition zone and lower mantle of the Earth, are considered as well.

2.1 High-Pressure Chromium-Bearing Phases in the Earth's Mantle

The major rock-forming minerals of the pyrolytic upper mantle (Ringwood 1966) are olivine, orthopyroxene, clinopyroxene, and garnet, which are replaced with majoritic garnet, akimotoite, wadsleyite (β-$(Mg,Fe)_2SiO_4$), and ringwoodite with the spinel-type structure (γ-$(Mg,Fe)_2SiO_4$) in the transition zone. At pressures of >24 GPa, ringwoodite is decomposed to form ferropericlase and bridgmanite $(Mg,Fe)SiO_3$ with the perovskite-type structure (Liu 1976; Ringwood and Irifune 1988; Ito and Takahashi 1989; Fei et al. 2004). Among the most important chromium-bearing phases in the Earth's upper mantle are chrome spinel, Cr-bearing pyroxene, and knorringitic garnet, whereas the content of chromium in olivine is very low.

The major host phases for chromium in the transition zone are knorringite-majoritic garnet (Zou and Irifune 2012), $MgCr_2O_4$ with the calcium titanate-type structure ($CaTi_2O_4$) (Yamamoto et al. 2009; Wang et al. 2002; Chen et al. 2003), and $(Mg,Fe)_2SiO_4$ wadsleyite (Ringwood and Major 1966a, b) being replaced with $(Mg,Fe)_2SiO_4$ ringwoodite (Ringwood and Major 1970) at higher pressure. As is evident from the experimental data (Ito and Navrotsky 1985; Ito and Takahashi 1989; Gasparik 1990; Sawamoto 1987; Yusa et al. 1993), akimotoite $(Mg,Fe)SiO_3$ with the ilmenite-type structure occurs in the transition zone of the Earth as well.

Ferropericlase (Mg,Fe)O and (Mg,Fe)SiO_3 bridgmanite may be considered as the host phases for chromium under the lower mantle conditions. $CaSiO_3$ with the perovskite-type structure, which is not considered in this monograph, is another very likely host for chromium.

2.1.1 (Mg,Fe)Cr_2O_4 Polymorphs

Chromite (chrome spinel) and its high-pressure polymorphs are the most chromium-rich phases in the Earth's mantle.

Chrome spinel shows a negative correlation between the concentrations of Al and Cr (Fig. 2.3). Spinels from inclusions in diamonds are characterized by very high contents of magnesiochromite ($MgCr_2O_4$), >80 mol% (e.g., Meyer and Boyd 1972; Sobolev 1977). The concentrations of Cr_2O_3 and Al_2O_3 vary within fairly narrow limits and reach 63–68 and 4–8 wt%, respectively. Chromite from inclusions in diamonds and garnet peridotite xenoliths basically has a high Cr# (Cr/(Cr + Al) × 100 = 86−91 and 80–86%, respectively) (Fig. 2.3) (e.g., Sobolev et al. 1997; Stachel et al. 2003; Davies et al. 2004). The lowest concentration of Cr_2O_3 (25–38 wt%) is typical of spinel from spinel peridotite xenoliths in kimberlite and alkaline basalt (Gregoire et al. 2006; Ionov et al. 2010). Spinel from dunite and harzburgite of ophiolitic complexes occupies an intermediate position between the minerals in garnet and spinel peridotite xenoliths. Chromite from harzburgite of ophiolitic complexes has the lower concentrations of TiO_2 (up to 0.1 wt%) than those in chromite from dunite (up to 0.5 wt%).

Chromite from ophiolite complexes is characterized by the highest Cr# (75–82%) and Mg# (Mg/(Mg + Fe) × 100, up to 77%). They also show moderate TiO_2 concentrations (0.15–0.25 wt%).

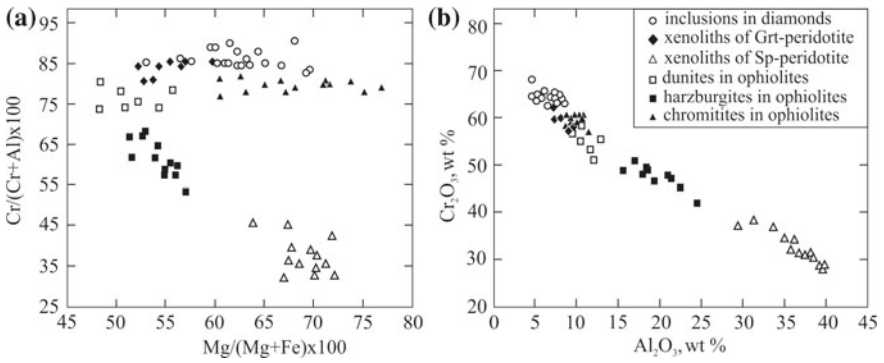

Fig. 2.3 Compositions of chrome spinel from inclusions in diamonds (Davies et al. 2004; Pokhilenko et al. 2004; Deines and Harris 2004), xenoliths in kimberlite, and ophiolites (e.g., Menzies et al. 2004; Aulbach et al. 2004; Gregoire et al. 2006; Zhou et al. 1996)

The concentration of chromium in Cr-rich spinel has the positive correlation with both the degree of partial melting and pressure (Dick and Bullen 1984).

Chromite is observed in almost all types of meteorites being the most important phase concentrating chromium. The concentrations of Cr, Fe, and Mg in chondrites depend on Mg# in coexisting silicates (olivine and/or orthopyroxene) and oxygen fugacity. Chromite in the most reduced meteorites (except for enstatite chondrites and achondrites, in which chromite is not found) is characterized by the highest Mg# and concentrations of Cr_2O_3, whereas chromite from the most oxidized types of meteorites usually shows low concentrations of Cr_2O_3 and Mg# (Bunch and Olsen 1975).

Most of chromites from meteorites are characterized by a quite high Cr# (>83%) (Fig. 2.4), whereas those from lunar rocks have a lower Cr# (<80%).

With increasing pressure ($P > 20$ GPa) chrome spinel adopts the calcium titanate-type ($CaTi_2O_4$) structure. Chrome spinel associated with ferropericlase and a $(Mg,Fe)SiO_3$ phase (bridgmanite?) was described in the Pandrea and Juina kimberlite pipes (Brazil) (Kaminsky et al. 2009). The discovered grains have lower concentrations of chromium (35–55 wt% Cr_2O_3), and higher contents of iron (33–34 wt% FeO) and titanium (10–11 wt% TiO_2) in comparison with chrome spinels included in upper mantle diamonds.

Mg–Cr–Fe and Ca–Cr oxides (up to 46 wt% Cr_2O_3, up to 13 wt% FeO) with post-spinel structures were found in polymineral inclusions in diamond from Rio Soriso (Brazil) in association with Fe-rich periclase (Kaminsky et al. 2015). In opinion of the authors, this assemblage formed under lower mantle conditions.

The studied Mg–Cr–Fe oxide has an orthorhombic symmetry (Kaminsky et al. 2015). The phase with the composition of $\left(Mg_{0.90}Mn_{0.18}\right)_{\Sigma 1.08}\left(Cr_{1.37}Fe^{3+}{}_{0.39}V_{0.11}Al_{0.05}\right)_{\Sigma 1.92}O_4$ (Mg# = 70%) is the chemical analog of chrome spinel. The authors compared the diffraction pattern of

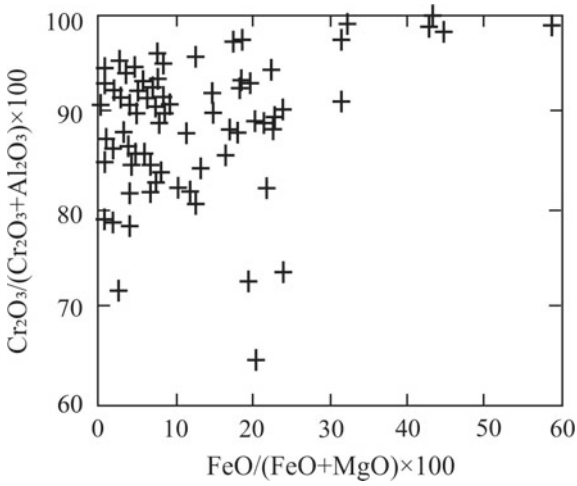

Fig. 2.4 Composition of chrome spinels from meteorites (e.g., Snetsinger et al. 1967; Bunch et al. 1967; Bunch and Keil 1971)

this phase with the patterns of cubic chromite (Chen et al. 2003), as well as orthorhombic phases with the calcium titanate-type ($CaTi_2O_4$, *Ct*) (Chen et al. 2003) and $CaCr_2O_4$-type (Hörkner and Müller-Buschbaum 1976) structures. The diffraction pattern they observed did not match that of cubic chromite; however, it was not possible to distinguish between the different orthorhombic structures (*Ct* or $CaCr_2O_4$). The analogous, iron-dominant mineral with formula $(Fe_{0.87}Mg_{0.13}Mn_{0.01})_{\Sigma 1.01}(Cr_{1.62}Al_{0.25}Ti_{0.08}V_{0.02})_{\Sigma 1.97}O_4$ (xieite) and with unit-cell parameters ($a = 9.462$ Å, $b = 9.562$ Å, $c = 2.916$ Å) close to those of the phase with the calcium titanite-type structure ($a = 9.467$ Å, $b = 9.550$ Å, $c = 2.905$ Å) has been found in the Suizhou meteorite (Chen et al. 2008).

A polymineral inclusion in the lower mantle diamond from Rio Soriso (Brazil) contains Ca–Cr oxide with the composition of $\left(Ca_{1.07}Mg_{0.02}Mn_{0.02}\right)_{\Sigma 1.11}\left(Cr_{1.71}Fe^{3+}{}_{0.06}V_{0.06}Ti_{0.03}Al_{0.03}\right)_{\Sigma 1.89}O_4$. This phase is orthorhombic and its diffraction pattern is similar to that of pure synthetic $CaCr_2O_4$ post-spinel phase (Hörkner and Müller-Buschbaum 1976).

2.1.2 Majoritic and Knorringitic Garnets

Garnet of an essentially knorringite and knorringite–majorite composition is certainly one of the most chromium-rich phase in the Earth's mantle.

Garnets are widely abundant as inclusions in natural diamonds and occur in xenoliths of garnet peridotite and eclogite in kimberlite. Their study is of special importance, since the composition of garnet is very sensitive to the *P*–*T* conditions of the formation of mineral assemblages in the Earth's upper mantle and transition zone. Garnets included in diamond crystals are often enriched in two high-pressure components: majorite (mostly eclogitic assemblages, E-type garnets) and knorringite (peridotitic or ultrabasic assemblages, P-type garnets).

The composition of E- and P-type garnets, abundant as inclusions in diamonds and in deep-seated xenoliths including diamondiferous varieties, may be expressed by the following general formula: $\{X^{2+}\}_3[Y^{3+}]_2(Si)_3O_{12}$, where the distorted eight-fold site {X} is occupied by divalent cations (mainly Mg, Ca, Fe^{2+}, and Mn), the octahedral site [Y] includes trivalent cations (Al, Cr, Fe^{3+}), and Si occurs in tetrahedra (three atoms per 12 oxygens). With increasing depth, garnet is progressively enriched in Si and depleted in Al and Cr due to dissolution of pyroxene components in it.

Such complex solid solutions between cubic garnet, $\{Mg\}_3[Mg,Si]_2(Si)_3O_{12}$ and $\{Ca,Mg\}_3[Mg,Si]_2(Si)_3O_{12}$ end-members (enstatite $MgSiO_3$ and diopside $CaMgSi_2O_6$ at low pressures, respectively) are traditionally called *majoritic garnets*. Garnets are attributed to the majoritic type if the concentration of Si exceeds 3 p.f.u. (Gasparik 2002).

Experimental studies of the systems with majoritic garnet unequivocally establish the relationship of the $2Al^{3+} = Mg^{2+} + Si^{4+}$ isomorphism with pressure (Akaogi and Akimoto 1977; Irifune 1987). Such chemical relationships may also provide

approximate estimates of the depth of crystallization for diamond crystals with inclusions of such majoritic garnets (e.g., Stachel 2001).

Actually, "majorite" is the mineral with the "pyroxene" composition and garnet structure (Ringwood and Major 1971); the only find of this mineral on the Earth was reported in the Zhamanshin astrobleme (Kazakhstan) (Badyukov 1985). Majoritic garnets were then described as inclusions in diamonds from the Monastery kimberlite pipe (South Africa) (Moore and Gurney 1985). This find showed that diamonds could contain asthenospheric and transition zone materials (the concentration of Si in garnets was 3.43 p.f.u.). Later, majoritic garnets were found in diamonds from different regions worldwide including Yakutia, Canada, Brazil, and China (Stachel 2001). Garnets included in diamonds from kimberlitic dykes of the Helam Mine deposit (South Africa) (McKenna et al. 2004) have the highest concentrations of majorite (3.508–3.534 Si p.f.u.).

In many cases, majoritic garnets contain significant admixture of Cr_2O_3 (up to a few wt%), which provides unambiguous evidence for their belonging to the ultrabasic paragenesis. The first finds of pyropic garnets with significant concentrations of chromium were reported during the study of inclusions in diamonds from kimberlite pipes of Lesotho and Yakutia (Sobolev and Sobolev 1967; Nixon and Hornung 1968). To describe the composition of high-chromium garnets syngenetic to P-type diamonds, the Mg–Cr end-member $Mg_3Cr_2Si_3O_{12}$ (Nixon and Hornung 1968) was named "knorringite" in honor of the famous Russian geologist Oleg von Knorring (1915–1994).

Oleg von Knorring (1915–1994)

Chromium-bearing garnets enriched in the knorringitic ($Mg_3Cr_2Si_3O_{12}$) component, as well as garnets of the majoritic type, are formed at significant depth in the diamondiferous assemblages. The characteristic features in the composition of P-type garnet syngenetic to diamond made possible to distinguish the dunite–harzburgite paragenesis within the area of diamond stability (Fig. 2.5). The minerals of this paragenesis show clear tendency towards lower concentrations of iron and calcium and higher concentration of chromium (>5 wt% Cr_2O_3) in comparison with garnets forming inclusions in diamonds of the lherzolite, wehrlite, and eclogite types (Sobolev et al. 1973). Such garnets are applied in prospecting for productive kimberlite bodies as a reliable mineralogical criterion of their diamond potential (Grütter et al. 2006).

Garnets having both the high-pressure components (majorite and knorringite) are of significant interest. Analysis of the composition of chromium-bearing majoritic garnets included in natural diamonds (Table 2.2) allows us to establish some regularities clearly observed when the concentrations of Si, Cr, Al are plotted against pressure (Fig. 2.6a). With increasing pressure, mantle garnets become undersaturated in Al^{3+} and Cr^{3+}, whereas the concentration of Si in the octahedral site progressively increases. Compositional peculiarities of the same garnets on the Cr–Si diagram (Fig. 2.6b) show two major compositional trends: pyrope–majorite and pyrope–knorringite. At the same time, some analyses of garnets (with the low-concentration of the pyrope end-member) line up on the diagram in parallel with the *majorite–knorringite* trend, which is indicated by a dashed line in the graph. This peculiarity of natural garnets is of decisive importance in the choice of one of the systems ($Mg_4Si_4O_{12}$–$Mg_3Cr_2Si_3O_{12}$) for experimental studies.

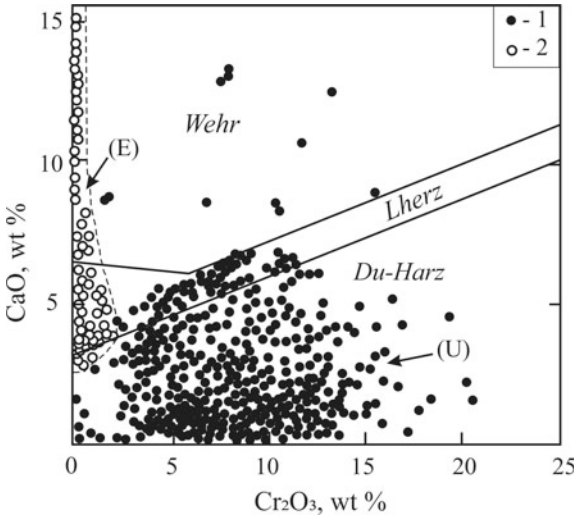

Fig. 2.5 Subdivision of garnets of the ultrabasic association (1) into the dunite-harzburgite (*Du-Harz*), lherzolite (Lherz), and wehrlite types in comparison with the garnet compositions of the eclogite (2) association, using data from Sobolev (1977), Meyer (1987), Garanin et al. (1991), and Taylor and Anand (2004). The compositional fields of garnet from diamonds of the ultrabasic (U) and eclogitic (E) assemblages in the different deposits worldwide are shown, after Griffin et al. (1993)

Table 2.2 Representative analyses of chromium-bearing majoritic garnets from inclusions in natural diamonds

Sample	G303-305	Sl3-30	Yum-27	HM009a	HM009b	K47
SiO_2	40.8	42.3	42.8	47.44	47.98	39.92
TiO_2	0.02	0.06	0.33	0.60	0.60	0.11
Al_2O_3	7.00	9.46	6.79	10.19	9.71	9.74
FeO	6.73	7.64	5.67	3.33	3.39	7.73
MnO	0.29	0.33	0.28	0.18	0.2	0.60
MgO	22.7	21.2	12.2	13.67	13.7	16.97
CaO	1.57	5.11	20.8	20.18	20.45	8.14
Na_2O	0.11	0.01	0.04	0.99	1.00	0.00
Cr_2O_3	20.56	12.8	10.2	2.19	2.20	17.47
Total	99.78	98.91	99.11	98.77	99.23	100.68
Formula units per 12 oxygens						
Si	3.063	3.166	3.300	3.508	3.534	3.015
Ti	0.001	0.003	0.019	0.033	0.033	0.006
Al	0.619	0.834	0.617	0.888	0.843	0.867
Fe	0.422	0.478	0.365	0.206	0.209	0.488
Mn	0.018	0.021	0.018	0.011	0.012	0.038
Mg	2.538	2.364	1.401	1.506	1.503	1.909
Ca	0.126	0.410	1.717	1.598	1.613	0.658
Na	0.016	0.001	0.006	0.142	0.143	0.000
Cr	1.220	0.757	0.621	0.128	0.128	1.043
Total	8.024	8.035	8.065	8.021	8.019	8.024

Note G303-305, Birim, West Africa (Stachel and Harris 1997); Sl3-30, Snap Lake, Slave Craton, Canada (Pokhilenko et al. 2004); Yum-27, Yubileinaya pipe, Yakutia, Russia (Sobolev et al. 2004); HM009a and HM009b, Helam Mine, South Africa (McKenna et al. 2004); K47, Kao kimberlite pipe, Lesotho (Nixon and Hornung 1968)

It should be noted that majoritic and especially chromium-bearing majoritic garnets were observed only as inclusions in diamonds, but did not occur in mantle xenoliths, even in their diamondiferous varieties. However, there are finds of mantle xenoliths, in which garnets contain exsolution textures providing evidence for initial high-pressure origin of such rocks.

Thus, garnets from peridotite and eclogite xenoliths in kimberlite from South Africa described by Haggerty and Sautter (1990) and Sautter et al. (1991) contain pyroxene lamellae oriented along (111) of the host mineral (Fig. 2.7a), which are assumed to be formed as a result of exsolution of majoritic garnet upon decompression. The reconstructed composition of the initial garnet shows high Si and Na and low Al contents indicative of a pressure of ~13 GPa (a depth of ~400 km) (Irifune 1987; Akaogi and Akimoto 1979).

Harte and Cayzer (2007) reported garnet inclusions in diamond crystals from the Juina province in the San Lois River valley, Brazil. These inclusions are actually

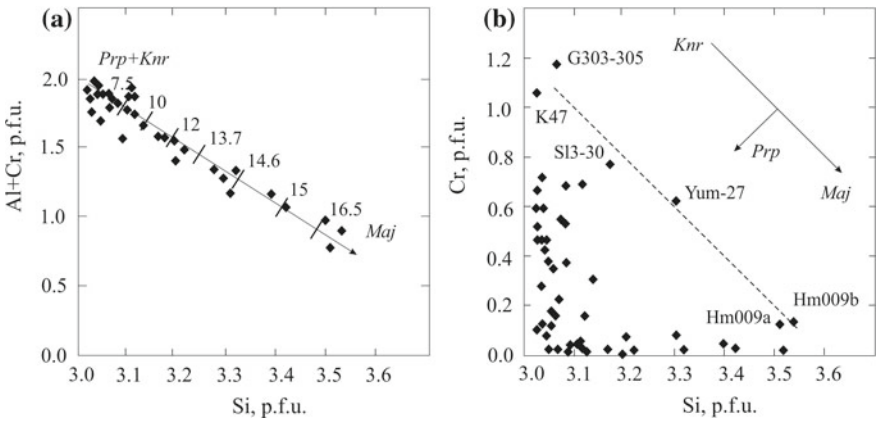

Fig. 2.6 Compositional peculiarities of chromium-bearing majoritic garnets from inclusions in natural diamonds (Table 2.2, using the data from reviews (Stachel 2001; Taylor and Anand 2004)). Solid lines with arrows show the compositional trends of garnet in the pyrope–majorite (**a**) and knorringite–majorite (**b**) series

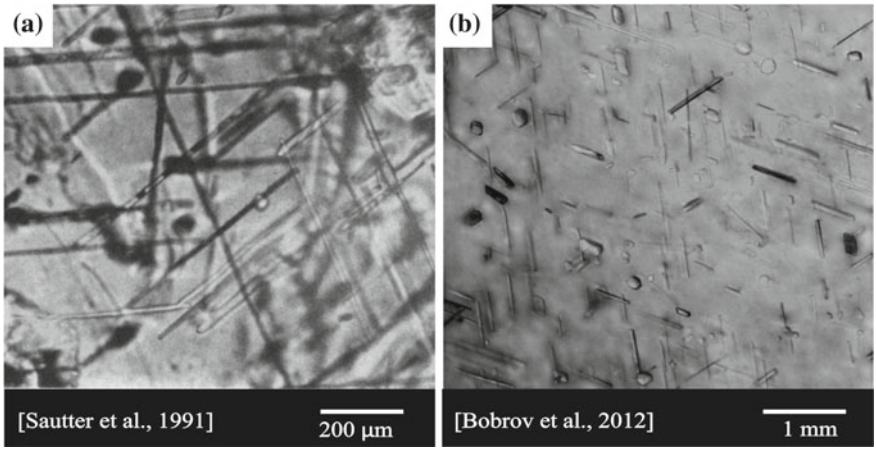

Fig. 2.7 Examples of garnets with pyroxene exsolution textures (images in transmitting light)

composed of complex intergrowths of garnet and monoclinic pyroxene. Garnet is characterized by high concentration of silicon (3.06–3.24 Si p.f.u.), but the content of the majoritic component regularly decreases towards the grain boundary where majorite-free garnet coexisting with clinopyroxene appears. Such garnet–pyroxene association for grains with normal silica content is very similar to that observed in many eclogite xenoliths. This allows us to assume that primarily majoritic garnets formed at higher depths in the lowermost upper mantle and transition zone and then underwent exsolution upon uplift to the surface with the formation of the garnet—clinopyroxene assemblage.

Spengler et al. (2006) showed examples of garnets with exsolution textures, in which pyroxene and sometimes olivine grains occur in two situations. In the first case, grains of orthopyroxene, rarely olivine, are located between garnet grains; in the second case, needles of orthorhombic and sometimes monoclinic pyroxenes occur in garnet grains. The same orientation of pyroxene needles provides evidence for exsolution of garnet with decreasing pressure and/or temperature. As it is evident from calculations (Spengler et al. 2006), the initial majoritic garnet contained ~19 mol% of majorite (3.19 p.f.u. Si per 12 O atoms), which indicates its crystallization at a pressure of ~11 GPa (~350 km).

In relation to the origin of high-pressure chromium-bearing phases in the Earth's mantle, of special interest are finds of oriented inclusions of chromite, as well as Cr-rich ilmenite and rutile in garnets. Such inclusions may be interpreted by decompressional exsolution of chromium-rich garnets. Oriented inclusions of ilmenite, chrome spinel, and rutile were originally described in garnets from the Mir and Udachnaya kimberlitic pipes (Yakutia, Russia) (Lazko 1979). Characteristically, chrome spinel inclusions of such type from heavy fraction of the Udachnaya pipe contain 50–55 wt% Cr_2O_3.

Alifirova et al. (2012) studied garnets in mantle xenoliths from the Mir, Udachnaya, and Obnazhennaya pipes containing intergrowths of spinel, ilmenite, rutile (all minerals contain admixture of chromium), and chromite (Fig. 2.8). All inclusions are parallel to (110) of host minerals and intersect in rhombododecahedral planes. Thus, it may be suggested that in this case we deal with exsolution textures in primarily high-pressure chromium-bearing garnets as well.

Bobrov et al. (2012) studied three pyrope-rich garnet megacrysts with numerous inclusions of monoclinic pyroxene and olivine oriented along (110) of garnet from the Mir kimberlite pipe (Yakutia) (Fig. 2.7b). Garnets are characterized by a moderate concentration of CaO (4.5–5.8 wt%) and relatively low concentration of Cr_2O_3 (up to 0.59 wt%), which corresponds to garnet of the lherzolitic paragenesis (Garanin et al. 1991). The calculated initial composition of garnets shows that the concentration of Si exceeds 3 p.f.u., and since the minerals contain admixture

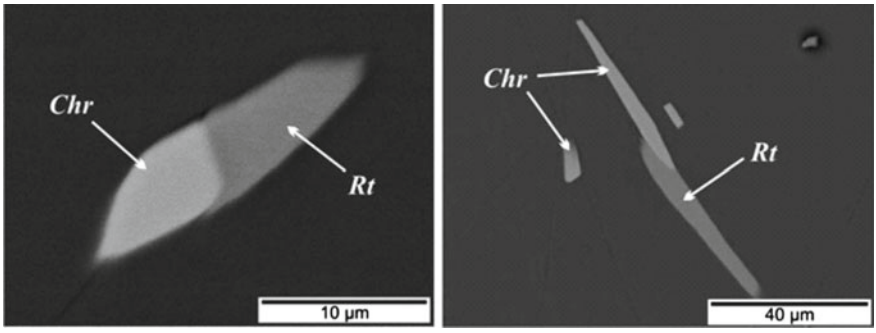

Fig. 2.8 Chromite and rutile oriented inclusions in garnet from peridotite xenoliths of the Mir pipe (Yakutia, Russia) (Alifirova et al. 2012)

of sodium, their primary composition corresponds to sodium-rich majorite. It was established that such garnets formed at pressures of >7.5 GPa, which correspond to a depth of >250 km. Incorporation of Ni in pyroxene lamellae and extremely high NiO concentration in olivine (up to 2.8 wt%) allowed the authors to suggest a high Ni content in the reconstructed composition of garnet, which, in turn, indicated a high temperatures of crystallization of primary majoritic garnets (~1500 °C). Subsequent decrease in pressure resulted in exsolution of garnets. The estimated *P–T* parameters of decompressional decomposition of garnet obtained using the methodology of Nikitina (1993), were 2.3–3.2 GPa and 820–880 °C.

The similar majoritic garnets (including chromium-rich) subjected to decompressional exsolution with the formation of pyroxene lamellae were found in rocks of different UHP metamorphic complexes worldwide (Van Roermund et al. 2001; Song et al. 2004; Zhang and Liou 2003; Scambelluri et al. 2008).

2.1.3 Clinopyroxenes

Clinopyroxenes from inclusions in diamonds and mantle xenoliths of the peridotitic assemblage are characterized by a high concentration of chromium (up to 3.2 wt% Cr_2O_3), moderate concentration of aluminum (0.63–3.52 wt% Al_2O_3), and low concentration of titanium (up to 0.4 wt% TiO_2) (Sobolev 1977). The high chromium content in the monoclinic pyroxene determines its name, *chrome diopside*. Figure 2.9b shows that there are two mechanisms of chromium incorporation in monoclinic pyroxene. At high concentrations of aluminum and low contents of chromium and sodium, all sodium is consumed to form the jadeite component ($NaAlSi_2O_6$). As a result, its content in clinopyroxene increases significantly against the background of a slight increase in the concentration of chromium in the

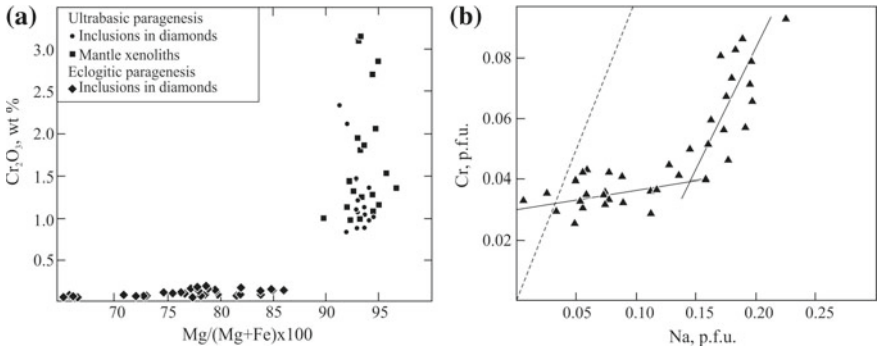

Fig. 2.9 Compositional peculiarities of pyroxenes from inclusions in diamonds and mantle xenoliths (Sobolev 1977; Bulanova et al. 1993; Aulbach et al. 2004; Davies et al. 2004; Phillips et al. 2004; Promprated et al. 2004). Solid lines show the compositional trends of pyroxenes; dashed line indicates the kosmochlor character of isomorphism

form of Cr analogues of Tschermak's molecules ($CaCrAlSiO_6$ and $MgCrAlSiO_6$). Pyroxenes with the highest concentrations of Cr_2O_3 and Na_2O and quite low concentrations of Al_2O_3 are characterized by a different substitution mechanism: $2^{VI}Mg^{2+} = {}^{VI}Na^{+} + {}^{VI}Cr^{3+}$, with the formation of the kosmochlor component ($NaCrSi_2O_6$).

The maximal concentrations of Cr_2O_3 (up to 7.3 wt%) were found in chrome diopsides from diamondiferous xenoliths and clinopyroxene intergrowths with diamonds (Bulanova et al. 1993). They are characterized by high concentrations of Al_2O_3 (up to 6.5 wt%) and Na_2O (up to 8.4 wt%) as well.

Monoclinic pyroxenes of the eclogite paragenesis show high concentrations of Al_2O_3 (up to 14 wt%) and Na_2O (up to 7 wt%), as well as low Mg# (65–86%). The concentrations of Cr_2O_3 do not exceed 0.2 wt% (Fig. 2.9).

2.1.4 Olivine and Its Polymorphs

As it is known, phases with the composition of $(Mg,Fe)_2SiO_4$ (forsterite–wadsleyite–ringwoodite) are widely abundant in the Earth's mantle.

Octahedral, trivalent chromium was originally discovered in olivine megacrysts with inclusions of high-Cr low-Ca garnet from the Udachnaya pipe (Matsyuk et al. 1985). Registration of trivalent chromium impurity in olivine, rather the incorporation of divalent chromium, as considered above (Burns 1975), is the radically new fact in the study of olivine crystal chemistry. The concentration of Cr_2O_3 in mantle olivine associated with orthopyroxene and/or garnet is low and reaches only 0.2 wt% (Sobolev et al. 2004; Phillips et al. 2004). Olivine coexisting with chromite is sometimes characterized by extremely high concentrations of chromium (up to 1.10 wt% Cr_2O_3) (Phillips et al. 2004).

The primary deep genesis of high-pressure $(Mg,Fe)_2SiO_4$ polymorphs (wadsleyite and ringwoodite) is not often directly supported owing to decompressional structural transformations.

The fact that a mineral belongs to an ultrabasic association of the lower mantle of the Earth is determined by its intergrowths with ferropericlase and bridgmanite, as well as by the high concentrations of Al and Cr admixtures. Thus, a mineral phase with the olivine composition was found in diamonds from placers of the Juina area (Brazil), closely associated with ferropericlase and bridgmanite (Wilding et al. 1991; Hayman et al. 2005; Kaminsky et al. 2001). These grains show wide variations in Mg# and moderate concentrations of Cr_2O_3 (up to 0.24 wt%) (Table 2.3). In addition, this "olivine" phase was characterized by low concentrations of Ni, which may be explained by its coexistence with ferropericlase (e.g., Kaminsky et al. 2001; Hayman et al. 2005). These authors interpret the formation of this phase by retrograde transformation of a high-pressure mineral, most likely ringwoodite. The Mg_2SiO_4 phase having the higher concentration of chromium (0.36 wt% Cr_2O_3) (Table 2.3) was described as an intergrowth with ferropericlase in diamond from placer of the Kankan area (Guinea) (Stachel et al. 2000b). Micron- and submicron-sized exsolution textures of spinel and high concentrations of Al_2O_3 (0.39 wt%) and Cr_2O_3 in olivine

Table 2.3 Representative compositions of chromium-bearing mantle phases from inclusions in natural diamonds

Sample	KK-109	5-54	SL-13	BZ210	VR16320	5-5
Phase	*"Ol"*	*"Ol"*	*Brd*	*Brd*	*Per*	*Per*
SiO_2	40.23	40.4	39.10	51.41	0.03	0.01
TiO_2	0.01	0.03	5.33	0.02	0.03	0.03
Al_2O_3	0.39	0.03	18.30	10.04	0.09	0.25
FeO	4.59	11.84	8.85	5.14	24.9	34.96
MnO	0.12	0.36	0.18	0.93	0.38	0.71
MgO	53.96	47.01	24.81	30.21	70.5	59.08
CaO	0.03	0.03	0.01	0.65	0.06	0.03
Na_2O	0.03	0.04	0.06	1.05		1.14
K_2O	0.01	0.04			0.77	0.04
NiO	0.28	0.14		0.02	0.33	0.5
Cr_2O_3	0.36	0.24	1.33	1.19	2.56	2.26
Total	100.01	100.16	97.99	100.66	97.1	99.01
Formula units per n oxygens						
N	4	4	3	3	1	1
Si	0.968	1.000	0.712	0.887	0.000	0.000
Ti	0.000	0.001	0.073	0.000	0.000	0.000
Al	0.011	0.001	0.393	0.204	0.001	0.002
Fe	0.092	0.245	0.135	0.074	0.160	0.238
Mn	0.002	0.008	0.003	0.014	0.002	0.005
Mg	1.935	1.733	0.673	0.777	0.806	0.718
Ca	0.001	0.001	0.000	0.012	0.000	0.000
Na	0.001	0.002	0.002	0.035	0.000	0.018
K	0.000	0.001	0.000	0.000	0.008	0.000
Ni	0.005	0.003	0.000	0.000	0.001	0.002
Cr	0.007	0.005	0.019	0.016	0.016	0.015
Total	3.023	2.998	2.010	2.020	0.995	0.999

Note "*Ol*", phase of the olivine composition. KK–109 and KK-44, placer of the Kankan area (Guinea) (Stachel et al. 2000b); 5-54 and 5-5, Juina area (Brazil) (Kaminsky et al. 2001); SL-13 and BZ210, San Luis (Brazil) (Harte et al. 1999; Zedgenizov et al. 2015); VR16320, DO27 pipe (Canada) (Davies et al. 2004)

provided evidence for the lower mantle conditions of the origin of ferropericlase and bridgmanite, which formed an association of ferropericlase + ringwoodite upon decompression (Stachel et al. 2000b).

The most chromium-rich phases with the composition of olivine (presumably former ringwoodite, judging from the octahedral crystal habit (Robinson et al. 2004; Griffin et al. 2016) were described in ultrahigh-pressure podiform chromitites from ophiolites of Tibet (South China). The concentrations of Cr_2O_3 in them reach 1.49 wt% (Liang et al. 2014). Among extraterrestrial rocks, Cr-bearing $(Mg,Fe)_2SiO_4$ ringwoodite was found in the Tenham meteorite (Binns 1970). In addition to meteorites, to date ringwoodite was only registered in impact pumice of El Gasco (Estremadura, Spain) (Diaz-Martinez et al. 2001; Glazovskaya and Trubkin 2005) and as rare inclusion in super-deep diamonds (Pearson et al. 2014).

The data on mineralogy of the deep Earth may be obtained not only in studies of inclusions in diamonds, but from *exsolution textures in deep minerals*. For example, peridotite of the Alpe Arami massif (Switzerland) contain olivines with acicular chromite and ilmenite inclusions, which were most likely formed as a result of exsolution of chromium-rich wadsleyite crystallized in the transition zone of the Earth at a pressure of 10–15 GPa (300–450 km) (Dobrzhinetskaya et al. 1996). The authors report that olivine contains ~0.25 vol.% of chromite lamellae and ~1 wt% of ilmenite lamellae, which corresponds to ~0.2 wt% Cr_2O_3 and ~0.6 wt% TiO_2 in primary wadsleyite $(Mg,Fe)_2SiO_4$.

Zhang et al. (1999) discovered olivines with exsolution textures of chromium-rich magnetite in ultrabasic rocks of the Dabie–Sulu ultrahigh-pressure complex (Central China). The authors suggest that these inclusions were formed by decomposition of the Cr-Fe_3O_4–$(Fe,Mg)_2SiO_4$ solid solution with decreasing pressure. In opinion of the authors, primary Cr–Fe wadsleyite was formed at a pressure of >13 GPa (Zhang et al. 1999).

Cr-bearing wadsleyite was registered in the Peace River meteorite crater as well (Price et al. 1983).

2.1.5 High-Pressure $(Mg,Fe)SiO_3$ Polymorphs

Orthorhombic pyroxenes from inclusions in diamonds and mantle xenoliths have low total admixtures of trivalent cations (i.e., Al and Cr). The concentration of chromium in these pyroxenes does not exceed 1 wt% Cr_2O_3; the concentration of aluminum reaches 3.5 wt% Al_2O_3. It was discovered that chromium may enter the structure of magnesium-rich pyroxene by the "jadeite" substitution scheme: $2^{VI}Mg^{2+} = {}^{VI}Na^{+} + {}^{VI}(Al,Cr)^{3+}$ (Bulanova et al. 1993).

Probability of this scheme is supported by very low concentrations of aluminum and chromium, as well as by the positive correlation between Na and Cr + Al. Based on these observations, Sobolev (1977) originally suggested that Cr^{3+} is incorporated in high-pressure orthorhombic pyroxenes via the "jadeitic" mechanism.

Cr^{3+} may enter the composition of orthopyroxenes as an analog of the Tschermak's molecule ($MgCrAlSiO_6$) via the following substitution scheme: $^{VI}Mg^{2+}+^{IV}Si^{4+} = {}^{VI}Cr^{3+}+{}^{IV}Al^{3+}$. In addition, we may consider the scheme of heterovalent isomorphism like $^{VI}Mg^{2+}+^{IV}Si^{4+} = {}^{VI}Cr^{3+}+{}^{IV}Cr^{3+}$, in which Cr occupies both octahedral (substituting for Mg) and tetrahedral (substituting for Si) sites, by analogy with the orthocorundum ($AlAlO_3$) pyroxene component (Berman and Aranovich 1996).

$(Mg,Fe)SiO_3$ phases under the conditions of the Earth's transition zone and lower mantle may crystallize with the *ilmenite*- or *perovskite*-type structures. Natural $(Mg,Fe)SiO_3$ ilmenite (akimotoite) has been not reported yet for mantle conditions. Most likely, this may be explained by the fact that the field of akimotoite stability is quite narrow, and this phase is formed in relatively cold zones of the mantle. $(Mg,Fe)SiO_3$ akimotoite with up to 0.5 wt% Cr_2O_3 was found in several meteorites (Tomioka and Fujino 1997, 1999; Sharp et al. 1997; Kimura et al. 2004; Xie and Sharp 2004; Ohtani et al. 2004).

$(Mg,Fe)SiO_3$ with the perovskite-type structure (bridgmanite) was found in meteorites as well (Tomioka and Fujino 1997; Sharp et al. 1997).

The phase $(Mg,Fe,Al)(Si,Al)O_3$ named 'high-pressure enstatite' was originally described under mantle conditions in association with ferropericlase as inclusions in diamonds from the Koffiefontein kimberlite pipe (South Africa) (Scott Smith et al. 1984; Moore et al. 1986). It is important that such paragenesis ($MgSiO_3$ + (Mg,Fe)O) is "forbidden" under the upper-mantle conditions. These phases may be formed syngenetically in the Earth's lower mantle as an association of bridgmanite and ferropericlase.

The number of such finds increased significantly from the end of past century. Lower-mantle $(Mg,Fe)SiO_3$ bridgmanites were registered in diamonds from San Luis (Brazil) (Harte et al. 1999; Wilding 1990), Kankan (Guinea) placers and in kimberlite rocks from pipes of the Slave province (Canada) (Stachel et al. 2000b, 2002; Davies et al. 2004). These phases often contain admixture of chromium (up to 0.39 wt% Cr_2O_3), and the maximal concentration of Cr_2O_3 (1.33 wt%) was registered in high-Al bridgmanite from Brazilian diamond SL-13 (Table 2.3).

It is established that under lower-mantle conditions iron-rich bridgmanite $(Fe,Mg)SiO_3$ is not stable and decomposes to form an association of $MgSiO_3$ (*Brd*) + FeO + SiO_2. Such transformation was supported experimentally only for iron-rich systems (Stachel et al. 2000b). This reaction may explain the predomination of high-Mg $(Mg,Fe)SiO_3$ bridgmanites (Mg# = 88 − 96) and Fe-rich ferropericlase (Fe,Mg)O in the lower mantle.

2.1.6 Other Chromium-Bearing Phases in the Earth's Mantle

Ferropericlase (Mg,Fe)O (*fPer*) or magnesiowüstite (Fe,Mg)O associated and sometimes intergrown with $(Mg,Fe)SiO_3$ bridgmanite and $(Mg,Fe)_2SiO_4$ polymorphs, are among the most abundant minerals of the ultrabasic assemblage in the Earth's mantle (Liu 1975). Ferropericlase in association with a phase with olivine composition was

registered in inclusions in diamonds from placers of the Kankan and Juina areas (Brazil) (Table 2.3). In addition, single ferropericlase inclusions (not associated with silicates) were found in diamonds from several regions worldwide; however, these finds cannot provide evidence for the lower-mantle origin of host diamonds. As it was shown by Stachel et al. (2000), ferropericlase could be found as inclusions in upper-mantle diamonds as well if the activity of Si was quite low. In contrast to monomineral ferropericlase inclusions, the close association of ferropericlase and enstatite (former $MgSiO_3$ bridgmanite) discovered in diamonds from the Koffiefontein pipe indicates belonging of these diamonds to the lower-mantle association (Scott Smith et al. 1984). Based on these data, some authors (Wilding 1990; Harte and Harris 1994) identified a similar lower-mantle associations in diamonds from the San Luis area (Brazil).

In addition to Ni, Mn, and Na, chromium is one of the most important minor components in the composition of ferropericlase. It is considered that the high concentrations of Na and Cr in ferropericlase are reliable indicators of the lower-mantle origin of ferropericlase (Kesson and Gerald 1992). The concentration of Cr_2O_3 in ferropericlase from inclusions in diamonds from the San Luis area (Brazil) reaches 2.56 wt%. *fPer* (Harte et al. 1999; Wilding 1990), 0.76 wt%, in diamonds from the Kankan area (Stachel et al. 2000b) and from kimberlite of the Slave Craton (Canada) (Tappert et al. 2005; Davies et al. 2004).

We should also mention the only find of eskolaite (Cr_2O_3) in association with magnesiochromite as inclusions in octahedral diamond from the Udachnaya pipe (Logvinova et al. 2008). In contrast to eskolaite from low-pressure skarn associations in Finland (Kouvo and Vuorelainen 1958), high-pressure eskolaite from inclusion in diamond contains up to 4 wt% TiO_2, which may be an indicator of pressure. In addition, the mantle origin of eskolaite is supported by inclusion of magnesiochromite in it with the composition typical of that of mantle chromites from inclusions in diamonds. Logvinova et al. (2008) inferred a formation at a pressure of 7 GPa (a depth of ~210 km) and suggested that the crystallochemical parameters of eskolaite may be applied for estimation of the conditions of its formation.

2.2 Cr-Rich Rocks and Mechanisms of Cr Concentration in the Earth's Mantle

Chrome is a lithophile element, and in the processes of partial melting, it is accumulated in chrome-spinel or monoclinic pyroxene rather than in melt within the Earth's upper mantle. Being stable in the mantle, these phases are not typical of the crustal conditions; therefore, the concentration of Cr in the crust does not exceed 100 ppm.

Chromite $(Fe,Mg)(Cr,Al)_2O_4$ containing up to ~55 wt% Cr_2O_3 is the major ore mineral of chromium and is an accessory mineral in many ultramafic rocks. Chromitite forms Cr-rich ore bodies, in which the content of chromite exceeds 30 vol.%; this results in local increase in the chromium concentration in the Earth's mantle.

Most of the world resources of chromite ores occur in original (primary) deposits; others form placers and laterite crusts of weathering. The problems relevant to the origin and setting of chromitite are very important for understanding of the deep structure of the Earth and evolution of its mantle and crust, because chromite carries information on the processes of partial melting in the mantle. In this regard, it is appropriate to consider the largest chromite deposits and the models of their formation.

It has been established that about 95% of reserves and 90% of resources are accounted for only three countries in the world, in which unique deposits are located: Bushveld in South Africa, Kempirsai in Kazakhstan, and the Great Dyke in Zimbabwe. According to the conditions of the origin and morphology of ore bodies, the chromitite deposits are subdivided into the *stratiform* chromitite deposits in large stratified mafic–ultramafic intrusions and the *podiform* deposits in ophiolites.

The stratiform chromitite deposits are located within the ancient continental cratons: on the Baltic Shield (Monchepluton and Bolshaya Varaka Complexes in Russia), in North America (Stillwater Complex in the United States), in South Africa (Bushveld in South Africa and Great Dyke in Zimbabwe), e.g., (Prendergast et al. 1989). In this type of deposits, chromitites are hosted by the layered intrusions of gabbro–chromitite composition containing a wide compositional variety of rocks from dunite and harzburgite to gabbronorite and anorthosite. The ore layers are stretched for great distances and lie in the lower part of the intrusive bodies. The typical mineral association includes chrome-spinel, olivine, augite, and bronzite.

Despite the complexity of the layered intrusions, the general mineralogical sequence of their crystallization follows the Bowen's reaction series and experimentally determined phase relations during progressive crystallization of mafic magma (Ridley 2013). The typical sequence of mineral crystallization is the following: olivine, chromite (with ~1% of modal content in the lower layers), orthopyroxene, plagioclase, and clinopyroxene. Crystallization proceeds at a relatively low depth, which is evident from the presence of the equilibrium association of olivine + plagioclase.

The concentration of Cr_2O_3 ranges from 30% in Brazilian deposits to 45–50% in the Bushveld Complex. Chromite ores in these deposits usually occur within the cumulate series as thin layers with a thickness from tens centimeters to ~1 m. Ore-forming chromite is characterized by a relatively low chromium content and associates with such *intercumulus* phases as olivine, plagioclase, orthopyroxene, or secondary hydrous minerals formed after olivine (serpentine) and bronzite (talc).

A number of different chemical and physical processes are considered to explain accumulation of chromite and the formation of chromitite bodies in layered intrusions. It is generally accepted that stratiform chromitites are formed as a result of crystallization differentiation of magma in intrusions on ancient platforms (Stowe 1994). Differential settling of chromitite, due to its higher density, results in the formation of layering in the magmatic chamber. Mass crystallization of chromite drives the composition of magma back to the olivine–chromite or orthopyroxene–chromite cotectic (Irvine 1977), so that olivine and chromite would crystallize as *intercumulus* phases within the chromitite layer. The presence of multiple chromitite layers within

the cumulate sequences may be interpreted by (1) repeated episodes of input of new magma portions almost of a similar composition and/or (2) periodic oxidation of magma controlled by addition of water, which should give rise to short periods of chromite settling (Ridley 2013).

The podiform chromitite deposits are spatially controlled by ophiolites of different ages and occur in the Urals (Russia), in China, Mongolia, Iran, etc. The huge resources of Cr in chromitite ores are hosted by the Kempirsai massif (South Urals, Kazakhstan) (Melcher et al. 1999; Distler et al. 2008), and complexes of New Caledonia (LeBlanc and Nicolas 1992). The main unsolved question concerning podiform chromitites (González-Jiménez et al. 2014) is how can chromium, a minor element in mantle peridotite and their derived partial melts, be concentrated to produce large bodies of massive chromitite.

Chromite bodies in ophiolite are characterized by different morphologies: irregular, lens-like, with sharp angular boundaries, and dyke-like. In most cases chromitites are separated from harzburgite by a dunite shell.

Chromites show significant compositional variations: from high-Cr to Al-rich. The podiform chromitites were interpreted as the products of reactional interaction of primitive mantle melts with restitic mantle peridotite (harzburgite) with further mixing of magmas of different compositions under the conditions of the upper mantle (Noller and Carter 1986; Arai and Yurimoto 1994; Zhou and Robinson 1994; Arai 1997). This process is characterized by incongruent dissolution of orthopyroxene, which is accompanied by removal of this mineral from peridotite with the formation of secondary dunite and melt enriched in silicon and chromium. Further mixing of such melt with primitive mantle melt would result in precipitation and accumulation of chromite crystals (Zhou et al. 1996). Such chromites sometimes contain inclusions of Na-rich pargasite, phlogopite, and pyroxenes (Augé 1987; Lorand and Ceuleneer 1989; Borisova et al. 2012), which provides evidence for the low-pressure character of the ore formation (Kushiro 1969).

However, podiform chromitites often contain ***ultrahigh-pressure minerals***, such as diamond (Robinson et al. 2004; Yang et al. 2007), coesite (Yang et al. 2007; Yamamoto et al. 2009), stishovite (Yang et al. 2007), and ringwoodite (Robinson et al. 2004; Bindi et al. 2018). Ultrahigh-pressure chromitites may be formed as a result of deep transformation of low-pressure chromitite upon the mantle convection. Such conclusion was made after the discovery of the structural and textural patterns generally typical of the low-pressure conditions in ultrahigh-pressure rocks (Arai 2013).

As it was mentioned above, knorringitic garnet is the major mineral host for chromium within ***the depth facies of garnet peridotite***. Therefore, the concentration of chromium in diamond-bearing rocks of the dunite–harzburgite association (Sobolev 1977) may be several times higher than the bulk concentration of chromium in the Earth's mantle. It was established that garnets with the highest contents of the knorringite end-member could crystallize only in the substrate (protolith) with high Cr/Al ratio (Kesson and Ringwood 1989; Canil and Wei 1992; Stachel et al. 1998). Such a protolith may be formed as a residue from partial melting in the area of stability of spinel peridotite, and high-Cr garnets crystallize in such substrate upon

subduction into the garnet stability field (Bulatov et al. 1991; Stachel et al. 1998). In particular, such mechanism is suggested for diamond-bearing garnet harzburgite with high-Cr low-Ca garnet. However, the described model requires a quantitative experimental approval.

References

Akaogi M (2007) Phase transitions of minerals in the transition zone and upper part of the lower mantle, vol 421 (Special papers). Geological Society of America pp 1–13

Akaogi M, Akimoto A (1977) Pyroxene-garnet solid-solution equilibria in the system $Mg_4Si_4O_{12}$-$Mg_3Al_2Si_2O_{12}$ and $Fe_4Si_4O_{12}$-$Fe_3Al_2Si_3O_{12}$ at high pressures and temperatures. Phys Earth Planet Inter 111:90–106

Akaogi M, Akimoto A (1979) High pressure phase equilibria in a garnet lherzolite, with special reference to Mg^{2+}-Fe^{2+} partitioning among constituent minerals. Phys Earth Planet Inter 19:31–51

Alekseev YV (1987) Heavy metals in soils and plants. Agropromizdat, Leningrad, p 95. [in Russian]

Alifirova TA, Pokhilenko LN, Ovchinnikov YI, Donnelly CL, Riches AJV, Taylor LA (2012) Petrologic origin of exsolution textures in mantle minerals: evidence in pyroxenitic xenoliths from Yakutia kimberlites. Int Geol Rev 54(9):1071–1092

Andrault D (2007) Properties of lower-mantle Al-(Mg, Fe)SiO3 perovskite, vol 421 (Special papers). Geological Society of America, pp 15–36

Arai S (1997) Origin of podiform chromitites. J Asian Earth Sci 15:303–310

Arai S, Yurimoto H (1994) Podiform chromitites of the Tari-Misaka ultramafic complex, southwestern Japan, as mantle–melt interaction products. Econ Geol 89:1279–1288

Arai S (2013) Conversion of low-pressure chromitites to ultrahigh-pressure chromitites by deep recycling: a good inference. Earth Planet Sci Lett 379:81–87

Augé T (1987) Chromite deposits in the northern Oman ophiolite: mineralogical constraints. Miner Deposita 22(1):1–10

Aulbach S, Griffin WL, Pearson NJ, O'Reilly SY, Kivi K, Doyle BJ (2004) Mantle formation and evolution, Slave Craton: constraints from HSE abundances and Re–Os isotope systematics of sulfide inclusions in mantle xenocrysts. Chem Geol 208(1):61–88

Badyukov DD (1985) High-pressure phases in impactites of the Zhamanshin crater (USSR)/XVI. In: Lunar and planetary science conference, Houston abstracts, pp 21–22

Berman RG, Aranovich LY (1996) Optimized standard state and solution properties of minerals: I. Model calibration for olivine, orthopyroxene, cordierite, garnet, and ilmenite in the system FeO-MgO-CaO-Al_2O_3-TiO_2-SiO_2. Contrib Mineral Petrol 126:1–24

Bindi L, Griffin WL, Panero WR, Sirotkina EA, Bobrov AV, Irifune T (2018) Synthesis of inverse ringwoodite sheds light on the subduction history of Tibetan ophiolites. Sci Rep 8:5457

Bindi L, Sirotkina EA, Bobrov AV, Irifune T (2014a) Chromium solubility in $MgSiO_3$ ilmenite at high pressure. Phys Chem Miner 41:519–526

Bindi L, Sirotkina EA, Bobrov AV, Irifune T (2014b) Chromium solubility in perovskite at high pressure: the structure of (Mg1–xCrx)(Si1–xCrx)O3 (with x = 0.07) synthesized at 23 GPa and 1600 °C. Am Mineral 99:866–869

Bindi L, Sirotkina EA, Bobrov AV, Irifune T (2014c) X-ray single-crystal structural characterization of MgCr2O4, a post-spinel phase synthesized at 23 GPa and 1600 °C. J Phys Chem Solids 75:638–641

Binns RA (1970) (Mg, Fe)2SiO4 spinel in a meteorite. Phys Earth Planet Inter 3:156–160

Bobrov AV, Sirotkina EA, Garanin VK, Bovkun AV, Korost DV, Shkurskii BB (2012) Majoritic garnets with exsolution textures from the Mir Kimberlitic Pipe (Yakutia). Dokl Earth Sci 444(1):574–578

Borisova AY, Ceuleneer G, Kamenetsky VS, Arai S, Béjina F, Abily B, Bindeman IN, Polvé M, De Parseval P, Aigouy T, Pokrovski GS (2012) A new view on the petrogenesis of the Oman ophiolite chromitites from microanalyses of chromite-hosted inclusions. J Petrol 53(12):2411–2440

Brey G, Wanke H (1983) Partitioning of cr, mn, V and NI between fe melt, magnesiowuestite and olivine at high pressures and temperatures, vol 14. In: Lunar and planetary science conference, pp 71–72

Bulanova GP, Barashkov YP, Tal'nikova SB, Smelova GB (1993) Natural diamond: genetic aspects. Nauka, Novosibirsk, p 168. [in Russian]

Bulatov V, Brey GP, Foley SF (1991) Origin of low-Ca, high-Cr garnets by recrystallization of low-pressure harzburgites, vol 5. In: International kimberlite conference: extended abstracts, pp 29–31

Bunch TE, Fuchs LH (1969) A new mineral: brezinaite, Cr_3S_4, and the Tucson meteorite. Amer Mineral 54:1509–1518

Bunch TE, Keil K (1971) Chromite and ilmenite in non-chondritic meteorites. Am Mineral 56:146–157

Bunch TE, Keil K, Snetsinger KG (1967) Chromite composition in relation to chemistry and testure of ordinary chondrites. Geochim Cosmochim Acta 31:1569–1582

Bunch TE, Olsen E (1975) Distribution and significance of chromium in meteorites. Geochim Cosmochim Acta 39(6–7)

Burns RG (1975) On the occurrence and stability of divalent chromium in olivines included in diamonds. Contrib Mineral Petrol 51(3):213–221

Canil D, Wei K (1992) Constraints on the origin of mantle-derived low Ca garnets. Contrib Mineral Petrol 109(4):421–430

Chen M, Shu J, Mao HK (2008) Xieite, a new mineral of high-pressure $FeCr_2O_4$ polymorph. Chin Sci Bull 53(21):3341–3345

Chen M, Shu J, Xie X, Mao H (2003) Natural $CaTi_2O_4$-structured $FeCr_2O_4$ polymorph in the Suizhou meteorite and its significance in mantle mineralogy. Geochim Cosmochim Acta 67:3937–3942

Davies RM, Griffin WL, O'Reilly SY, McCandless TE (2004) Inclusions in diamond from the K14 and K10 kimberlites, Buffalo Hills, Alberta, Canada: diamond growth in a plume. Lithos 77:99–111

Deines P, Harris JW (2004) New insights into the occurrence of 13 C-depleted carbon in the mantle from two closely associated kimberlites: Letlhakane and Orapa, Botswana. Lithos 77:1–4

Diaz-Martinez E, Sanz-Rubio E, Fernandez C, Martinez-Frias J (2001) Evidence for a small meteorite impact in Extremadura (W. Spain). In: Proceedings of the 6th European science foundation, impact workshop on impact markers in the stratigraphic record, Granada, Spain, pp 21–22

Dick HJB, Bullen TB (1984) Chromian spine1 as a petrogenetic indicator in abyssal and alpine-type peridotites. In: Komprobst J (ed) Kimberlites II: the mantle and crust-mantle relationships, pp 295–308

Distler VV, Kryachko VV, Yudovskaya MA (2008) Ore petrology of chromite-PGE mineralization in the Kempirsai ophiolite complex. Mineral Petrol 92(1–2):31–58

Dobrzhinetskaya L, Green HW, Wang S (1996) Alpe Arami: a peridotite massif from depths of more than 300 kilometers. Science 271:1841–1845

Donath IM (1962) Die Metullischen Rohstoffe. Band 14: Chrom, p 2. Ferdinand Enke, p 371

Dreibus G, Wanke H (1979) On the chemical composition of the Moon and the eucrite parent body and a comparison with the composition of the Earth; the case of Mn, Cr, and V, vol 10. In: Lunar and planetary science conference, pp 315–317

Fanfani L, Zanazzi PF (1967) Structural similarities of some secondary lead minerals. Miner Mag 36:522–529

Fanfani L, Zanazzi PF (1968) The crystal structure of vauquelinite and the relationships to fornacite. Zeits Krist 126:433–443

Fei Y, Van Orman J, Li J, van Westrenen W, Sanloup C, Minarik W, Hirose K, Komabayashi T, Walter M, Funakoshi K (2004) Experimentally determined postspinel transformation boundary in Mg_2SiO_4 using MgO as an internal pressure standard and its geophysical implications. J Geophys Res 109

Frondel C, Klein C (1965) Ureyite, $NaCrSi_2O_6$: a new meteorite pyroxene. Science 149:742–744

Garanin VK, Kudryavtseva GP, Marfunin AS, Mikhailichenko OA (1991) Inclusions in diamond and diamondiferous rocks. Izd Mos Universiteta, Moscow, p 240. [in Russian]

Gasparik T (1990) Phase relations in the transition zone. J Geophys Res 95:15751–15769

Gasparik T (2002) Experimental investigations of the origin majoritic garnet inclusions in diamonds. Phys Chem Miner 29:170–180

Glazovskaya LI, Trubkin NV (2005) Ringwoodite in pumice of the El Gasco region (Extremadura, Western Spain). Dokl Earth Sci 405A(9):1317–1320

Gonzalez-Jimenez JM, Griffin WL, Proenza JA, Gervilla F, O'Reilly SY, Akbulut M, Pearson NJ, Arai S (2014) Chromitites in ophiolites: how, where, when, why? Part II. The crystallization of chromitites. Lithos 189:140–158

Gregoire M, Bell DR, Le Roex AP (2006) Garnet lherzolithes from the Kaapraval Craton (South Africa): trace element evidence for a metasomatic history. J Petrol 44:629–657

Griffin WL, Afonso JC, Belousova EA, Gain SE, Gong XH, González-Jiménez JM, Howell D, Huang JH, McGowan N, Pearson NJ, Satsukawa T, Shi R, Williams P, Xiong Q, Yang JS, Zhang M, O'Reilly SY (2016) Mantle recycling: transition zone metamorphism of Tibetan ophiolitic peridotites and its tectonic implications. J Petrol 57(4):655–684

Griffin WL, Sobolev NV, Ryan CG, Pokhilenko NP, Win TT, Yefimova ES (1993) Trace elements in garnets and chromites: diamond formation in the Siberian lithosphere. Lithosphere 29:235–256

Grütter H, Latti D, Menzies A (2006) Cr-saturation arrays in concentrate garnet compositions from kimberlite and their use in mantle barometry. J Petrol 47:801–820

Haggerty SE (1978) The redox state of planetary basalts. Geophys Res Lett 5(6):443–446

Haggerty SE, Boyd FR, Bell PM, Finger LW, Bryan WB (1970) Opaque minerals and olivine in lavas and breccias from Mare Tranquillitatis. Geochimica et Cosmoc Acta Supplement 1:513

Haggerty SE, Sautter V (1990) Ultradeep (greater than 300 kilometers), ultramafic upper mantle xenoliths. Science 248:993–996

Hanson B, Jones JH (1998) The systematics of Cr^{3+} and Cr^{2+} partitioning between olivine and liquid in the presence of spinel. Am Mineral 83:669–684

Harte B, Cayzer N (2007) Decompression and unimixing of crystals include in diamonds. Phys Chem Miner 34:647–656

Harte B, Harris JW (1994) Lower mantle mineral association preserved in diamonds. Miner Mag 58A:384–385

Harte B, Harris JW, Hutchison MT, Watt GR, Wilding MC (1999) Lower mantle mineral associations in diamonds from Sao Luiz, Brazil. Mantle petrology: field observations and high pressure experimentation: a tribute to Francis R. (Joe) Boyd (The Geochemical Society, Houston) 6:125–153

Hartmann G, Wedepohl KH (1993) The composition of peridotite tectonites from the Ivrea complex, northern Italy: residues from melt extraction. Geochim Cosmochim Acta 57:1761–1782

Hayman PC, Kopylova MG, Kaminsky FV (2005) Lower mantle diamonds from Rio Soriso (Juina area, Mato Grosso, Brazil). Contrib Mineral Petrol 149(4):430–445

Hörkner W, Hk Müller-Buschbaum (1976) Einkristalluntersuchungen von β-$CaCr_2O_4$. Zeitschrift für Naturforschung, Teil B, Anorganische Chemie Organische Chemie 31:1710–1711

Hutchison MT, Hurtshouse MB, Light ME (2001) Mineral inclusions in diamonds: associations and chemical distinctions around the 670-km discontinuity. Contrib Mineral Petrol 142(2):119–126

Ionov DA, Doucet LS, Ashchepkov IV (2010) Composition of the Lithospheric Mantle in the Siberian Craton: new constraints from Fresh Peridotites in the Udachnaya-East Kimberlite. J Petrol 51:2177–2210

Irifune T (1987) An experimental investigation of the pyroxene–garnet transformation in a pyrolite composition and its bearing on the constitution of the mantle. Phys Earth Planet Inter 45:324–336
Irvine TN (1977) Origin of chromitite layers in the Muskox intrusion and other stratiform intrusions: a new interpretation. Geology 5:273–277
Ito E, Navrotsky A (1985) $MgSiO_3$ ilmenite: calorimetry, phase equilibria, and decomposition at atmospheric pressure. Am Mineral 70:1020–1026
Ito E, Takahashi E (1989) Postspinel transformations in the system Mg_2SiO_4-Fe_2SiO_4 and some geophysical implications. J Geophys Res 94(B8):10637–10646
Jagoutz E, Palme H, Baddenhausen H, Blum K, Cendales M, Dreibus G, Spettel B, Lorenz V, Wanke H (1979) The abundances of major, minor and trace elements in the earth's mantle as derived from primitive ultramafic nodules. In: Proceedings of the 10th lunar planet science conference, Lunar and Planetary Science Institute, Houston, pp 2031–2050
Jones RH (1990) Petrology and mineralogy of type II, FeO-rich chondrules in Semarkona (LL3. 0): origin by closed-system fractional crystallization, with evidence for supercooling. Geochim Cosmochim Acta 54(6):1785–1802
Jones RH, Scott ERD (1989) Petrology and thermal history of type IA chondrules in the Semarkona (LL3. 0) chondrite, vol 19. In: Lunar and planetary science conference proceedings, pp 523–536
Joswig W, Stachel T, Harris JW, Baur WH, Brey G (1999) New Ca-silicate inclusions in diamonds—tracers from the lower mantle. Earth Planet Sci Lett 173:1–6
Kaminsky FV, Khachatryan GK, Andreazza P, Araujo D, Griffin WL (2009) Superdeep diamonds from kimberlites in the Juina area, Mato Grosso State, Brazil. Lithos 112S(2):833–842
Kaminsky FV, Wirth R, Schreiber AA (2015) Microinclusion of lower-mantle rock and other minerals and nitrogen lower-mantle inclusions in a diamond. Canad Mineral 53:83–104
Kaminsky FV, Zakharchenko OD, Davies R, Griffin WL, Khachatryan-Blinova GK, Shiryaev AA (2001) Superdeep diamonds from the Juina area, Mato Grosso State, Brazil. Contrib Mineral Petrol 140:734–753
Keil K (1968) Mineralogical and chemical relationships among enstatite chondrites. J Geophys Res 73(22):6945–6976
Kesson SE, Gerald JDF (1992) Partitioning of MgO, FeO, NiO, MnO and Cr_2O_3 betweem magnesian silicate perovskite and magnesiowustite implications for the origin of inclusions in diamond and the composition of the lower mantle. Earth Planet Sci Lett 111:229–240
Kesson SE, Ringwood AE (1989) Slab-mantle interactions: 1. Sheared and refertilised garnet peridotite xenoliths—samples of Wadati-Benioff zones? Chemical Geol 78(2):83–96
Kimura M, Chen M, Yoshida Y, El Goresy A, Ohtani E (2004) Backtransformation of high-pressure phases in a shock melt vein of an Hchondrite during atmospheric passage: implications for the survival of high-pressure phases after decompression. Earth Planet Sci Lett 217:141–150
Kouvo O, Vuorelainen Y (1958) Eskolaite, a new chromium mineral. Am Mineral 43:1098–1106
Kushiro I (1969) The system forsterite–diopside–silica with and without water at the high pressures. Am J Sci 267A:269–294
Lazko EE (1979) Accessory minerals of diamond and the genesis of kimberlite rocks. Nedra, Moscow, p 192. [in Russian]
Leblanc M, Nicolas A (1992) Ophiolitic chromitites. Int Geol Rev 34(7):653–686
Leshin LA, Rubin AE, McKeegan KD (1997) The oxygen isotopic composition of olivine and pyroxene from CI chondrites. Geochim Cosmochim Acta 61(4):835–845
Liang F, Yang J, Xu Z, Zhao J (2014) Moissanite and chromium-rich olivine in the Luobusa mantle peridotite and chromitite, Tibet: deep mantle origin implication. J Himalayan Earth Sci (Special Volume) 103
Liu L (1975) Post-oxide phases of forsterite and enstatite. Geophys Res Lett 2:417–419
Liu L (1976) Orthorhombic perovskite phases observed in olivine, pyroxene and garnet at high pressures and temperatures. Phys Earth Planet Inter 11:289–298
Logvinova A, Wirth R, Sobolev NV, Seryotkin YV, Yefimova ES, Floss C, Taylor LA (2008) Eskolaite associated with diamond from the Udachnaya kimberlite pipe, Yakutia, Russia. Am Mineral 93:685–690

Lorand JP, Ceuleneer G (1989) Silicate and base-metal sulfide inclusion in chromites from the Maqsad area (Oman ophiolite, Gulf of Oman): a model for entrapment. Lithos 22:173–190
Lozanovskaya JH, Orlov DS, Sadovnikova LK (1998) Ecology and biosphere protection under chemical pollution. Vysshaya Shkola, Moscow, p 287. [in Russian]
Matsyuk SS, Platonov AN, Khomenko VM (1985) Optical spectra and colors of mantle minerals from kimberlites. Kiev, Nukova Dumka. [in Russian]
McCoy TJ, Scott ERD, Jones RH, Keil K, Taylor GJ (1991) Composition of chondrule silicates in LL3-5 chondrites and implications for their nebular history and parent body metamorphism. Geochim Cosmochim Acta 55:601–619
McKenna NM, Gurney JJ, Klump J, Davidson JM (2004) Aspects of diamond mineralisation and distribution at the Helam Mine, South Africa. Lithos 77:193–208
Melcher F, Grum W, Thalhammer TV, Thalhammer OAR (1999) The giant chromite deposits at Kempirsai, Urals: constraints from trace element (PGE, REE) and isotope data. Mineral Depos 34(3):250–272
Menzies A, Westerlund K, Grütter H, Gurney J, Carlson J, Fung A, Nowicki T (2004) Peridotitic mantle xenoliths from kimberlites on the Ekati Diamond Mine property, NWT, Canada: major element compositions and implications for the lithosphere beneath the central slave craton. Lithos 77(1):395–412
Meyer HOA (1987) Inclusions in diamond. In: Nixon PH (ed) Mantle xenoliths. Wiley, Chichester pp 501–522
Meyer HOA, Boyd FR (1972) Composition and origin of crystalline inclusions in natural diamonds. Geochim Cosmochim Acta 59:110–119
Moore RO, Gurney JJ (1985) Pyroxene solid solution in garnets included in diamond. Nature 318:553–555
Moore RO, Otter ML, Rickard RS, Harris JW, Gurney JJ (1986) The occurrence of moissanite and ferro-periclase as inclusions in diamond, vol 16. In: 4th international kimberlite conference extended abstracts. Perth. Geological society of Australia abstract, pp 409–411
Nikitina LP (1993) The consistent system of thermometers and barometers for the basic and ultrabasic rocks and reconstruction of thermal conditions in the mantle based on Xenolites in Kimberlites. Zapiski Vseross Mineral Obshchestva 122(5):6–19
Nixon PH, Hornung G (1968) A new chromium garnet end member, knorringite from kimberlite. Am Mineral 53:1833–1840
Noller JS, Carter B (1986) The origin of various types of chromite schlieren in the Trinity Peridotite, Klamath Mountains, California. In: Carter B, Chowdhury MKR, Jankovic S, Marakushev AA, Morten L, Onikhimovsky VV, Raade G, Rocci G, Augustithis SS (eds) Metallogeny of basic and ultrabasic rocks (regional presentations) Theophrastus Athens, pp 151–178
Ohtani E, Kimura Y, Kimura M, Takata T, Kondo T, Kubo T (2004) Formation of high-pressure minerals in shocked L6 chondrite Yamato 791384: constraints on shock conditions and parent body size. Earth Planet Sci Lett 227:505–515
Olsen E, Fuchs L (1968) Krinovite, $NaMg_2CrSi_3O_{10}$: a new meteorite mineral. Science 161:786–787
Olsen E, Fuchs LH, Forbes WC (1973) Chromium and phosphorus enrichment in the metal of Type II (C2) carbonaceous chondrites. Geochim Cosmochim Acta 37:2037–2042
O'Neill HSC (1991) The origin of the moon and the early history of the earth—a chemical model. Part 1: the moon. Geochim Cosmochim Acta 55(4):1135–1157
Papike JJ (1998) Comparative planetary mineralogy: chemistry of melt-derived pyroxene, feldspar, and olivine, vol 29. In: Lunar and planetary science conference
Papike JJ, Karner JM, Shearer CK (2004) Comparative planetary mineralogy: V/(Cr + Al) systematics in chromite as an indicator of relative oxygen fugacity. Am Mineral 89:1557–1560
Pearson DG, Brenker FE, Nestola F, McNeill J, Nasdala L, Hutchison MT, Matveev S, Mather K, Silversmit G, Schmitz S, Vekemans B, Vincze L (2014) Hydrous mantle transition zone indicated by ringwoodite included within diamond. Nature 507(7491):221–224
Perel'man AI (1989) Geochemistry. Vysshaya Shkola, Moscow, p 582. [in Russian]

Phillips D, Harris JW, Viljoen KS (2004) Mineral chemistry and thermobarometry of inclusions from De Beers Pool diamonds, Kimberley, South Africa. Lithos 77:155–179
Pokhilenko NP, Sobolev NV, Reutsky VN, Hall AE, Taylor LA (2004) Crystalline inclusions and C isotope rations in diamonds from the Snap Lake/King Lake kimberlite dyke system: evidence of ultradeep and enriched lithospheric mantle. Lithos 77:57–67
Prendergast MD, Wilson AH, Jones MJ (1989) The Great Dyke of Zimbabwe-II: mineralization and mineral deposits. In: Magmatic sulfides—the Zimbabwe volume. Institute of Mining and Metallurgy, London, pp 21–42
Price GD, Putnis A, Agrell SO, Smith DGW (1983) Wadsleyite, natural β-(Mg, Fe)2SiO4 from the Peace River meteorite. Canad Mineral 21:29–35
Promprated P, Taylor LA, Anand M, Floss C, Sobolev NV, Pokhilenko NP (2004) Multiple-mineral inclusions in diamonds from the Snap Lake/King Lake kimberlite dike, Slave craton, Canada: a trace-element perspective. Lithos 77(1):69–81
Pushcharovsky DYu, Pushcharovsky YuM (2012) The mineralogy and the origin of deep geospheres: a review. Earth Sci Rev 113:94–109
Rammensee W, Palme H, Wanke H (1983) Experimental investigation of metal-silicate partitioning of some lithophile elements (Ta, Mn, V, Cr). Lunar Planet Sci XIV:628–629
Ridley J (2013) Ore deposit geology. Cambridge University Press, Cambridge
Ringwood AE (1966) The chemical composition and origin of the earth. In: Hurley PM (ed) Advances in earth science. M.I.T. Press, Cambridge, pp 287–356
Ringwood AE, Irifune T (1988) Nature of the 650-km seismic discontinuity: implications for mantle dynamics and differentiation. Nature 331:131–136
Ringwood AE, Major A (1966a) Synthesis of Mg_2SiO_4-Fe_2SiO_4 solid solutions. Earth Planet Sci Lett 1:241–245
Ringwood AE, Major A (1966b) Some high-pressure transformations in olivines and pyroxenes. J Geophys Res 71:4448–4449
Ringwood AE, Major A (1970) The system Mg_2SiO_4-Fe_2SiO_4 at high pressures and temperatures. Phys Earth Planet Int 89:3
Ringwood AE, Major A (1971) Synthesis of majorite and other high pressure garnets and perovskites. Earth Planet Sci Lett 12:411–418
Robinson PT, Bai WJ, Malpas J, Yang JS, Zhou MF, Fang QS, Hu XF, Cameron S, Standigel H (2004) Ultra-high pressure minerals in the Luobusa Ophiolite, Tibet, and their tectonic implications. In: Malpas J, Fletcher CJN, Ali JR, Aitchison JC (eds) Aspects of the tectonic evolution of China. Geological society of London, pp 247–271
Ryabchikov ID, Green DH, Wall VJ, Brey GP (1981) The oxidation state of carbon in the reduced-velocity zone. Geochem Int 18:148–158
Sato M (1976) Oxygen fugacity and other thermochemical parameters of Apollo 17 high-Ti basalts and their implications on the reduction mechanism, vol 7. In: Lunar and planetary science conference proceedings, pp 1323–1344
Sato M, Hickling NL, McLane JE (1973) Oxygen fugacity values of Apollo 12, 14, and 15 lunar samples and reduced state of lunar magmas, vol 4. In: Lunar planetary science conference proceedings, p 1061
Sautter V, Haggerty SE, Field S (1991) Ultradeep (>300 kilometers) ultramafic xenoliths: petrological evidence from the transition zone. Science 252:827–830
Sawamoto H (1987) Phase diagram of MgSiO3 at pressures up to 24 GPa and temperatures up to 2200 °C: phase stability and properties of tetragonal garnet. In: Manghnani MH, Syono Y (eds) High-pressure research in mineral physics, pp 209–219
Scambelluri M, Pettke T, van Roermund HLM (2008) Majoritic garnets monitor deep subduction fluid flow and mantle dynamics. The geological society of America, Geology 36:59–62
Scott Smith BH, Danchin RV, Harris JW, Stracke KJ (1984) Kimberlites near Orroroo, South Australia, vol 1. In: Kimberlites I: Kimberlites and Related Rocks. Elsevier, pp 121–142

Shannon RT (1976) Revised effective ionic radii and systematic studies of interatomic distances in halides and chalcogenides. Acta Crystallogr Sect A Cryst Phys Diffr Theor Gen Crystallogr 32(5):751–767

Shannon RT, Prewitt CT (1969) Effective ionic radii in oxides and fluorides. Acta Crystallogr Sect B Struct Crystallogr Cryst Chem 25(5):925–946

Sharp TG, Lingemann CM, Dupas C, Stoffler D (1997) Natural occurrence of $MgSiO_3$-ilmenite and evidence for $MgSiO_3$-perovskite in a shocked L chondrite. Science 277:352–355

Sirotkina EA, Bindi L, Bobrov, AV, Aksenov SM, Irifune T (2018) Synthesis and crystal structure of chromium-bearing anhydrous wadsleyite. Phys Chem Miner, 1–6

Snetsinger KG, Keil K, Buncii TE (1967) Chromite from 'equilibrated' chondrites. Am Mineral 52:1322–1331

Sobolev NV (1977) Deep-seated inclusions in kimberlites and the problem of the composition of the upper mantle. American Geophysical Union, Washington, DC, p 279

Sobolev NV, Kaminsky FV, Griffin WL, Efimova ES, Win TT, Ryan CG, Botkunov AI (1997) Mineral inclusions in diamonds from the Sputnik kimberlite pipe, Yakutia. Lithos 39:135–157

Sobolev NV, Lavrent'ev YG, Pokhilenko NP, Usova LV (1973) Chrome-rich garnets from the kimberlites of Yakutia and their parageneses. Contrib Mineral Petrol 40(1):39–52

Sobolev NV, Logvinova AM, Zedgenizov DA, Seryotkin YV, Yefimova ES, Floss C, Taylor LA (2004) Mineral inclusions in microdiamonds and macrodiamonds from kimberlites of Yakutia: a comparative study. Lithos 77:225–242

Sobolev VS, Sobolev NV (1967) On chromium and chromium-bearing minerals in deep-seated xenoliths of kimberlite pipes. Geol Rudn Mestorozhd 2:10–16 [in Russian]

Song S, Zhang L, Niu Y (2004) Ultra-deep origin of garnet peridotite from the North Qaidam ultrahigh-pressure belt, northern Tibetan Plateau, NW China. Am Mineral 89:1330–1336

Spengler D, Van Roermund HL, Drury MR, Ottolini L, Mason PR, Davies GR (2006) Deep origin and hot melting of an Archaean orogenic peridotite massif in Norway. Nature 440(7086):913–917

Stachel T, Viljoen KS, Brey G, Harris JW (1998) Metasomatic processes in lherzolitic and harzburgitic domains of diamondiferous lithospheric mantle: REE in garnets from xenoliths and inclusions in diamonds. Earth Planet Sci Lett 159(1–2):1–12

Stachel T (2001) Diamonds from the asthenosphere and the transition zone. Eur J Mineral 13:883–892

Stachel T, Brey GP, Harris JW (2000a) Kankan diamonds (Guinea) I: from the lithosphere down to the transition zone. Contib Mineral Petrol 140:1–15

Stachel T, Harris JW (1997) Diamond precipitation and mantle metasomatism-evidence from the trace element chemistry of silicate inclusions in diamonds from Akwatia. Ghana Contrib Mineral Petrol 129(2–3):143–154

Stachel T, Harris JW, Aulbach S, Deines P (2002) Kankan diamonds (Guinea) III: $\delta^{13}C$ and nitrogen characteristics of deep diamonds. Contrib Mineral Petrol 142(4):465–475

Stachel T, Harris JW, Brey GP, Joswig W (2000b) Kankan diamonds (Guinea) II: lower mantle inclusion parageneses. Contib Mineral Petrol 140:16–27

Stachel T, Harris JW, Tappert R, Brey GP (2003) Peridotitic diamonds from the Slave and the Kaapvaal cratons—similarities and differences based on a preliminary data set. Lithos 71(2–4):489–503

Stowe CW (1994) Compositions and tectonic settings of chromite deposits through time. Econ Geol 89(3):528–546

Sutton SR, Jones KW, Gordon B, Rivers ML, Bajt S, Smith JV (1993) Reduced chromium in olivine grains from lunar basalt 15555: X-ray absorption near edge structure (XANES). Geochim Cosmochim Acta 57:461–468

Tappert R, Stachel T, Harris JW, Muehlenbachs K, Ludwig T, Brey G (2005) Mineral inclusions in diamonds from the Slave Province. Canada Eur J Miner 17(3):423–440

Taylor LA, Anand M (2004) Diamonds: time capsules from the Siberian Mantle. Chem Erde 64:1–74

Tomioka N, Fujino K (1997) Natural (Mg, Fe)SiO3-ilmenite and -perovskite in the Tenham meteorite. Science 277:1084–1086

Tomioka N, Fujino K (1999) Akimotoite, (Mg, Fe)SiO3, a new silicate mineral of the ilmenite group in the Tenham chondrite. Am Mineral 84:267–271
Van Roermund HLM, Drury MR, Barnhoorn A, De Ronde AA (2001) Relict majoritic garnet microstructures from ultra-deep orogenic peridotites in Western Norway. J Petrol 42:117–130
Wang Z, O'Neill HSC, Lazor P, Saxena SK (2002) High pressure Raman spectroscopic study of spinel $MgCr_2O_4$. J Phys Chem Solids 63:2057–2061
Wänke H, Dreibus G, Palme H (1978) Primary matter in the lunar highlands—the case of the siderophile elements, vol 9. In: Lunar and planetary science conference proceedings, pp 83–110
Weinbruch S, Armstrong J, Palme H (1994) Constraints on the thermal history of the Allende parent body as derived from olivine-spinel thermometry and Fe/Mg interdiffusion in olivine. Geochim Cosmochim Acta 58(2):1019–1030
Wijbrans CH, Rohrbach A, Klemme S (2016) An experimental investigation of the stability of majoritic garnet in the Earth's mantle and an improved majorite geobarometer. Contrib Mineral Petrol 171. https://doi.org/10.1007/s00410-016-1255-7
Wilding MC (1990) A study of diamonds with syngenetic inclusions. Unpublished Ph.D. thesis, University of Edinburgh, UK, p 281
Wilding MC, Harte B, Harris JW (1991) Evidence for a deep origin for the Sao Luiz diamonds. In: Fifth international kimberlite conference extended abstracts, Araxa, pp 456–458
Xie Z, Sharp TG (2004) High-pressure phases in shock-induced melt veins of the Umbarger L6 chondrite: constraints of shock pressure. Meteorit Planet Sci 39:2043–2054
Yamamoto S, Komiya T, Hirose K, Maruyama S (2009) Coesite and clinopyroxene exsolution lamellae in chromites: in-situ ultrahigh-pressure evidence from podiform chromitites in the Luobusa ophiolite, southern Tibet. Lithos 109:314–322
Yang J-S, Dobrzhinetskaya L, Bai W-J, Fang Q-S, Robinson PT, Zhang J, Green HW (2007) Diamond- and coesite-bearing chromitites from the Luobusa ophiolite. Tibet Geol 35:875–878
Yusa H, Akaogi M, Ito E (1993) Calorimetric study of $MgSiO_3$ garnet and pyroxene: heat capacities, transition enthalpies, and equilibrium phase relations in $MgSiO_3$ at high pressures and temperatures. J Geophys Res 98:6453–6460
Zedgenizov DA, Shatsky VS, Panin AV, Evtushenko OV, Ragozin AL, Kagi H (2015) Evidence for phase transitions in mineral inclusions in superdeep diamonds of the São Luiz deposit (Brazil). Russ Geol Geophys 56(1–2):296–305
Zhang RY, Liou JG (2003) Clinopyroxenite from the Sulu ultrahigh-pressure terrane, eastern China: origin and evolution of garnet exsolution in clinopyroxene. Am Mineral 88:1591–1600
Zhang RY, Shu JF, Mao HK, Liou JG (1999) Magnetite lamellae in olivine and clinohumite from Dabie UHP ultramafic rocks, central China. Am Mineral 84(4):564–569
Zhou MF, Robinson PT (1994) High-Cr and high-Al podiform chromitites, Western China: relationship to partial melting and melt/rock reaction in the upper mantle. Int Geol Rev 36(7):678–686
Zhou MF, Robinson PT, Malpas J, Li Z (1996) Podiform chromitites from the Luobusa ophiolite (Southern Tibet): implications for melt/rock interaction and chromite segregation in the upper mantle. J Petrol 37:3–21
Zou Y, Irifune T (2012) Phase relations in $Mg_3Cr_2Si_3O_{12}$ and formation of majoritic knorringite garnet at high pressure and high temperature. J Miner Petrol Sci 107:197–205

Chapter 3
Experimental Study of Cr-Bearing Phases at High Pressures

3.1 Experimental and Analytical Techniques

Experimental studies of the systems $Mg_4Si_4O_{12}$–$Mg_3Cr_2Si_3O_{12}$ and Mg_2SiO_4–$MgCr_2O_4$ (MgO–SiO_2–Cr_2O_3) were carried out on a Kawai-type multi-anvil apparatus at the Geodynamic Research Center, Ehime University (Matsuyama, Japan) and at the Bayerisches Geoinstitut, University of Bayreuth (Bayreuth, Germany) at $P = 10$–24 GPa and $T = 1600$ °C. Experiments on the study of the influence of the low aluminum concentrations on the conditions of crystallization and composition of majorite–knorringite garnets in the system $Mg_4Si_4O_{12}$–$Mg_3Cr_2Si_3O_{12}$ (MgO–SiO_2–$Cr_2O_3 \pm Al_2O_3$) at $P = 7$ GPa and $T = 1500$–1700 °C were performed on a toroidal ("anvil-with-hole") high-pressure apparatus at the Vernadsky Institute of Geochemistry and Analytical Chemistry, Russian Academy of Sciences. The composition of mineral phases synthesized in the runs was analyzed using the electron microprobe, Raman spectroscopy, and single-crystal X-ray diffraction.

3.1.1 Multi-anvil Apparatus

The high-pressure octahedral cell in the multi-anvil apparatus is compressed by eight tungsten carbide cubic anvils with 4.0- and 2.5-mm truncation edge length applied as the second-stage anvils of the high-pressure apparatus (Sirotkina et al. 2015). The high-pressure "split-sphere" multi-anvil apparatus is equipped with a 5000 t multi-anvil hydraulic press compressing two guide blocks. Each guide block consists of three external steel anvils separated by three supporting wedges along the outer circumference. The external anvils determine the size and cubic configuration of the volume subsequently compressed with eight internal anvils.

A tubular $LaCrO_3$ heater was inserted into a semi-sintered octahedron (MgO + 17 wt% CoO) of 8.0–10.0 and 8.0 mm in edge length (Fig. 3.1). Pyrophyllite gaskets

E. A. Matrosova et al., *Geochemistry of Chromium in the Earth's Mantle*,
Springer Geology, https://doi.org/10.1007/978-3-030-27018-6_3

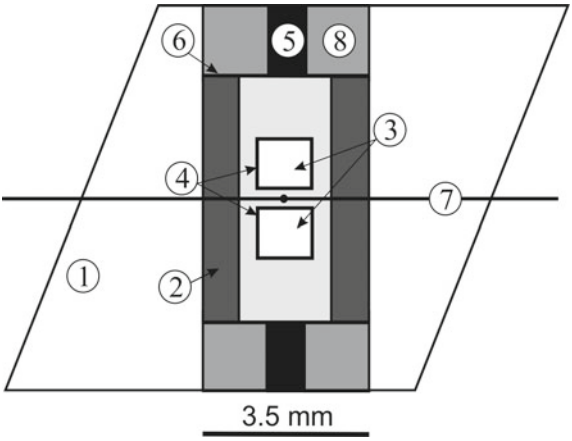

Fig. 3.1 The sample assembly of the Kawai-type apparatus used in our experimental studies (Sirotkina et al. 2015): (1) semisintered 8 mm edged (Mg,Co)O octahedron; (2) $LaCrO_3$ tubular heater; (3) starting material (sample); (4) platinum capsule; (5) Mo electrodes; (6) Mo discs; (7) $W_{97}Re_3$–$W_{75}Re_{25}$ thermocouple; (8) ZrO_2 plugs

with a width of 4 mm were used as the deformed hardening closing compressing volume. The samples (two in each cell assembly) were loaded into platinum capsules isolated from the heater by an MgO insulator.

Temperature and pressure measurement. The temperature was measured using a $W_{97}Re_3$–$W_{75}Re_{25}$ thermocouple with a hot junction positioned in the central part of the heater. Thermocouple was insulated with a BN tube. Thermocouple cold ends were connected to the automatic control unit. The temperature measurement accuracy was ±10 °C. The press load was selected in accordance with the calibration shown in Fig. 3.2.

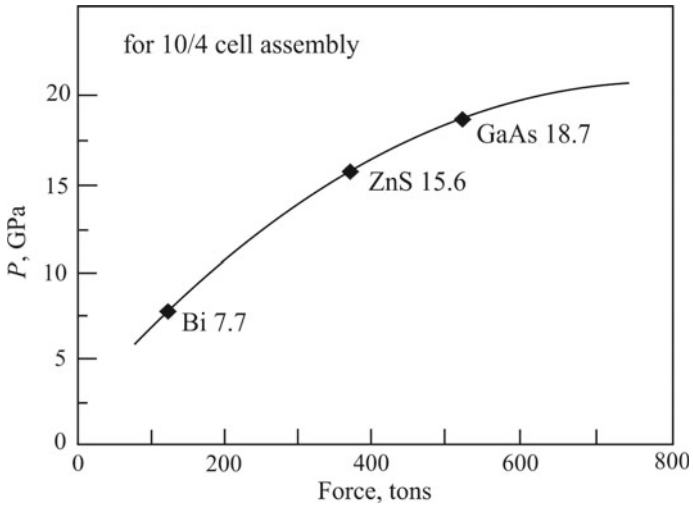

Fig. 3.2 Calibration of the pressure in the cell assembly against the load (oil pressure) of the press based on the pressure fixed points (Irifune et al. 2004; Zou and Irifune 2012)

Phase transitions in the pressure fixed points were diagnosed using Raman spectroscopy. Pressure values at room temperature were calibrated against the load (oil pressure) of the press based on the pressure fixed points (Fig. 3.2): Bi I–II transition at 2.55 GPa, Bi III–V transition at 7.7 GPa and semiconductor-metal transitions of ZnS at 15.5 GPa and GaAs at 18.3 GPa (Irifune et al. 2004; Zou and Irifune 2012). The effect of temperature on pressure was further corrected using the α–β and β–γ phase transitions in Mg_2SiO_4 (Katsura and Ito 1989). As a result, run pressure was controlled to ±0.5 GPa (Irifune et al. 1991).

Starting materials and experiment. The starting materials were prepared for the majorite ($Mg_4Si_4O_{12}$)–knorringite ($Mg_3Cr_2Si_3O_{12}$), magnesiochromite ($MgCr_2O_4$)–forsterite (Mg_2SiO_4) and majorite ($Mg_4Si_4O_{12}$)–knorringite ($Mg_3Cr_2Si_3O_{12}$)–pyrope ($Mg_3Al_2Si_3O_{12}$) systems corresponding to the following compositions: Knr_0Maj_{100}, $Knr_{05}Maj_{95}$, $Knr_{10}Maj_{90}$, $Knr_{15}Maj_{85}$, $Knr_{30}Maj_{70}$, $Knr_{50}Maj_{50}$, $Knr_{60}Maj_{40}$, $Knr_{70}Maj_{30}$, $Knr_{90}Maj_{10}$, $Knr_{100}Maj_0$, $MChr_{10}Fo_{90}$, $MChr_{30}Fo_{70}$, $MChr_{40}Fo_{60}$, $MChr_{50}Fo_{50}$, $MChr_{80}Fo_{20}$, $Prp_5Knr_{47.5}Maj_{47.5}$, $Prp_{10}Knr_{45}Maj_{45}$, and $Prp_{20}Knr_{40}Maj_{40}$. Very fine powders (particle size <100 nm) of MgO, SiO_2, Al_2O_3, and Cr_2O_3 (a purity is 99.99%) were homogenized at room temperature using ethanol and agate mortar. Then, the prepared mixtures were dried at 100 °C for 24 h and enclosed in a Pt capsule. The use of fine-grained oxides helps to enhance chemical reactions in H*P*–H*T* runs, as demonstrated by Zou and Irifune (2012). The sample was pressurized at ambient temperature to 10–24 GPa. Subsequently, the charge was heated to the desired temperature. The duration of each run was 3–5 h, which is long enough for attaining chemical equilibrium between coexisting phases. After run, the sample was rapidly quenched to ambient temperature by switching off a power supply with a quench rate of 200 °C/s. Then, the apparatus was decompressed, and the cell assembly with the sample was removed from anvils. Each run sample was divided into several pieces for microprobe analysis and XRD measurements.

3.1.2 Toroidal ("Anvil-with-Hole") Apparatus

The experimental study was performed at a pressure of 7.0 GPa and temperatures of 1500–1700 °C on a toroidal "anvil-with-hole" apparatus NL-13T at the Institute of Geochemistry and Analytical Chemistry, Russian Academy of Sciences. The apparatus is a modification of the Bridgman-anvil type high-pressure apparatus (Litvin 1991).

The "anvil-with-hole" apparatus contains two identical coaxial hard-alloy anvils (tungsten carbide). This allows us to attain pressures of up to 10 GPa. To increase the efficiency, anvils are fastened with a set of steel rings pressed against each other. Cooling of the working matrices proceeds through the nozzle by supplying a flow of cooled water to the gap between the blocks supporting the working matrix and the base plate. A specially constructed cell assembly is placed between anvils, so that the closing layer is formed between the edges of anvils upon complete loading. This

layer prevents "leakage" of the sample and provides the stable lithostatic pressure in the cell assembly (Fig. 3.3).

A cell assembly is shown in Fig. 3.4. Solid-state cells of a 30-mm outer diameter were manufactured from the lithographic limestone (Algeti Mine, Georgia) and contained ultra-pure graphite heater of a 7-mm outer diameter and with a length of 7.5 mm. The heater had a hole with a 2.5 mm diameter and a 2.5 mm depth in the center of the cell, in which experimental starting materials were loaded. After pressurization, the sample volume was reduced to ~1.5 mm^3.

Temperature and pressure measurement. A special series of calibration experiments were performed, which made possible to achieve the highest accuracy in temperature and pressure estimations. The pressure was produced by the uniaxial compression of the upper and lower anvils and calibrated against the phase transition points of Bi at 2.55 GPa (Bi I–Bi II), 2.7 GPa (Bi II–Bi III) and 7.7 GPa (Bi III–Bi V), at room temperature (Homan 1975). The pressure was corrected for the high temperature with the diamond–graphite curve (Kennedy and Kennedy 1976)

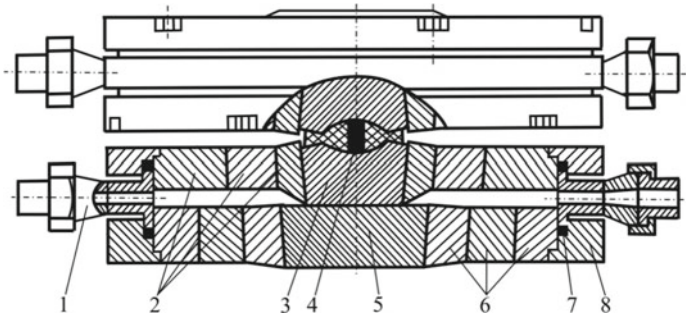

Fig. 3.3 Scheme of the high-pressure camera. (1) Nozzle of the cooling system; (2) rings supporting an anvil; (3) anvil; (4) reaction volume; (5) mounting; (6) system of mounting support; (7) hardening; (8) case (Litvin 1991)

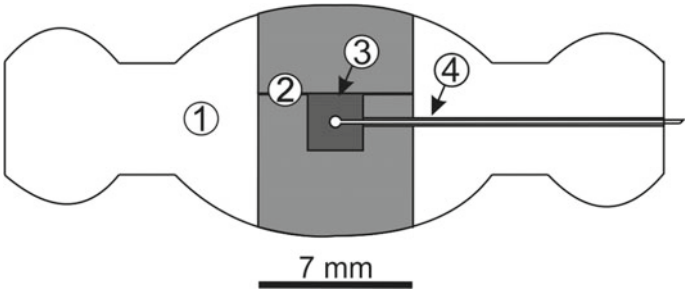

Fig. 3.4 The cell assembly of the toroidal "anvil-with-hole" apparatus used in our experimental studies (Sirotkina et al. 2016): (1) cell (pressed carbonate or lithographic limestone); (2) C (graphite) heater; (3) sample; (4) Pt–Rh thermocouple in an Al_2O_3 sleeve

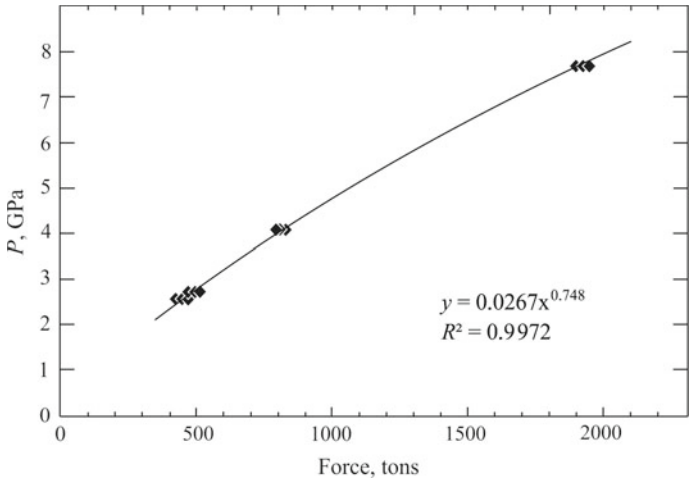

Fig. 3.5 Pressure calibration curve in the cell assembly (GPa) against the oil pressure (tons)

using growth/dissolution of diamond seeds in carbon-oversaturated multicomponent carbonate melts (Spivak and Litvin 2004). The pressure calibration curve is shown in Fig. 3.5.

The temperature was monitored (within ±10 °C) by the heating-power supply calibrated against $Pt_{70}Rh_{30}/Pt_{94}Rh_6$ thermocouples, and the distribution of temperature in the sample was close to isothermal because of its small size. This provided a homogeneous composition of the phases in subsolidus experiments and a uniform crystal-melt distribution in the samples molten close to the liquidus boundary. The results of calibration of cells with a graphite heater (diameter 7/0) are shown in Fig. 3.6.

3.1.3 Analytical Procedures

Run products were subjected to visual examinations for homogeneity by using a binocular microscope. Each sample was divided into several pieces for examination in reflective light, microprobe analysis, and XRD measurements. One/two pieces of each sample were embedded in epoxy and polished. The experimental products were studied on a scanning electron microscope Jeol JSM-6480LV (Japan) equipped with an INCA Energy-350 energy-dispersive analyser and an INCA Wave-500 wavelength diffraction spectrometer (Oxford Instrument Ltd., United Kingdom). Microprobe analyses were performed at an accelerating voltage of 20 kV, a beam current of 10 nA, and a beam diameter of 3 μm.

No normalization procedure was applied. Compositions of the phases in each run were determined from the average of 3–7 analyses. The chemical formulae were

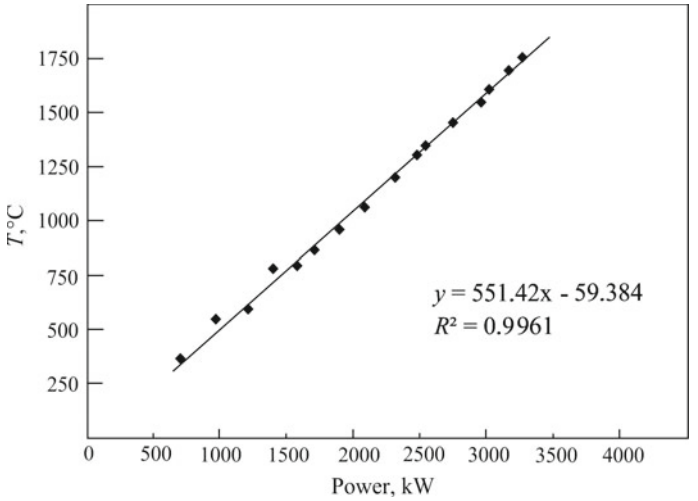

Fig. 3.6 Temperature calibration against the electric power at a pressure of 7 GPa for the cell assembly 7/0. The thermocouple $Pt_{70}Rh_{30}/Pt_{94}Rh_6$ with a diameter of 0.5 mm was applied

calculated on the basis of a specified number of oxygen atoms. No significant differences in sample textures and mineral compositions were observed for the runs with different durations; this confirms that the chemical equilibrium was achieved in our runs.

The modal proportions of minerals in the samples were estimated using the CT-An software from BSE images.

Raman spectroscopy. Raman spectra were recorded from polished surfaces of crystalline samples (mostly garnets) produced at 12–16 GPa. The main goal of the research was to obtain Raman spectra for knorringitic garnet, since such data were not available in literature.

The Lab Ram system (Micro-Raman RENISHAW) with a He–Nd-laser (an excitation wavelength of 532 nm) was used for the collection of the Raman spectra. The laser power was controlled by a series of density filters. The lateral and depth resolutions were ~2 and 5 μm, respectively. The system was calibrated using the 520.6 cm^{-1} Raman band of Si prior to the experimental session. The spectra were collected with multiple acquisitions (2–6) with single counting times ranging between 20 and 180 s. The spectra were recorded using the LabSpec 5 software from 150 to 1750 cm^{-1}. The studies were performed at the Geodynamics Research Center, Ehime University (Matsuyama, Japan) and Bayerisches Geoinstitut (Bayreuth, Germany).

Crystal-structure refinement. Small crystals of the studied phases (garnet, akimotoite, bridgmanite, $MgCr_2O_4$ and $Mg(Mg,Cr)(Mg,Si)O_4$ with the calcium titanate-type structure, and anhydrous phase B), handpicked under a reflected-light microscope from run products, were preliminarily examined with a Bruker-Enraf MACH3 single-crystal diffractometer using the graphite monochromatized Mo$K\alpha$ radiation. Then, the data collection was performed on a Supernova (Rigaku-Oxford Diffrac-

tion) single-crystal diffractometer equipped with the Mova microsource (a spot size of 0.120 mm, Mo$K\alpha$) and assembled with a Pilatus 200 K detector (Dectris). Intensity integration and standard Lorentz-polarization corrections were performed with the CrysAlis RED (Oxford Diffraction 2006) software package. The program ABSPACK of the CrysAlis RED package was used for the absorption correction.

Single-crystal X-Ray diffraction of the samples was carried out in two modes: (1) full intensity data collection and subsequent crystal structure refinement for a complete characterization (garnet, akimotoite, bridgmanite, $MgCr_2O_4$ and $Mg(Mg,Cr)(Mg,Si)O_4$ phases with the calcium titanate-type structures); (2) determination of unit cell parameters only for identification purposes (majorite–enstatite–akimotoite–bridgmanite and forsterite–wadsleyite–ringwoodite).

3.2 Review of the Experimental Data

Along with the analysis of mineralogical data, a significant amount of information on the composition and structure of the Earth's deep mantle areas were obtained from the experimental studies of the model (mostly simulating Mg–Fe-isomorphism in high-pressure phases) and multicomponent (corresponding to the peridotite/pyrolite and eclogite lithologies) systems. The new experimental information on the effect of minor elements on the compositions and structural patterns of the deep phases motivated more careful studies of some geophysically significant phase transformations, which account for variations in the composition of mantle minerals.

A number of experimental and thermodynamic studies of Cr-bearing mantle associations has been carried out over the past decades (Girnis et al. 2003; Brey et al. 1999; Klemme 2004). Most of these papers contained the data on the phase equilibria and conditions of the formation of high-pressure chromium-rich (knorringite) garnets. The solubility of chromium in other high-pressure phases, as well as the influence on the structural features and the *PT* parameters of stability of these phases, are poorly studied and restricted the influence of chromium on olivine and its polymorphs (Gudfinnsson and Wood 1998).

3.2.1 Systems with High-Pressure Components of Garnets

The natural garnets from garnet peridotite, eclogite, kimberlite, and other high-pressure rocks are characterized by the pyrope–grossular–almandine composition with minor impurities of high-pressure components. As it is evident from the experimental data, incorporation of knorringite ($Mg_3Cr_2Si_3O_{12}$) in garnet is registered at ~3 GPa, i.e., beyond the diamond depth facies (Malinovskii et al. 1975), whereas the concentration of chromium in garnets within the area of crystallization of most of natural diamonds (4–7 GPa) reaches significant values (5–10 wt% Cr_2O_3 and higher). Such garnets are mostly high-chromium subcalcic pyropes, which are indica-

tors of the diamondiferous dunite–harzburgite paragenesis in the lithospheric mantle (Sobolev 1974). The maximum concentration of Cr_2O_3 in natural garnet is 20.6 wt%, which corresponds to 60 mol% of knorringite (Stachel and Harris 1997).

Incorporation of excess silicon (majoritic component) is one more pattern of deep garnets. The concentration of chromium and aluminum in garnets decreases with increasing pressure (Akaogi and Akimoto 1977; Irifune 1987), whereas the concentration of silicon in the octahedral site and the concentration of divalent cations (Ca, Mg, and Fe) and sodium progressively increase (Ono and Yasuda 1996); as a result, garnet with Si >3 f.u. is formed. This results from the beginning of dissolution of the pyroxene (mostly (Mg, Fe)SiO_3) end members in garnet starting from a pressure of ~7.5 GPa (Akaogi and Akimoto 1979). With increasing pressure, the solubility of pyroxene in garnet becomes significant. In contrast to the knorringite component, the presence of majorite is mostly typical of eclogitic garnets.

According to the experimental and natural data, the minimum pressures of knorringite (~3 GPa) and majorite (~7.5 GPa) incorporation in natural garnets are different. Therefore, the relative saturation of garnet in knorringite is probable in the lithosphere, whereas high concentrations of the majoritic component (5–10 mol%) are typical of the sublithospheric mantle only. The presence of both knorringite and majorite in natural garnets is occasional (Stachel 2001; Taylor and Anand 2004). However, the simplified ternary system pyrope–majorite–knorringite ($MgO–Al_2O_3–Cr_2O_3–SiO_2$) may be applied for reconstruction of the formation of garnets in the lowermost upper mantle and transition zone.

From the first study of the pyrope–majorite join (Akaogi and Akimoto 1977), a huge database on the experimental investigation of the systems containing majoritic garnet was accumulated in a wide range of temperatures and pressures. Both relatively simple (model) and multicomponent systems with natural chemistry were studied. The main result of these studies was the demonstration of the linear correlation between the concentration of Si in the octahedral site and pressure, independently on the complexity of the systems studied experimentally.

Many authors have studied the change in the unit cell parameters with increasing content of the majoritic component in garnet (Parise et al. 1996; Nakatsuka et al. 1999). It was established that increase in the majorite component in garnet along the majorite–pyrope join resulted in the gradual increase in the cell parameters with further transition from cubic (space group $Ia\bar{3}d$) to tetragonal (space group $I4_1/a$) symmetry (Akaogi and Akimoto 1977; Parise et al. 1996). This transition occurs at high majorite contents in garnet (>80 mol% Maj) (Parise et al. 1996).

Although knorringite is an important end-member of garnet in the deep lithospheric mantle, the stability and high-pressure phase relations of knorringite are still controversial. Its stability field has been investigated in several studies (Ringwood 1977; Irifune et al. 1982; Turkin et al. 1983; Klemme 2004; Taran et al. 2004; Zou and Irifune 2012). The first synthesis of knorringite garnet was reported by Coes (1955) without any details about the run procedures and physical properties of the new phase. Later Ringwood (1977) synthesized knorringitic garnet in a quite wide pressure range (6–8 GPa) at temperatures of 1400–1500 °C. Irifune et al. (1982) demonstrated the stability of knorringite at pressures >11.5 GPa at 1200 °C and at

>11.8 GPa at 1400 °C. In contrast, Turkin et al. (1983) reported on the appearance of knorringite at significantly lower pressures of 8.0–9.5 GPa at 1200–1800 °C, with a negative slope of the phase boundary. Klemme (2004) synthesized knorringite coexisting with eskolaite (Cr_2O_3) at 16 GPa and 1600 °C. Taran et al. (2004) reported on the synthesis of knorringite at 9–16 GPa and 1300–1600 °C. Zou and Irifune (2012) noted that in all runs knorringite was associated to eskolaite. The authors explained this fact by incorporation of the majorite component in garnet.

The structure of knorringite was refined using X-ray single crystal (Bykova et al. 2014) and powder diffraction data (Juhin et al. 2010). Ottonello et al. (1996) performed calculations of the cell parameters of pure knorringite $Mg_3Cr_2Si_3O_{12}$ (a = 11.6040 Å).

Single-crystal X-ray diffraction studies of knorringitic garnets, as well as the study of the structural features of garnet solid solutions containing a significant portion of the knorringite end-member have not been carried out yet. The occurrence of the knorringite component in garnet was studied on the example of the model pyrope–knorringite system (Ringwood 1977; Klemme 2004; Turkin and Sobolev 2009). Turkin and Sobolev (2009) established that the maximum solubility of the knorringite component in garnet increased with pressure and temperature within the pressure range from 3 to 7 GPa. The authors of that study observed a negative slope of the isolines of the chromium content in garnet in the P–T coordinates (Malinovskii et al. 1975; Turkin and Sobolev 2009).

The P–X diagram for the pyrope–knorringite system, which summarizes the data of various studies, is shown in Fig. 3.7 (Malinovskii et al. 1975; Turkin et al. 1983; etc.). Addition of calcium to the system leads to the transformation of the reaction line to the four-phase field *OPx* + *Sp* + *Grt* + *Fo* (Fig. 3.8) in the CaO–MgO–Al_2O_3–SiO_2–Cr_2O_3 system (MacGregor 1964). It was also established that the increase in the Cr content in the CaO–MgO–Al_2O_3–SiO_2–Cr_2O_3 system moved the spinel-bearing association field to the higher pressure area (Fig. 3.8). The majorite–knorringite system has not been studied yet.

Recent experimental studies of the majorite–eskolaite ($MgSiO_3$–Cr_2O_3) system (Zou and Irifune 2012) at 8–16 GPa and 1200–1800 °C have shown that pyroxene and eskolaite are stable in the low-pressure area of the diagram (Fig. 3.9). With increasing pressure, this association is replaced by the knorringite-majorite garnet and eskolaite in the chromium-rich part of the system. The concentration of the knorringite end-member in garnet decreases with pressure, which results in an increase of the eskolaite content in the run products. As the authors performed their runs with the starting composition $Mg_3Cr_2Si_3O_{12}$ (pure knorringite), the fields *Px* + *Grt* and *Esk* were not supported experimentally.

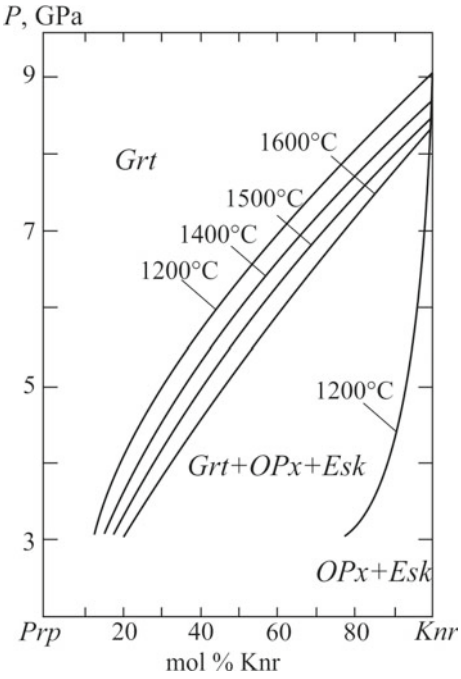

Fig. 3.7 Isothermal *P–X* section of the pyrope–knorringite system (Malinovskii et al. 1975; Babich 1980; Turkin et al. 1983; Doroshev et al. 1997; Turkin and Sobolev 2009)

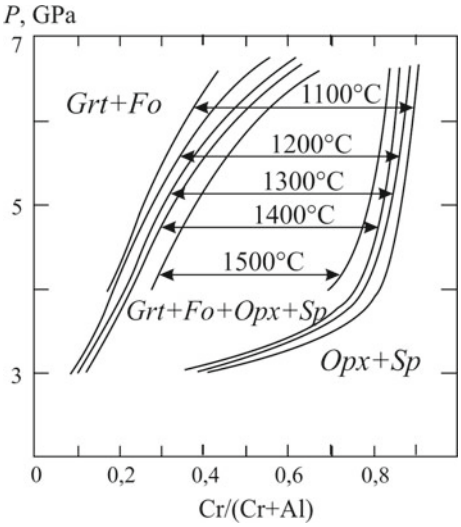

Fig. 3.8 Compositions of coexisting garnet and spinel in dependence on temperature, after (Malinovskii et al. 1975; Babich 1980; Turkin et al. 1983; Doroshev et al. 1997; Turkin and Sobolev 2009)

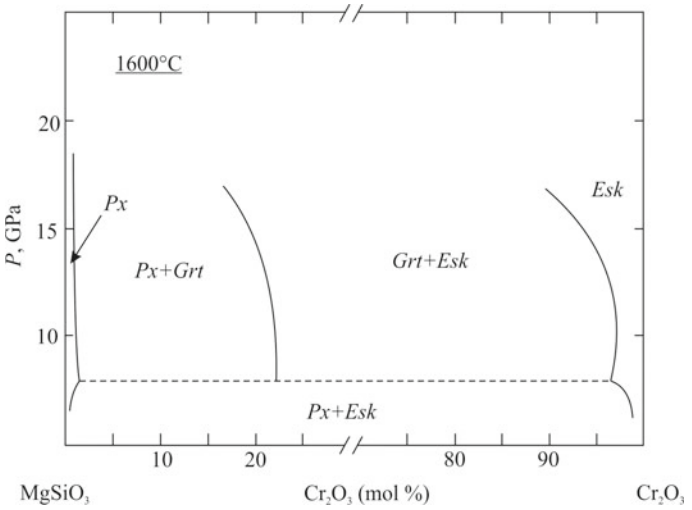

Fig. 3.9 Schematic diagram of phase relations in the system $MgSiO_3$–Cr_2O_3 at 8–16 GPa and 1600 °C (Zou and Irifune 2012)

3.2.2 *Influence of Cr and Other Minor Elements on Mg_2SiO_4 Polymorphs*

The study of the influence of minor elements on the *P–T* parameters of phase transformations and on the structural features of the high-pressure phases with composition $(Mg,Fe)_2SiO_4$ have been poorly studied over the past decades (Harte 2010).

Gudfinnsson and Wood (1998) investigated the effect of minor elements, such as Cr, Ni, Ti, Al, Ca, Na, and H, on the depth and pressure range of olivine–wadsleyite transformation. The authors demonstrated that the maximum concentration of Cr_2O_3 that could be dissolved in wadsleyite was ~2.0 wt% (~0.35 wt% in *Ol*) at 14 GPa and 1600 °C, whereas the solubility of TiO_2 in *Wad* at such conditions reached ~0.6 wt% (~0.1 wt% in *Ol*). This work confirms the conclusion of Dobrzhinetskaya et al. (1996) on the high-pressure formation of the Mg_2SiO_4 phase (initial wadsleyite) with exsolution textures of chromite and chromium-bearing ilmenite ($Cr–FeTiO_3$) in olivine from peridotite of the Alpe-Arami Massif (Switzerland). Gudfinnsson and Wood (1998) also suggested that effects of these minor elements on the properties of the 410 km seismic discontinuity (olivine/wadsleyite transition) were negligible.

Recent experimental studies of the Al-rich part of the Mg_2SiO_4–$MgAl_2O_4$ system (Kojitani et al. 2007) at pressures of 21–27 GPa and temperatures of 1600–2200 °C showed that the maximum solubility of Mg_2SiO_4 in $MgAl_2O_4$ with the calcium ferrite-type structure (*Cf*) was 34 mol% (14.3 wt% SiO_2) at 24 GPa. At 21–23 GPa, the association of corundum (*Crn*) + periclase (*Per*) was stable in the Al-rich part of the system; with increasing pressure, this assemblage is replaced with $MgAl_2O_4$ with the calcium ferrite-type structure.

In this chapter, we report the influence of chromium on the unit-cell parameters of the mantle high-pressure phases and thermodynamic conditions of their stability. We discuss the results of high-pressure experiments in the Cr-rich systems, such as majorite–knorringite, forsterite–magnesiochromite, and majorite—magnesiochromite, which are the petrologically significant sections of the model $MgO–SiO_2–Cr_2O_3$ system. Finally, we discuss the influence of Al on the phase relations in this system and consider the conditions of the formation of Cr-rich phases (mostly knorringitic garnet) in the multicomponent (pyrolite) system.

3.3 Experimental Study of the Model System SiO_2–MgO–Cr_2O_3 Under the Mantle *P–T* Parameters

With a certain degree of approximation, the model system $SiO_2–MgO–Cr_2O_3$ characterizes the phase associations of the different regions of the Earth's mantle. Despite absence of a number of the major components (CaO, FeO, Na_2O, K_2O, and others) in this system, its study in a wide pressure range (10–24 GPa) allows us to consider the most important phase transformations of Mg-rich silicate minerals in the upper mantle, transition zone, and lower mantle. Addition of chromium makes possible to understand the influence of the minor component on the structural patterns of these phases and on the parameters of their phase transformations. During the preliminary analysis, we selected two petrologically significant sections of the ternary diagram $SiO_2–MgO–Cr_2O_3$ for the experimental study: (1) the $Mg_4Si_4O_{12}–Mg_3Cr_2Si_3O_{12}$ system simulating the majorite–knorringite series of solid solutions in mantle garnets and the post-garnet phases with the ilmenite- and perovskite-type structures; (2) the $Mg_2SiO_4–MgCr_2O_4$ system simulating the major polymorph transitions olivine–wadsleyite–ringwoodite, the post-ringwoodite associations, as well as the phase transformations for the post-spinel phases. Our experimental studies were not restricted to the Mg-rich compositions, but were aimed at obtaining of complete experimental information for the abovementioned systems, including the Cr-rich starting compositions; therefore, the *P–X* phase diagrams were studied for each system at a constant temperature of 1600 °C, which is close to the mantle geotherm (Stixrude and Lithgow-Bertelloni 2007). In addition, to study the influence of the small concentrations of Al on the parameters of crystallization and composition of majorite–knorringite garnets, we carried out the series of experiments in the $SiO_2–MgO–Cr_2O_3 \pm Al_2O_3$ system at 7 GPa and 1500–1700 °C. The main experimental results obtained in our study are considered below.

3.3.1 $Mg_4Si_4O_{12}$–$Mg_3Cr_2Si_3O_{12}$ Section at 10–24 GPa and 1600 °C

Due to the important role of chromium in the mineralization of the upper mantle and the widely abundant association of knorringitic garnet with natural diamond, the $Mg_4Si_4O_{12}$–$Mg_3Cr_2Si_3O_{12}$ section was selected as the model one for the experimental study of regularities in the formation of knorringite–majorite garnets. Both high-pressure components (majorite and knorringite) are very important for barometry of the mantle mineral associations; however, their simultaneous incorporation in garnet has been not studied yet. Here we report the results of the experimental study of the majorite–knorringite system on a high-pressure multianvil apparatus (Sirotkina et al. 2015).

Phase relations. At 10–24 GPa and 1600 °C, we studied the full range of the starting compositions in the knorringite–majorite series with increments of 10–20 mol% *Knr* and 1–2 GPa, which allowed us to synthesize Cr-bearing phases of a wide compositional range. The phases obtained in our runs include pyroxene, garnet of the knorringite–majorite composition (Juhin et al. 2010; Zou and Irifune 2012; Bykova et al. 2014), Cr-bearing $MgSiO_3$ with the ilmenite- (Kawai et al. 1974; Bindi et al. 2014a) and perovskite-type (Liu 1974; Bindi et al. 2014b) structures, eskolaite Cr_2O_3, $MgCr_2O_4$ with the calcium titanate-type structure (Wang et al. 2002; Chen et al. 2003; Bindi et al. 2014c), and stishovite. The run conditions, phase assemblages, and compositions of the phases produced in experiments in the system $Mg_4Si_4O_{12}$–$Mg_3Cr_2Si_3O_{12}$ (majorite–knorringite) at 10–24 GPa and 1600 °C are reported in Table 3.1. The phase assemblages in the experimental samples were established using a scanning electron microscope with an energy-dispersive spectrometer, and after all runs, the results were controlled by single-crystal X-ray diffraction and Raman spectroscopy.

As it was shown by Zou and Irifune (2012) and Sirotkina et al. (2016), at relatively low pressures ($P < 8$ GPa), pyroxene associates with eskolaite Cr_2O_3 (*Esk*) in the whole compositional range. Increase in pressure results in appearance of knorringite–majorite garnet in association with pyroxene (*Grt* + *Px*, 0–90 mol% *Knr* in the starting composition), according to the reaction *Px* + *Esk* = *Grt*, and eskolaite (*Grt* + *Esk*, 90–100 mol% *Knr* in the starting composition).

At 10–14 GPa and low Cr contents in the starting composition, Cr-bearing majoritic garnet is in the equilibrium with low-Cr pyroxene. The texture of samples is characterized by relatively large isometrical (a diameter of 10–100 μm) garnet crystals and large, often elongated (a length up to 120 μm) pyroxene grains with clear cleavage (Fig. 3.10a). With increasing Cr concentration in the starting composition, the bulk garnet content in the sample increases. Thus, the content of garnet in Sample 2520-5 (the starting composition $Maj_{95}Knr_{05}$) does not exceed ~12 vol.%, whereas the estimated content of this mineral in Sample 2423-15 (the starting composition $Maj_{85}Knr_{15}$) reaches 40 vol.%.

Further increase in pressure and $Mg_3Cr_2Si_3O_{12}$ in the starting composition stimulates appearance of the single-phase field of garnet with the knorringite–majorite

Table 3.1 Conditions, phase assemblages, and compositions of the phases produced in experiments in the system $Mg_4Si_4O_{12}$–$Mg_3Cr_2Si_3O_{12}$ at 10–24 GPa and 1600 °C

Run no. (sample)	*P* (GPa); *T* (°C)	Starting composition	Heating duration (hours)	Run products	Mean composition of the phases				
					Phase	MgO	SiO_2	Cr_2O_3	Total
2526-100	10; 1600	$Knr_{100}Maj_0$	5	*Grt* + *Esk*	*Grt*[a]	28.16 (0.54)	41.24 (0.43)	30.78 (0.20)	100.18
					Esk	0.30 (0.11)	0.47 (0.2)	98.45 (0.79)	99.22
2521-100	12; 1600	$Knr_{100}Maj_0$	5	*Grt* + *Esk*	*Grt*	29.01 (0.05)	43.21 (0.12)	28.70 (0.09)	100.91
					Esk	1.55 (0.40)	1.54 (0.28)	94.99 (0.35)	98.08
2404-50	12; 1600	$Knr_{50}Maj_{50}$	4	*Grt* + *Px*[b]	*Grt*	31.01 (0.39)	45.81 (0.48)	23.79 (0.36)	100.61
2533-100	14; 1600	$Knr_{100}Maj_0$	5	*Grt* + *Esk*	*Grt*	32.35 (0.31)	47.93 (0.30)	19.99 (0.25)	100.27
					Esk	1.51 (0.32)	1.69 (0.31)	96.26 (0.45)	99.46
2403-50	14; 1600	$Knr_{50}Maj_{50}$	4	*Grt*	*Grt*	33.52 (0.28)	49.48 (0.20)	17.74 (0.21)	100.74
2423-15	14; 1600	$Knr_{15}Maj_{85}$	4	*Grt* + *Px*	*Grt*	34.62 (0.25)	50.59 (0.37)	14.35 (0.08)	99.56
					Px	39.73 (0.20)	58.71 (0.21)	0.6 (0.08)	99.04
2520-5	14; 1600	Knr_5Maj_{95}	5	*Grt* + *Px*	*Grt*	34.36 (0.31)	50.83 (0.42)	14.99 (0.44)	100.18
					Px	39.86 (0.37)	59.26 (0.32)	0.00	99.12
2425-5	15; 1600	Knr_5Maj_{95}	5	*Grt*	*Grt*[a]	39.62 (0.12)	59.01 (0.24)	1.17 (0.11)	99.80
2401-100	16; 1600	$Knr_{100}Maj_0$	5	*Grt* + *Esk*	*Grt*	29.98 (0.34)	44.81 (0.30)	25.54 (0.40)	100.33
					Esk	1.75 (0.31)	1.74 (0.20)	95.89 (50)	99.37
2399-90	16; 1600	$Knr_{90}Maj_{10}$	4	*Grt* + *Esk*	*Grt*	29.71 (0.39)	43.44 (0.46)	25.02 (0.15)	98.17
					Esk	1.70	1.82	96.03	99.55
2397-70	16; 1600	$Knr_{70}Maj_{30}$	4	*Grt*	*Grt*	30.34 (0.29)	44.83 (0.36)	24.22 (0.38)	99.39
2398-50	16; 1600	$Knr_{50}Maj_{50}$	4	*Grt*	*Grt*	32.47 (0.31)	48.67 (0.19)	18.02 (0.17)	99.16

(continued)

Table 3.1 (continued)

Run no. (sample)	*P* (GPa); *T* (°C)	Starting composition	Heating duration (hours)	Run products	Mean composition of the phases				
					Phase	MgO	SiO_2	Cr_2O_3	Total
2418-15	16; 1600	$Knr_{15}Maj_{85}$	5	*Grt*	*Grt*	38.16 (0.10)	57.22 (0.20)	5.63 (0.39)	101.04
2399-10	16; 1600	$Knr_{10}Maj_{90}$	4	*Grt*	*Grt*[a]	38.95 (0.09)	57.61 (0.08)	3.74 (0.05)	100.30
2408-100	17; 1600	$Knr_{100}Maj_{0}$	5	*Grt* + *Esk*	*Grt*	30.50 (0.13)	45.69 (0.38)	23.57 (0.30)	99.56
					Esk	3.02 (0.31)	3.84 (0.21)	92.23 (0.56)	99.09
2415-100	18; 1600	$Knr_{100}Maj_{0}$	5	*Grt* + *Ct* + *Sti*	*Grt*	31.19 (0.49)	46.45 (0.34)	21.85 (0.30)	99.49
					Ct	24.46 (0.45)	3.52 (0.35)	71.82 (0.53)	99.80
2438-60	18; 1600	$Knr_{60}Maj_{40}$	5	*Grt*	*Grt*[a]	31.97 (0.44)	47.32 (0.31)	21.31 (0.23)	100.60
2410-30	18; 1600	$Knr_{30}Maj_{70}$	5	*Grt* + *Ak*	*Grt*	33.63 (0.36)	49.74 (0.28)	17.09 (0.37)	100.46
					Ak[a]	37.94 (0.30)	56.55 (0.35)	5.71 (0.23)	100.20
2415-10	18; 1600	$Knr_{10}Maj_{90}$	5	*Grt*[b] + *Ak*	*Ak*[a]	38.51 (0.42)	57.39 (0.35)	3.42 (0.40)	99.32
2530-100	19; 1600	$Knr_{100}Maj_{0}$	5	*Grt* + *Ct*[b] + *Sti*	*Grt*	32.35 (0.12)	47.93 (0.24)	19.99 (0.11)	100.27
2531-30	19; 1600	$Knr_{30}Maj_{70}$	5	*Grt* + *Ak*	*Grt*	32.98 (0.21)	48.40 (0.19)	17.69 (0.15)	99.07
					Ak	39.04 (0.25)	57.67 (0.31)	3.59 (0.11)	100.3
2531-15	19; 1600	$Knr_{15}Maj_{85}$	5	*Grt* + *Ak*	*Grt*	33.38 (0.16)	49.74 (0.30)	17.73 (0.25)	100.85
					Ak	38.84 (0.34)	57.72 (0.14)	3.63 (0.03)	100.19
2530-5	19; 1600	$Knr_{5}Maj_{95}$	5	*Ak*	*Ak*[a]	39.12 (0.48)	58.31 (0.26)	2.24 (0.17)	99.67
2402-100	20; 1600	$Knr_{100}Maj_{0}$	3	*Grt* + *Ct* + *Sti*	*Grt*	32.81 (0.30)	48.68 (0.35)	17.54 (0.29)	99.03
					Ct	24.53	3.68	70.95	99.15

(continued)

Table 3.1 (continued)

Run no. (sample)	*P* (GPa); *T* (°C)	Starting composition	Heating duration (hours)	Run products	Mean composition of the phases				
					Phase	MgO	SiO_2	Cr_2O_3	Total
2407-90	20; 1600	$Knr_{90}Maj_{10}$	4	*Grt* + *Ct* + *Sti*	*Grt*	33.23 (0.48)	49.41 (0.31)	17.98 (0.49)	100.62
					Ct	24.42 (0.28)	3.81 (0.21)	70.79 (0.35)	99.02
2406-70	20; 1600	$Knr_{70}Maj_{30}$	4	*Grt* + *Ct*[b] + *Sti*	*Grt*	33.53 (0.28)	50.04 (0.21)	17.39 (0.20)	100.96
2402-50	20; 1600	$Knr_{50}Maj_{50}$	3	*Grt* + *Brd* + *Ct* + *Sti*	*Grt*	32.85 (0.38)	48.51 (0.35)	18.19 (0.23)	99.55
					Brd	36.64 (0.32)	54.24 (0.49)	8.23 (0.13)	99.11
					Ct	23.97 (0.74)	3.88 (0.21)	70.61 (0.76)	98.45
2407-30	20; 1600	$Knr_{30}Maj_{70}$	4	*Grt* + *Brd*	*Grt*	33.12 (0.13)	49.32 (0.26)	17.64 (0.24)	100.08
					Brd	37.16 (0.50)	55.24 (0.40)	6.86 (0.73)	99.26
2434-15	20; 1600	$Knr_{15}Maj_{85}$	5	*Brd*	*Brd*	37.93 (0.41)	56.39 (0.43)	5.62 (0.54)	99.94
2528-100	21; 1600	$Knr_{100}Maj_{0}$	5	*Brd* + *Ct* + *Sti*	*Brd*	36.66 (0.18)	54.24 (0.28)	8.31 (0.21)	99.21
					Ct	21.39	0.00	79.32	100.71
2528-30	21; 1600	$Knr_{30}Maj_{70}$	5	*Brd* + *Ct*[b] + *Sti*	*Brd*	37.09 (0.51)	54.94 (0.40)	8.05 (0.31)	100.08
2529-10	21; 1600	$Knr_{10}Maj_{90}$	5	*Brd*	*Brd*	39.14 (0.45)	57.66 (0.35)	3.78 (0.32)	100.58
2413-70	23; 1600	$Knr_{70}Maj_{30}$	4	*Brd* + *Ct* + *Sti*	*Brd*[a]	35.66 (0.24)	53.17 (0.48)	10.35 (0.44)	99.18
					Ct[a]	20.73 (0.25)	0.00	78.58 (0.35)	99.31
2424-50	24; 1600	$Knr_{50}Maj_{50}$	4	*Brd* + *Ct*[b] + *Sti*	*Brd*	36.05 (0.39)	53.96 (0.44)	10.92 (0.67)	100.93
2424-10	24; 1600	$Knr_{10}Maj_{90}$	4	*Brd*	*Brd*	39.07 (0.19)	57.36 (0.21)	4.03 (0.18)	100.46

[a]Crystals studied by X-ray diffraction (see Chap. 4)
[b]Because of the small grain sizes, compositions of the phases were not analyzed

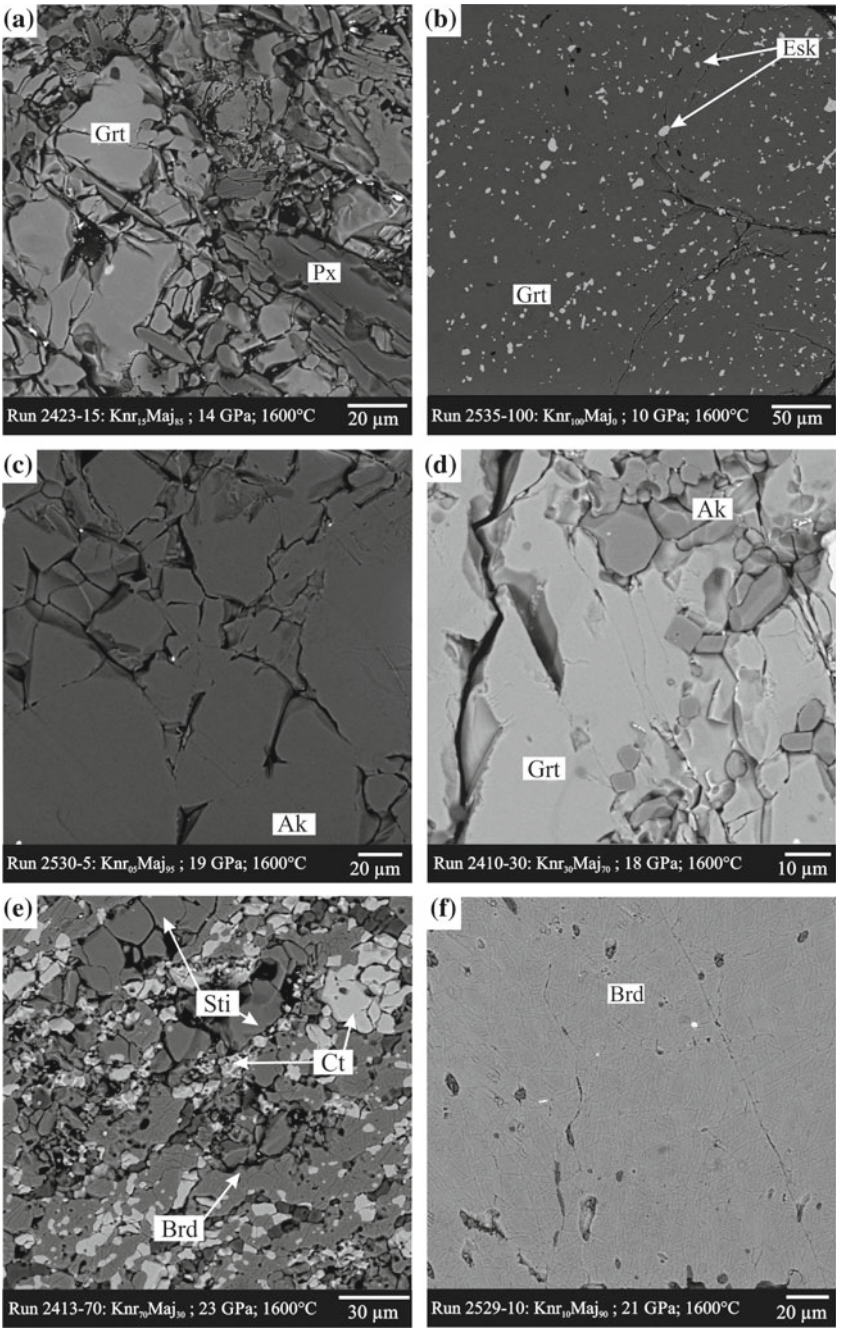
(a)
Grt
Px
Run 2423-15: $Knr_{15}Maj_{85}$; 14 GPa; 1600°C
20 µm
(b)
Esk
Grt
Run 2535-100: $Knr_{100}Maj_{0}$; 10 GPa; 1600°C
50 µm
(c)
Ak
Run 2530-5: $Knr_{95}Maj_{95}$; 19 GPa; 1600°C
20 µm
(d)
Ak
Grt
Run 2410-30: $Knr_{30}Maj_{70}$; 18 GPa; 1600°C
10 µm
(e)
Sti
Ct
Brd
Run 2413-70: $Knr_{70}Maj_{30}$; 23 GPa; 1600°C
30 µm
(f)
Brd
Run 2529-10: $Knr_{10}Maj_{90}$; 21 GPa; 1600°C
20 µm

◀**Fig. 3.10** BSE images of textural relationships and phase associations in run products in the system $Mg_4Si_4O_{12}$–$Mg_3Cr_2Si_3O_{12}$ at 10–24 GPa and 1600 °C: **a** aggregate of majorite–knorringite garnet and elongated prismatic pyroxene grains; **b** association of majorite–knorringite garnet and eskolaite, in which the latter occurs as inclusions in garnet and fills interstitials; **c** massive aggregate of subhedral $MgSiO_3$ akimotoite grains; **d** segregations of small $MgSiO_3$ akimotoite grains in majorite–knorringite garnet; **e** aggregate of $MgSiO_3$ bridgmanite, $MgCr_2O_4$ with a calcium titanate-type structure, and stishovite; **f** massive aggregate of bridgmanite grains with a dense system of fractures

composition. Garnets form large euhedral crystals with a size up to 150 μm. With increasing knorringite content in the starting material, an association of garnet and eskolaite does appear. The typical texture of the samples is shown in Fig. 3.10b: relatively large garnet crystals with a size of >150 μm and small, regularly distributed, often interstitial eskolaite segregations. Eskolaite often forms inclusions in garnet. The size of eskolaite segregations does not exceed 10 μm. It is defined that the stability of an association of *Grt* + *Esk* expands to the area of the lower content of *Knr* in the system with pressure, most likely, due to decrease in Cr solubility in garnet. Thus, it can be assumed that for each pressure value, a certain maximum solubility of chromium in garnet is established. With increasing Cr concentration in the starting material, the bulk content of eskolaite in this association does increase.

Increase in pressure in the area enriched in the majorite end-member (0–15 mol% *Knr*) results in the formation of a single-phase field of $MgSiO_3$ akimotoite (*Ak*). *Ak* forms a massive aggregate (Fig. 3.10c) with sizes of individual grains up to 100 μm. *Ak* associates with garnet in runs with the starting compositions with the moderate Cr concentrations (10–50 mol% *Knr*).

Akimotoite forming small euhedral crystals with a size of ≤50 μm associates with garnet (Fig. 3.10d). With increase in pressure up to 19 GPa for the same starting composition, the bulk content of garnet in the sample decreases. The paragenesis of garnet and bridgmanite appears at 20 GPa. The texture of the samples is characterized by relatively large euhedral garnet crystals and by smaller subhedral bridgmanite grains. Bridgmanite shows a small fracturing, most likely formed upon sample decompression after run.

The stability of garnet is limited by the pressure of 21 GPa. In the Cr-rich part of the system (>50 mol% *Knr*), the association of garnet and eskolaite is replaced with the paragenesis of garnet and $MgCr_2O_4$ with the calcium titanate-type structure (*Ct*) at ~17 GPa. With increasing pressure, the portion of garnet in run products gradually decreases, so that only single grains of garnet (not more than 5 vol.%) are registered at 21 GPa. $MgCr_2O_4$ in this association is represented by relatively large segregations with a size up to 50 μm. Characteristically, stishovite appears in association with chromium-rich garnet or chromium-bearing bridgmanite and the $MgCr_2O_4$ phase. Stishovite forms small anhedral grains with a size up to 10 μm.

The transition from the garnet-bearing associations (*Grt* + *Brd* and *Grt* + *Ct* + *Sti*) to the paragenesis of $MgSiO_3$ bridgmanite (*Brd* + *Ct* + *Sti*, Fig. 3.10e) proceeds at ~20 GPa in a wide range of starting compositions. The single-phase $MgSiO_3$ bridg-

manite field occurs for the low-Cr starting compositions above 20 GPa (Fig. 3.10f). This mineral forms massive fractured aggregates with a size of individual grains up to 50 μm.

Composition of the phases. Most of the phases synthesized in the $Mg_4Si_4O_{12}$–$Mg_3Cr_2Si_3O_{12}$ system at 10–24 GPa and 1600 °C show wide compositional variations (Table 3.1).

Pyroxene in the run products has the composition close to enstatite and contains a small chromium admixture (<0.6 wt% Cr_2O_3).

The main feature of *garnet* in all experimental samples is an excess of silicon (>3 Si p.f.u.), which is typical of garnets of the majoritic type. In association with pyroxene, garnet is characterized by quite high chromium contents (up to 24 wt% Cr_2O_3). With increasing pressure, the concentration of chromium in the mineral decreases (14 wt% Cr_2O_3 at 14 GPa), which results from increase in the bulk content of garnet and decrease in the portion of pyroxene in the sample.

The composition of garnets obtained in the single-phase field of the system depends on the starting composition, but not on pressure. With increasing content of the knorringite end-member in the starting material, its concentration in garnet regularly increases. The maximal concentration of knorringite in garnet from the single-phase field reaches 70 mol% (24 wt% Cr_2O_3) at 16 GPa for the starting composition $Knr_{70}Maj_{30}$.

The concentration of chromium in garnet associated with eskolaite decreases with pressure, whereas the concentration of silicon in the octahedral site (majoritic component) increases (Fig. 3.11a). There is a negative correlation between the concentrations of Mg and Cr in garnet (Fig. 3.11b), which, similarly to the Cr–Si relationships, is controlled by pressure and concentration of the knorringite end-member in the starting material.

With appearance of akimotoite at a pressure of >17 GPa, garnet becomes enriched in chromium (17 wt% Cr_2O_3). In this case, the composition of garnet does not depend on the Cr content in the starting material, but is controlled by pressure. The bulk content of garnet in the sample decreases with pressure, whereas the concentration

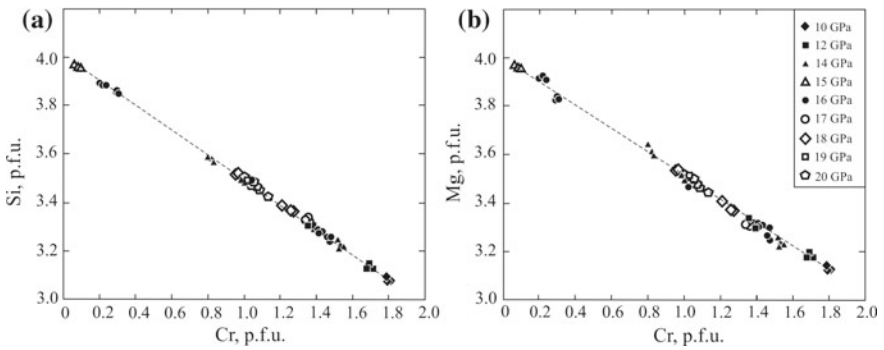

Fig. 3.11 Variations in the concentrations of Si, Mg, and Cr in garnets synthesized in the system $Mg_4Si_4O_{12}$–$Mg_3Cr_2Si_3O_{12}$ at 10–20 GPa and 1600 °C

of Cr in garnet does increase. Increase in pressure (>20 GPa) results in appearance of bridgmanite in association with garnet; the formation of bridgmanite does not influence significantly on the composition of garnet. The concentration of Cr_2O_3 in garnet associated with bridgmanite reaches 18 wt%.

Study of the starting material corresponding to pure $Mg_3Cr_2Si_3O_{12}$ (Table 3.1) is of key importance from the point of garnet composition and phase relations in the system. It should be emphasized that pure knorringite was not synthesized in a wide pressure range (10–20 GPa). Garnet with the highest chromium content (31 wt% Cr_2O_3) corresponding to ~90 mol% *Knr* was produced at 10 GPa. For this starting composition, increase in pressure results in a decrease of the chromium content in garnet (18 wt% Cr_2O_3, ~50 mol% *Knr* at 20 GPa). At a fixed pressure of 16 GPa, the concentration of the knorringite component in garnet increases with increasing bulk chromium content in the starting material (Table 3.1); however, as it is evident from Fig. 3.12, there is a certain limit for Cr incorporation in garnet, which, in our opinion, provides evidence for impossibility of pure knorringite synthesis.

The composition of $MgSiO_3$ *akimotoite* depends on the starting composition and pressure as well (Table 3.1). Increase in the chromium content in the starting composition results in an increase in the concentration of Cr_2O_3 concentration in akimotoite in the absence of other phases. The portion of akimotoite in association with garnet increases with pressure, and the concentration of chromium in it increases as well. The maximal solubility of chromium in akimotoite (~5.7 wt% Cr_2O_3) was registered in our runs at 18 GPa. There is a negative correlation of Mg and Si with Cr, which indicates decrease in the concentrations of Mg and Si in akimotoite with pressure (Fig. 3.13).

$MgSiO_3$ *bridgmanite* shows a higher solubility of chromium (4–11 wt% Cr_2O_3) than akimotoite. *Brd* associating with high-chromium garnet contains ≤8.5 wt%

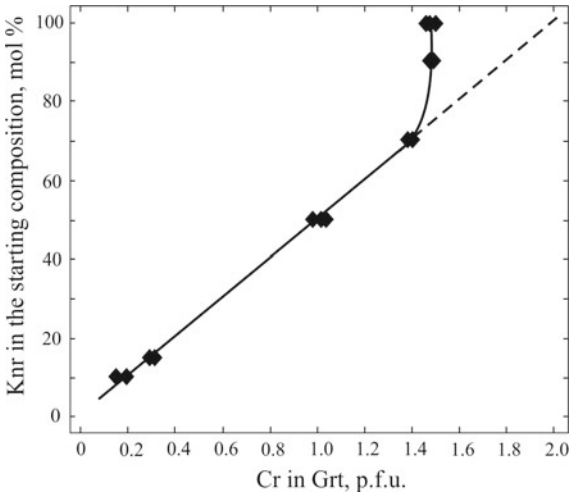

Fig. 3.12 Dependence of the Cr concentration in garnet on the bulk content of the knorringite component (mol%) in the starting material at 16 GPa

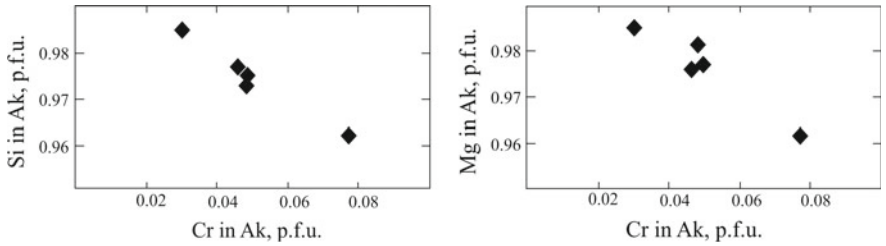

Fig. 3.13 Correlations between the concentrations of Mg, Si, and Cr in $MgSiO_3$ akimotoites synthesized in the system $Mg_4Si_4O_{12}$–$Mg_3Cr_2Si_3O_{12}$ at 18–19 GPa and 1600 °C

Cr_2O_3; upon disappearance of garnet (>21 GPa), the content of chromium in bridgmanite increases significantly.

The phase with the composition $MgCr_2O_4$ and the *calcium titanate-type structure* (*Ct*) associated with garnet and stishovite and synthesized in a pressure range from 18 to 20 GPa is characterized by the presence of silicon (up to 4 wt% SiO_2). Increase in pressure stimulates increase in Si solubility in the *Ct* structure. However, interestingly, at a pressure of >20 GPa, *Ct* in association with bridgmanite exhibits a stoichiometric composition (without Cr admixture).

Eskolaite in the system $Mg_3Cr_2Si_3O_{12}$–$Mg_4Si_4O_{12}$ was detected in association with garnet in a pressure range from 10 to 16 GPa for the knorringite-rich starting compositions. This phase contains significant admixtures of magnesium and silicon increasing with pressure (up to 3 wt% MgO and up to 3.5 wt% SiO_2).

Topology and phase diagram of the pseudobinary section $Mg_4Si_4O_{12}$–$Mg_3Cr_2Si_3O_{12}$. As it was mentioned above, the phase relations in the system $Mg_4Si_4O_{12}$–$Mg_3Cr_2Si_3O_{12}$ may be described within the three-component system SiO_2–MgO–Cr_2O_3 (Fig. 3.14). Garnet forms solid solutions of the majorite–knorringite series, and its stability at 1600 °C is limited by the lowest pressure of ~8 GPa; an association of pyroxene and eskolaite (*En* + *Esk*) is stable below (Zou and Irifune 2012; Sirotkina et al. 2016). The highest content of knorringite in garnets synthesized in our runs does not exceed 90 mol% (Fig. 3.14, point 1 on the line *a*), which is in good agreement with the experimental data (Juhin et al. 2010; Zou and Irifune 2012). Eskolaite is always formed in equilibrium with garnet due to incorporation of the majorite end-member in garnet via the reaction:

$$Mg_3Cr_2Si_3O_{12}(Knr) = 3MgSiO_3(Maj) + Cr_2O_3(Esk) \quad (3.1)$$

Since eskolaite on the SiO_2–MgO–Cr_2O_3 diagram (Fig. 3.14) plots outside the section $Mg_4Si_4O_{12}$–$Mg_3Cr_2Si_3O_{12}$ (line *a*), studied system should be considered as pseudobinary.

The formation of the phase $MgCr_2O_4$ with the calcium titanate ($CaTi_2O_4$)-type structure and stishovite representsadditional evidence for the pseudobinary nature of the studied system. The formation of this association (line *b* in Fig. 3.14) is first registered in the chromium-rich part of the system at a pressure of 18 GPa, according

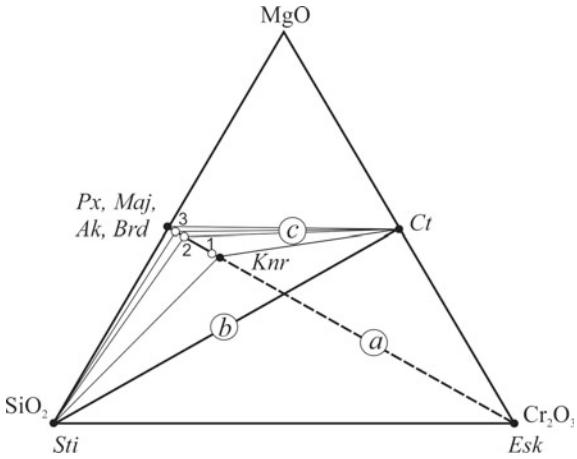

Fig. 3.14 Relative position of the phases and phase associations of the studied system $Mg_4Si_4O_{12}$–$Mg_3Cr_2Si_3O_{12}$ on the triangular diagram SiO_2–MgO–Cr_2O_3 (Sirotkina et al. 2015). (1–3) The maximum concentration of Cr_2O_3 in the phases synthesized in our experiments: (1) garnet, (2) $MgSiO_3$ bridgmanite, and (3) $MgSiO_3$ akimotoite. Letters in circles (*a*–*c*) correspond to the sequence of the chemical reactions with increasing pressure

to the following reactions:

$$Mg_3Cr_2Si_3O_{12}(Knr) + 2Cr_2O_3(Esk) = 3MgCr_2O_4(Ct) + 3SiO_2(Sti); \quad (3.2)$$

$$MgSiO_3(Maj) + Cr_2O_3(Esk) = MgCr_2O_4(Ct) + SiO_2(Sti). \quad (3.3)$$

These reactions with participation of the knorringitic and majoritic components of garnet control the abovementioned total decrease in the portion of garnet in experimental samples with increasing pressure. One more important feature of this reaction is the appearance of stishovite, a mineral that is not typical of the ultrabasic (pyrolytic) association, as an individual phase (Kaminsky 2012).

Complete disappearance of garnet at a pressure of >20 GPa occurs as a result of transformation of the $MgSiO_3$ component of garnet (majorite) into bridgmadite and decomposition of the knorringitic component of garnet via the reaction (compositional triangle *c* in Fig. 3.14):

$$MgSiO_3(Maj) = MgSiO_3(Brd); \quad (3.4)$$

$$Mg_3Cr_2Si_3O_{12}(Knr) = 2MgSiO_3(Brd) + MgCr_2O_4(Ct) + SiO_2(Sti). \quad (3.5)$$

In this association, bridgmanite contains ~30 mol% of the "knorringitic" component (11 wt% Cr_2O_3), whereas the remaining chromium goes into the $MgCr_2O_4$

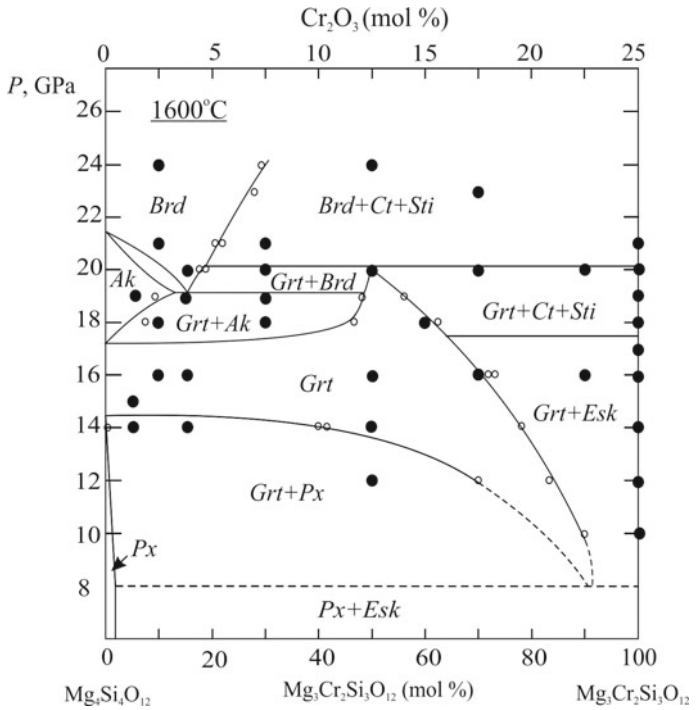

Fig. 3.15 Fragment of the isothermal *P–X* section of the phase diagram SiO_2–MgO–Cr_2O_3 (Fig. 3.14). Small circles show compositions of the phases synthesized in the *Maj–Knr* system (Sirotkina et al. 2015)

phase with the calcium titanate-type structure; as a result, similarly to the previous case, stishovite is formed to maintain the stoichiometry of the system.

Based on the results of the topological analysis and using the data of experiments on study of the phase relations, we plotted the isothermal *P–X* section of the phase diagram SiO_2–MgO–Cr_2O_3 (Fig. 3.15). The considered pseudobinary system $Mg_4Si_4O_{12}$–$Mg_3Cr_2Si_3O_{12}$ represents only a small fragment of the $MgSiO_3$–Cr_2O_3 section preliminarily studied by Zou and Irifune (2012) at pressures up to 16 GPa for the starting composition $Mg_3Cr_2Si_3O_{12}$.

3.3.2 Mg_2SiO_4–$MgCr_2O_4$ Section at 10–24 GPa and 1600 °C

As $(Mg,Fe)_2SiO_4$ polymorphs (olivine/wadsleyite/ringwoodite) are widely abundant in the Earth's mantle, and chrome spinel is a very important chromium-bearing phase of the upper-mantle rocks and often forms inclusions in natural diamonds (Sobolev 1983; Bulanova et al. 1993), we selected the model system Mg_2SiO_4–$MgCr_2O_4$ for multi-anvil experimental study of phase relations and interphase chromium compo-

nent partitioning (Sirotkina et al. 2018). Although the minerals of natural mantle associations are represented by relatively low-chromium silicates or, conversely, high-chromic oxides, the task was to study the full range of starting compositions of this system in order to construct the *P–X* phase diagram and establish the parameters and limits of isomorphism in chromium-bearing phases.

Phase relations. The forsterite–magnesiochromite (*Fo–MChr*) was studied experimentally at a temperature of 1600 °C in a pressure range of 10–24 GPa (with an increment of 1–3 GPa) for the starting compositions with an increment of 10–30 mol% $MgCr_2O_4$, which allowed us to synthesize chromium-bearing mantle phases of various depth levels and wide compositional range. Among the phases obtained in the study of the *Fo–MChr* system are chromium-bearing olivine (*Ol*), wadsleyite (*Wad*) (Price et al. 1983; Akaogi et al. 1989; Katsura and Ito 1989; Yu et al. 2008; Sirotkina et al. 2018), ringwoodite (*Rgw*) (Binns 1970; Akaogi et al. 1989; Yu et al. 2008), bridgmanite (*Brd*) (Tschauner et al. 2014; Bindi et al. 2014b), $Mg_2Cr_2O_5$ with modified ludwigite-type structure (*mLd*) (Ishii et al. 2015), $Mg(Mg,Cr)(Mg,Si)O_4$ phase with modified calcium titanate-type structure (*mCt*) (Bindi et al. 2015), knorringite–majorite garnet (Juhin et al. 2010; Zou and Irifune 2012; Bykova et al. 2014; Sirotkina et al. 2015), $MgCr_2O_4$ with the spinel-(*MChr*) and calcium titanate-type (*Ct*) structures (Bindi et al. 2014c), eskolaite (*Esk*), periclase (*Per*), and anhydrous phase B (*anhB*) (Herzberg and Gasparik 1989; Bindi et al. 2016). The run conditions, phase assemblages, and compositions of the phases produced in experiments in the system Mg_2SiO_4–$MgCr_2O_4$ (forsterite–magnesiochromite) at 10–24 GPa and 1600 °C are reported in Table 3.2.

At a moderate pressure (10 GPa), magnesiochromite ($MgCr_2O_4$) coexists with chromium-bearing olivine in a wide range of starting compositions. The typical texture of the sample is shown in Fig. 3.16a: large olivine crystals and relatively small *MChr* grains occurring either as inclusions in olivine or in interstitials.

$MgCr_2O_4$ magnesiochromite grains are predominantly isometric, subhedral (sometimes euhedral), rarely elongated. The size of olivine crystals ranges from 10 to 100 μm, whereas the length of magnesiochromite crystals reaches 50 μm. With increasing chromium concentration in the starting material, the content of chrome spinel increases in the sample (~27 vol.% in Sample 2632-30, ~85 vol.% in Sample 2632-80).

Increase in pressure in the area of the system enriched in the forsterite component (0–8 mol% *MChr*) results in the formation of the single-phase field of wadsleyite. At a pressure of >12 GPa, an association of knorringite–majorite garnet, $Mg_2Cr_2O_5$ phase with modified ludwigite-type structure, and $(Mg,Cr)_{14}(Si,Cr)_5O_{24}$ anhydrous phase B is formed in a wide compositional range (8–60 mol% *MChr*). Further increase in pressure (>13 GPa) results in the formation of an association of wadsleyite and $Mg(Mg,Cr)(Mg,Si)O_4$ phase with modified calcium titanate-type structure (*mCt*). The texture of the samples is characterized by relatively large (up to 70 μm) euhedral wadsleyite crystals and smaller subhedral *mCt* crystals (Fig. 3.16b).

Increase in the chromium content in the starting material (35–65 mol% $MgCr_2O_4$) results in the formation of garnet in association with the phase $Mg(Mg,Cr)(Mg,Si)O_4$. Preserving the stoichiometry of the system requires the formation of the phase

Table 3.2 Conditions, phase assemblages, and compositions of the phases produced in experiments in the system Mg_2SiO_4–$MgCr_2O_4$ at 10–24 GPa and 1600 °C

Run no. (sample)	*P* (GPa); *T* (°C)	Starting composition	Heating duration (hours)	Run products	Mean composition of the phases				
					Phase	MgO	SiO_2	Cr_2O_3	Total
2632-80	10; 1600	$MChr_{80}Fo_{20}$	4	*Ol* + *MChr*	*Ol*	58.19 (0.85)	40.97 (0.57)	2.5 (0.46)	101.66
					MChr	22.14 (0.69)	1.64 (0.40)	74.27 (0.43)	98.05
2632-30	10; 1600	$MChr_{30}Fo_{70}$	4	*Ol* + *MChr*	*Ol*	55.14 (0.95)	41.2 (0.47)	3.21 (0.57)	99.55
					MChr	21.94 (0.39)	1.85 (0.19)	74.62 (0.70)	98.41
2627-40	12; 1600	$MChr_{40}Fo_{60}$	3.5	*anhB* + *mLd*[a] + *Grt*	*anhB*[b]	62.6	32.1	5.37	100.07
					Grt	29.65 (0.22)	43.59 (0.34)	26.38 (0.37)	99.62
2627-10	12; 1600	$MChr_{10}Fo_{90}$	3.5	*anhB*[a] + *mLd* + *Grt*	*Grt*	29.77 (0.54)	43.91 (0.61)	26.51 (0.33)	100.19
					mLd	33.87 (0.21)	0.45 (0.09)	65.59 (0.58)	99.91
2653-80	13; 1600	$MChr_{80}Fo_{20}$	5	*Grt* + *mLd* + *Esk*	*Grt*	29.89 (0.25)	43.87 (0.57)	25.98 (0.85)	99.74
					mLd	33.31 (0.73)	0.52 (0.03)	65.17 (0.86)	99.00
					Esk	0.41 (0.08)		98.63 (0.18)	99.04
2653-30	13; 1600	$MChr_{30}Fo_{70}$	5	*Wad* + *mCt*	*Wad*	54.28 (0.41)	39.18 (0.96)	6.31 (0.08)	99.77
					mCt	39.62 (0.16)	21.22 (0.17)	39.7 (0.18)	100.54
2646-50	14; 1600	$MChr_{50}Fo_{50}$	4	*mCt* + *mLd* + *Grt*	*Grt*	29.96 (0.35)	44.85 (0.59)	24.91 (0.21)	99.72
					mLd	32.96 (0.13)	0.74 (0.04)	63.68(0.4)	97.38
					mCt	40.16 (0.57)	21.81 (0.54)	38.33 (0.60)	100.30
2646-10	14; 1600	$MChr_{10}Fo_{90}$	4	*Wad* + *mCt*	*Wad*	53.75 (0.46)	39.39 (0.12)	6.1 (0.08)	99.24
					mCt	40.57 (0.61)	22.51 (0.20)	38.69 (0.51)	101.77
2629-80	16; 1600	$MChr_{80}Fo_{20}$	5	*Grt* + *mLd* + *Esk*	*Grt*	29.97 (0.71)	44.74 (0.52)	24.68 (0.83)	99.39

(continued)

Table 3.2 (continued)

Run no. (sample)	*P* (GPa); *T* (°C)	Starting composition	Heating duration (hours)	Run products	Mean composition of the phases				
					Phase	MgO	SiO_2	Cr_2O_3	Total
					mLd	34.28	0.92	65.27	100.47
					Esk	0.77 (0.58)	0.43 (0.87)	98.33 (0.93)	99.54
2629-40	16; 1600	$MChr_{40}Fo_{60}$	5	*Grt* + *mLd* + *mCt*	*Grt*	29.92 (0.92)	44.69 (0.38)	24.72 (0.52)	99.33
					mLd	33.95 (0.25)	0.81 (0.20)	64.25 (0.21)	99.01
					mCt[b]	40.06 (0.39)	22.43(0.18)	37.27(0.27)	99.76
2639-30	18; 1600	$MChr_{30}Fo_{70}$	5	*Wad* + *mCt*	*Wad*	54.86 (0.57)	40.57 (0.64)	4.78 (0.11)	100.21
					mCt	41.25	23.23	35.85	100.33
2639-10	18; 1600	$MChr_{10}Fo_{90}$	5	*Wad* + *mCt*	*Wad*	54.7 (0.88)	39.71 (0.56)	5.29 (0.05)	99.70
					mCt	40.76 (0.49)	22.92 (0.47)	34.94 (0.57)	98.62
2651-80	19; 1600	$MChr_{80}Fo_{20}$	5	*Grt* + *Ct* + *mLd*[a]	*Grt*	30.78 (0.73)	46.17 (0.56)	21.41 (0.61)	98.36
					Ct	22.52 (0.16)	1.82 (0.05)	75.35 (0.53)	99.69
2651-50	19; 1600	$MChr_{50}Fo_{50}$	5	*Wad* + *Grt* + *mLd*	*Wad*	53.29 (0.37)	40.11 (0.54)	7.29 (0.84)	100.69
					Grt	32.81 (0.23)	48.5 (0.30)	19.59 (0.12)	100.90
					mLd	34.87 (0.10)	0.92 (0.05)	65.25 (0.45)	101.04
2645-10	19; 1600	$MChr_{10}Fo_{90}$	4	*Wad* + *Grt* + *mLd*[a]	*Wad*	53.81 (0.11)	38.65 (0.72)	7.36 (0.19)	99.82
					Grt	32.11 (0.17)	47.34(0.61)	20.65 (0.21)	100.10
2635-80	20; 1600	$MChr_{80}Fo_{20}$	4	*Grt* + *Ct* + *mLd*	*Grt*	33.36 (0.34)	49.24 (0.23)	18.29 (0.19)	100.89
					Ct	23.87 (0.23)	2.39 (0.11)	74.71 (0.30)	100.98

(continued)

Table 3.2 (continued)

Run no. (sample)	*P* (GPa); *T* (°C)	Starting composition	Heating duration (hours)	Run products	Mean composition of the phases				
					Phase	MgO	SiO_2	Cr_2O_3	Total
					mLd	34.55 (0.87)	1.23 (0.09)	63.36 (0.56)	98.59
2635-40	20; 1600	$MChr_{40}Fo_{60}$	4	*Rgw + Grt + mLd*	*Rgw*	52.12 (0.85)	35.88 (0.27)	11.87 (0.18)	99.87
					Grt	32.28 (0.85)	47.92 (0.24)	18.41 (0.77)	98.61
					mLd	34.85 (0.46)	1.21 (0.07)	64.12(0.18)	100.18
2634-40	21; 1600	$MChr_{40}Fo_{60}$	5	*Rgw + Brd + mLd*	*Rgw*	50.89	32.98	17.07	100.94
					Brd	39.02 (0.58)	58.33 (0.40)	3.42 (0.42)	100.77
					mLd	34.66 (0.64)	2.04 (0.06)	62.36 (0.59)	99.06
2649-30	21; 1600	$MChr_{30}Fo_{70}$	5	*Rgw + Brd + mLd*[a]	*Rgw*	51.04 (0.26)	33.86 (0.35)	15.26 (0.12)	100.16
					Brd	39.99 (0.68)	59.15 (0.10)	2.82 (0.13)	101.96
2649-10	21; 1600	$MChr_{10}Fo_{90}$	4	*Rgw (with minor Ct)*	*Rgw*	56.35	41.58	2.15	100.08
2647-80	23; 1600	$MChr_{80}Fo_{20}$	4	*Brd + Ct + mLd*	*Brd*	39.33 (0.41)	58.92 (0.55)	3.71 (0.08)	101.96
					Ct	23.87 (0.47)	3.22 (0.10)	72.08 (0.55)	99.77
					mLd	34.69 (0.14)	2.13 (0.08)	62.08 (0.53)	98.90
2647-30	23; 1600	$MChr_{30}Fo_{70}$	4	*Rgw + Brd + mLd*[a]	*Rgw*	49.85 (0.35)	32.89 (0.28)	18.54 (0.5)	101.28
					Brd	38.31 (0.38)	57.14 (0.91)	4.81 (0.12)	100.26
2631-50	24; 1600	$MChr_{50}Fo_{50}$	5	*Brd + Ct + mLd*	*Brd*	37.48 (0.23)	55.63 (0.43)	6.85 (0.83)	99.96
					Ct	29.98 (0.33)	7.9 (0.17)	62.38 (0.16)	100.26

(continued)

Table 3.2 (continued)

Run no. (sample)	*P* (GPa); *T* (°C)	Starting composition	Heating duration (hours)	Run products	Mean composition of the phases				
					Phase	MgO	SiO_2	Cr_2O_3	Total
					mLd	37.86 (0.06)	3.94 (0.01)	55.67 (0.04)	97.47
2631-10	24; 1600	$MChr_{10}Fo_{90}$	5	*Brd* + *Per*	*Brd*	39.49	54.08	6.77	100.34
					Per	71.99 (0.60)	3.77 (0.30)	22.37 (0.12)	98.13

[a]Because of the small grain sizes, compositions of the phases were not analyzed
[b]Crystals studied by X-ray diffraction (see Chap. 4)

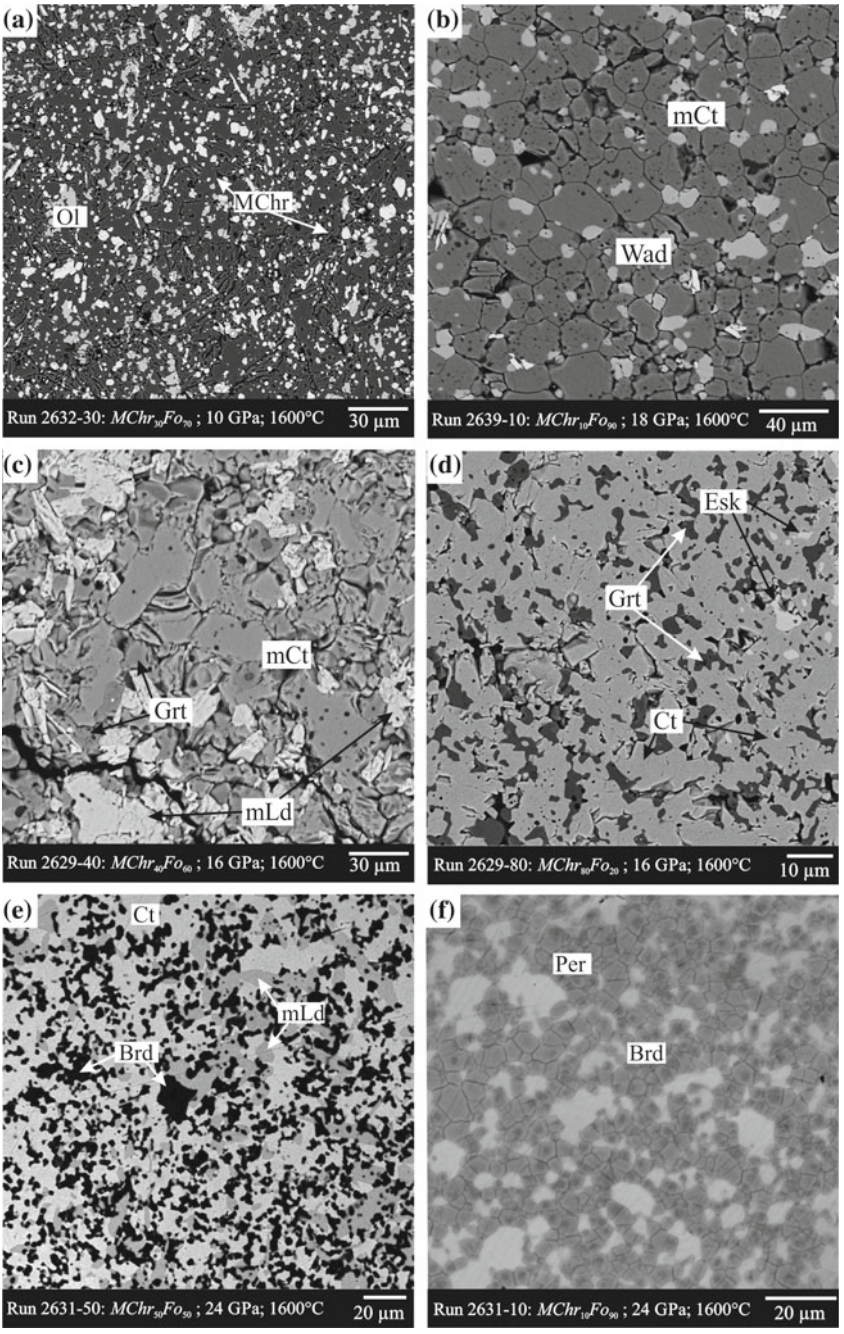
(a)
Ol
MChr
Run 2632-30: $MChr_{30}Fo_{70}$; 10 GPa; 1600°C
30 µm
(b)
mCt
Wad
Run 2639-10: $MChr_{10}Fo_{90}$; 18 GPa; 1600°C
40 µm
(c)
mCt
Grt
mLd
Run 2629-40: $MChr_{40}Fo_{60}$; 16 GPa; 1600°C
30 µm
(d)
Esk
Grt
Ct
Run 2629-80: $MChr_{80}Fo_{20}$; 16 GPa; 1600°C
10 µm
(e)
Ct
mLd
Brd
Run 2631-50: $MChr_{50}Fo_{50}$; 24 GPa; 1600°C
20 µm
(f)
Per
Brd
Run 2631-10: $MChr_{10}Fo_{90}$; 24 GPa; 1600°C
20 µm

◀**Fig. 3.16** BSE images of textural relationships and phase associations in run products in the section Mg_2SiO_4–$MgCr_2O_4$ at 10–24 GPa and 1600 °C: **a** aggregate of olivine and small grains of magnesiochromite in the experimental sample; **b** association of wadsleyite and *mCt*; **c** small *mCt* crystals with small prismatic crystals of $Mg_2Cr_2O_5$ phase with modified ludwigite-type structure (*mLd*) and small isometric garnet grains; **d** association of garnet, wadsleyite, and *mLd*; **e** aggregate of $MgSiO_3$ bridgmanite, $MgCr_2O_4$ with the calcium titanate-type structure, and *mLd*; (f) aggregate of bridgmanite with the typical dense system of small fractures and periclase in the experimental sample

$Mg_2Cr_2O_5$ with modified ludwigite-type structure (*mLd*) in association with garnet. The texture of the samples obtained is formed by predominant relatively large (up to 60 μm) crystals with small (up to 20 μm) prismatic crystals of *mLd*, as well as relatively small (<15 μm) isometric garnet crystals filling interstitials (Fig. 3.16c). With further increase in the chromium content in the starting composition, an association of *mLd* + *Grt* + *Esk* is formed.

An association of *mLd* + *Esk* is formed in the chromium-rich part of the system (>92 mol% *MChr*) in the pressure range of 12–18 GPa; its stability field slightly expands with pressure. Increase in pressure (>18 GPa) results in the formation of the single-phase field of $MgCr_2O_4$ with the calcium titanate-type structure (*Ct*). It is shown that with increasing pressure, the field of *Ct* expands to the area of the higher forsterite content in the system due to increase in silicon solubility in $MgCr_2O_4$.

Two garnet-bearing associations are formed at a pressure of >18 GPa. In total, they cover almost complete range of the starting compositions (10–90 mol% *MChr*): *Grt* + *Wad* + *mLd* (Fig. 3.16d) and *Grt* + *Ct* + *mLd*. The first of them was detected only in two samples (2651-50 and 2645-10) at 19 GPa; at 20 GPa wadsleyite is replaced with ringwoodite in this association. In the forsterite-rich part of the system, the single-phase field of Mg_2SiO_4 ringwoodite replacing Cr-*Wad* is formed at ≥21 GPa. Ringwoodite composes massive aggregates with a grain size up to 50 μm.

At ~21 GPa, the garnet-bearing associations (*Grt* + *Rgw* + *mLd* and *Grt* + *Ct* + *mLd*) are replaced with the parageneses of $MgSiO_3$ bridgmanite (*Brd* + *Rgw* + *mLd* and *Brd* + *Ct* + *mLd*) in a wide range of starting compositions (15–85 mol% *MChr*). In these assemblages, bridgmanite composes small, intensely fractured, euhedral crystals with a size up to 20 μm. The phases *mLd* and *Ct* are represented by relatively large segregations with a size up to 50 μm (Fig. 3.16e). Further increase in pressure results in decomposition of ringwoodite with the formation of the association of bridgmanite and periclase in the forsterite-rich part of the system. This association was detected in one run (2631-10) performed at 24 GPa. The forsterite-rich part of the system *Fo–MChr* (0–20 mol% *MChr*), does not contain any other phases, except for *Brd* and *Per* (Fig. 3.16f), whereas the starting compositions with the moderate chromium contents (20–45 mol% *MChr*) demonstrate the presence of the more chromium-rich phase $Mg_2Cr_2O_5$ in association with $MgSiO_3$ bridgmanite and periclase.

Composition of the phases. The phases synthesized in the system Mg_2SiO_4–$MgCr_2O_4$ at 10–24 GPa and 1600 °C are characterized by the wide compositional ranges (Table 3.2).

All phases with the composition Mg_2SiO_4 obtained in the *Fo–MChr* system contain chromium and show the negative correlation of Cr with Mg and Si concentrations (Fig. 3.17). The concentration of Cr_2O_3 in *olivine* (forsterite) synthesized at 10 GPa reaches 3.2 wt%. At ~12 GPa and quite high content of $MgCr_2O_4$ in the starting material (~40 mol%) olivine transforms to the denser phase, *wadsleyite*. Increase in pressure stimulates increase in the concentration of chromium in wadsleyite (Fig. 3.18). The composition of wadsleyite practically does not change with the evolution of the phase assemblages. The highest content of $MgCr_2O_4$ in wadsleyite reaches 7.3 mol% (~7.6 wt% Cr_2O_3) at a pressure of 19 GPa.

The composition of Mg_2SiO_4 *ringwoodite* is significantly controlled by pressure. With increasing pressure, the concentration of chromium in ringwoodite increases (Fig. 3.18). Thus, the maximal solubility of chromium was registered for ringwoodite in the *Fo–MChr* system (~18.5 wt% Cr_2O_3) at a pressure of 23 GPa, which is close to the upper boundary of the stability of this phase.

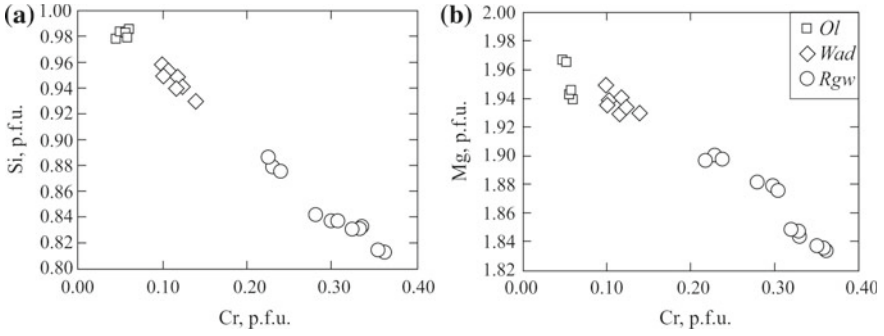

Fig. 3.17 Variations in the concentrations of Si, Mg, and Cr in chromium-bearing Mg_2SiO_4 polymorphs synthesized in the system Mg_2SiO_4–$MgCr_2O_4$ at 10–23 GPa and 1600 °C

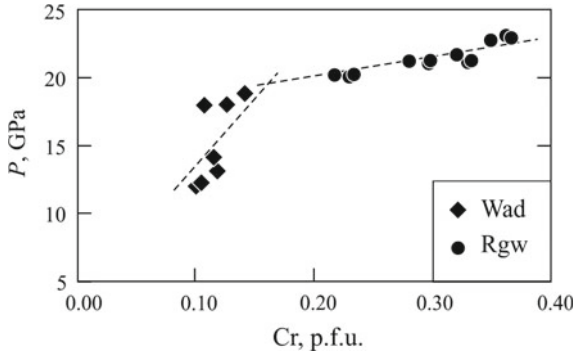

Fig. 3.18 Dependence on the concentration of Cr in wadsleyite and ringwoodite on pressure

Chromite ($MgCr_2O_4$) associated with olivine contains a small silicon impurity (<1.85 wt% SiO_2, which corresponds to 6 mol% *Fo*).

$Mg(Mg,Si,Cr)_2O_4$ *with modified (distorted) calcium titanate-type structure* (*mCt*) is stable at pressures of 12–18 GPa in association with wadsleyite. In all experimental samples, this phase is characterized by significant incorporation of silicon (58–63 mol% *Fo*) and shows slight compositional variations. There is the negative correlation of Cr with Mg and Si, which indicates substitution of Cr with Si and Mg in the octahedral sites (Fig. 3.19). With increasing pressure, the phase $Mg(Mg,Si,Cr)_2O_4$ becomes depleted in chromium, whereas the concentration of silicon in the octahedral site regularly increases.

The phase $MgCr_2O_4$ with the calcium titanate-type structure (*Ct*) synthesized at a pressure of >18 GPa in the chromium-rich part of the system is characterized by a relatively wide compositional range. This phase contains significant admixture of Si in the composition of Mg_2SiO_4. Excessive Mg and Si substitute Cr in the octahedral sites of *Ct*. Within the pressure range of 18–21 GPa, the concentration of SiO_2 in $MgCr_2O_4$ *Ct* associating with garnet and $Mg_2Cr_2O_5$ with modified ludwigite-type structure does not exceed 2.5 wt%. At a pressure of >21 GPa, the concentration of SiO_2 increases significantly up to 8 wt%, which corresponds to 23 mol% *Fo*. Such high concentrations of SiO_2 are typical of $MgCr_2O_4$ with the calcium titanate-type structure (*Ct*) synthesized at a maximal pressure of 24 GPa. Thus, increase in pressure in the *Fo–MChr* system stimulates increase in solubility of the forsterite component in $MgCr_2O_4$.

Comparing peculiarities of the phases with the calcium titanate-type structures in the *Fo–MChr* and *Maj–Knr* systems, we should note that the concentrations of SiO_2 in $MgCr_2O_4$ *Ct* synthesized in the *Maj–Knr* system are much lower. The dependence of the silicon content on pressure is very unclear and is violated by the complete absence of SiO_2 in *Ct* synthesized at 24 GPa (Sample 2413-70). In addition, *mCt*, the phase with the very high silicon content resulting in distortion of the structure in relation to that of *Ct* was not detected in the *Maj–Knr* system.

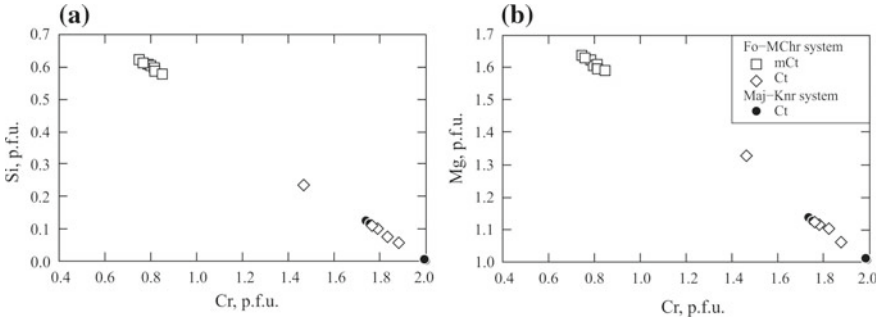

Fig. 3.19 Variations in the concentrations of Si, Mg, and Cr in the phases with the calcium titanate-type structure (*Ct* and *mCt*) synthesized in the Mg_2SiO_4–$MgCr_2O_4$ system (Sirotkina et al. 2018) in comparison with the data on the $Mg_4Si_4O_{12}$–$Mg_3Cr_2Si_3O_{12}$ system (Sirotkina et al. 2015)

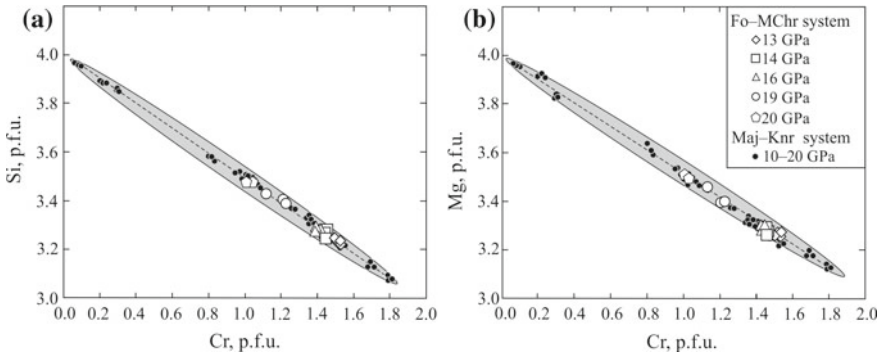

Fig. 3.20 Variations in the concentrations of Si, Mg, and Cr in garnets synthesized in the system Mg_2SiO_4–$MgCr_2O_4$ at pressures of 13–20 GPa and a temperature of 1600 °C, in comparison with the data on the system $Mg_4Si_4O_{12}$–$Mg_3Cr_2Si_3O_{12}$ (Sirotkina et al. 2015). The trend of the evolution of garnet composition is shown by the dashed line

Garnets in the run products show a relatively narrow compositional range and are characterized by an excessive silicon content (>3 Si p.f.u.); the content of the majoritic component does not exceed 50 mol% (Fig. 3.20). With increasing pressure, the concentration of chromium in garnet decreases, whereas the concentration of silicon in the octahedral site regularly increases, which is in a good agreement with the data on the composition of garnets synthesized in the *Maj–Knr* system (Sirotkina et al. 2015). The highest content of the knorringite end-member in garnet, 75 mol% (26 wt% Cr_2O_3), was registered at a pressure of 13 GPa; at 20 GPa, the content of knorringite decreases to 50 mol%, which is consistent with the data obtained for garnets in the *Knr–Maj* system (Fig. 3.11). However, garnets synthesized in the *Knr–Maj* system are characterized by the higher chromium concentrations (90 mol% *Knr*, 30.78 wt% Cr_2O_3) at a pressure of 10 GPa. Such high contents of knorringite are not typical of garnets produced in the *Fo–MChr* system due to impossibility of garnet synthesis at a pressure below ~12 GPa, because of the stability of the phase association *Ol* + *MChr* under these conditions.

The phase $Mg_2Cr_2O_5$ *with modified ludwigite-type structure* (*mLd*) was detected in a wide range of pressures and starting compositions. At relatively low pressures (13–16 GPa), *mLd* is characterized by the small concentration of Si, deficiency in Mg, excess of Cr. This fact is explained by substitution of Mg with Cr and Mg in the ludwigite-type structure. With increasing pressure, the concentrations of Si and Mg in garnet increase against the background of decrease in the solubility of Cr (Fig. 3.21). The maximal concentration of SiO_2 in *mLd* obtained in the *Fo–MChr* system reaches 2.8 wt% (~0.12 Si p.f.u.).

The composition of $MgSiO_3$ *bridgmanite* changes insignificantly (2.8–6.7 wt% Cr_2O_3) and depends on pressure as well. The lowest concentrations of chromium were registered in bridgmanite associated with ringwoodite at a pressure of 21 GPa. The maximal solubility of Cr_2O_3 (~6.7 wt%) was registered in bridgmanite synthesized in the system *Fo–MChr* at a pressure of 24 GPa.

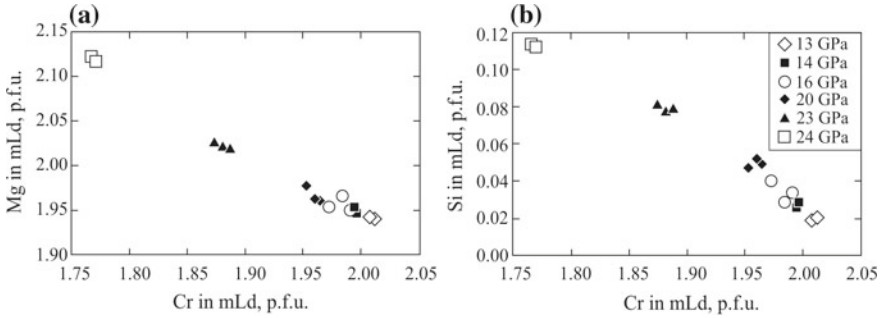

Fig. 3.21 Compositional variations of Si, Mg, and Cr in *mLd* synthesized in the system Mg_2SiO_4–$MgCr_2O_4$ at pressures of 13–24 GPa and a temperature of 1600 °C

Periclase was detected in the system *Fo–MChr* in association with bridgmanite in the range of starting compositions of 0–50 mol% *MChr* at a pressure of >23 GPa. Periclase is characterized by significant concentrations of silicon (~3.8 wt% SiO_2) and chromium (22.4 wt% Cr_2O_3). The latter fact emphasizes the need to consider periclase as one of the potential chromium concentrators in the Earth's lower mantle.

Topology and phase diagram of the pseudobinary section Mg_2SiO_4–$MgCr_2O_4$. The phase relations in the section Mg_2SiO_4–$MgCr_2O_4$ may be considered in terms of the ternary system SiO_2–MgO–Cr_2O_3 (Fig. 3.22).

The stability of the *Ol* + *MChr* association is limited to a pressure of ~12 GPa, above which the formation of the association of wadsleyite and the phase $Mg(Mg,Cr)(Mg,Si)O_4$ with modified calcium titanate-type structure is registered.

An association of knorringite–majorite garnet, $Mg_2Cr_2O_5$ phase with modified ludwigite-type structure, and $(Mg,Cr)_{14}(Si,Cr)_5O_{24}$ anhydrous phase B (*Anh B*) is formed at a pressure of >12 GPa in a wide range of starting compositions (8–65 mol% $MgCr_2O_4$) via the following reactions (*a* and *b* in Fig. 3.22):

$$\begin{aligned} &Mg_2SiO_4(Ol/Wad/mCt) + MgCr_2O_4(Sp/mCt) \\ &\quad = Mg_{14}Si_5O_{24}(Anh\ B) + Mg_3Cr_2Si_3O_{12}(Knr); \end{aligned} \tag{3.6}$$

$$\begin{aligned} &5MgCr_2O_4(MChr/mCt) + 3Mg_2SiO_4(Ol/Wad/mCt) \\ &\quad = Mg_3Cr_2Si_3O_{12}(Knr) + 4Mg_2Cr_2O_5(mLd); \end{aligned} \tag{3.7}$$

$$\begin{aligned} &MgCr_2O_4(MChr/mCt) + Mg_2SiO_4(Ol/Wad/mCt) \\ &\quad = MgSiO_3(Maj) + Mg_2Cr_2O_5(mLd). \end{aligned} \tag{3.8}$$

Since the compositions of knorringite–majorite garnet, ludwigite, and anhydrous phase B plot outside the Mg_2SiO_4–$MgCr_2O_4$ section corresponding to the studied system on the SiO_2–MgO–Cr_2O_3 diagram, this system should be considered as pseudobinary.

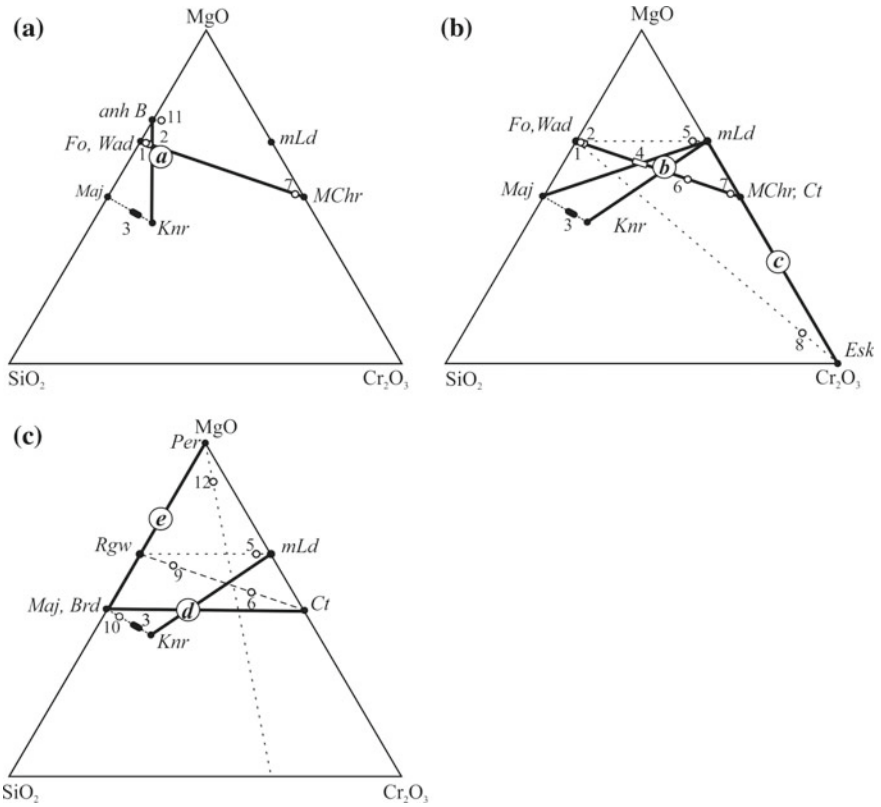

Fig. 3.22 Relative position of the phases and phase associations in the system Mg_2SiO_4–$MgCr_2O_4$ on the triangular diagram SiO_2–MgO–Cr_2O_3. Numerals (1–4, 9–11) characterize the concentration limits of $MgCr_2O_4$/Cr_2O_3 registered in our runs for olivine (1), wadsleyite (2), knorringite–majorite garnet (3), *mCt* (4), ringwoodite (9), bridgmanite (10), and anhydrous phase B; numerals (5–8) characterize the concentration limits of the forsterite component registered in our runs for *mLd* (5), *Ct* (6), magnesiochromite (7), and eskolaite (8). Letters in circles (*a*–*e*) show the sequence of chemical reactions with increasing pressure and decreasing chromium concentration in the starting composition

The formation of an association of wadsleyite and $Mg(Si,Mg)(Cr,Mg)O_4$ phase with modified calcium titanate-type structure proceeds via the same reactions at a pressure of >13 GPa.

In the chromium-rich part of the system (>93 mol% $MgCr_2O_4$), $MgCr_2O_4$ with the spinel-type structure decomposes to form an association *mLd* + *Esk* by the reaction (line *c* in Fig. 3.22):

$$2MgCr_2O_4(Sp) = Mg_2Cr_2O_5(mLd) + Cr_2O_3(Esk). \quad (3.9)$$

Appearance of an eskolaite–ludwigite assemblage provides additional evidence for the pseudobinary character of the Mg_2SiO_4–$MgCr_2O_4$ section.

Crystallization of the $MgCr_2O_4$ phase with the calcium titanate-type structure (*Ct*) in association with knorringite–majorite garnet (*Ct* + *Grt* + *mLd*) or chromium-bearing bridgmanite (*Ct* + *Brd* + *mLd*) proceeds at a pressure of >18 GPa. As it is evident from our runs, the stability field of $MgCr_2O_4$ *Ct* expands with pressure to the area of the lower chromium concentrations.

The pseudobinary character of the section is also evident from appearance of the knorringite–majorite garnet (Fig. 3.22, Sect. 3.3) in the following phase associations: *Rgw/Wad* + *Grt* + *mLd*, *Grt* + *mLd* + *Esk*, and *Grt* + *mLd* + *mCt/Ct*.

The narrow range of garnet composition is controlled by the relative position of connodes and is highly dependent on pressure. In this situation, it is very important that the compositions of *mCt* occur on intersection of the connodes *Ol/Wad–MChr* connodes (with a slight shift of the compositional range towards *MChr*) and *Maj–mLd*. Based on the defined phase relations, the portion of the majorite component in garnet coexisting with *mCt* cannot exceed 50 mol%. In contrast to the *Maj–Knr* system, further increase in the content of the majorite end-member in garnet will be hindered by the reaction of this mineral with $Mg_2Cr_2O_5$ (*mLd*) with the formation of $Mg(Mg,Si,Cr)_2O_4$ (*mCt*).

Complete disappearance of garnet at a pressure of >21 GPa proceeds via the reaction of interaction of the knorringite component of garnet with the $Mg_2Cr_2O_5$ phase and the reaction of transition of the $MgSiO_3$ component of garnet (majorite) into bridgmanite (Fig. 3.22, *d*):

$$\begin{aligned} &Mg_3Cr_2Si_3O_{12}(Knr) + Mg_2Cr_2O_5(mLd) \\ &\quad = 2MgCr_2O_4(Rgw/Ct) + 3MgSiO_3(Brd); \end{aligned} \tag{3.10}$$

$$MgSiO_3(Maj) = MgSiO_3(Brd). \tag{3.11}$$

The formation of periclase in association with bridgmanite results from decomposition of ringwoodite at a pressure of >23 GPa in the silicon-rich part of the system via the reaction (Fig. 3.22, line *e*):

$$Mg_2SiO_4(Rgw) = MgSiO_3(Brd) + MgO(Per). \tag{3.12}$$

Based on the results of topological analysis and using the data of experiments on the study of phase relations considered above, the *P–X* phase diagram of the pseudobinary system Mg_2SiO_4–$MgCr_2O_4$ was plotted (Fig. 3.23); this diagram represents an isothermal section of the phase diagrams SiO_2–MgO–Cr_2O_3 (Fig. 3.22).

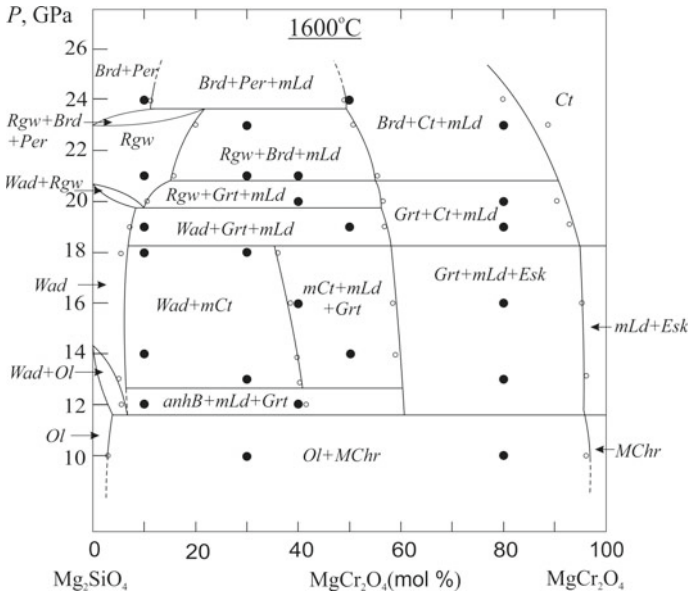

Fig. 3.23 *P–X* phase diagram of the pseudobinary system Mg_2SiO_4–$MgCr_2O_4$ at 1600 °C (Sirotkina et al. 2018). The pressures of the phase transformations in Mg_2SiO_4 (forsterite/wadsleyite at 14.8 GPa and wadsleyite/ringwoodite at 20.2 GPa) are given after (Akaogi et al. 1989). Small circles denote the compositions of the phases synthesized in the *Fo–MChr* system

3.3.3 $Mg_4Si_4O_{12}$–$MgCr_2O_4$ Section at 10–24 GPa and 1600 °C and General Topology of the SiO_2–MgO–Cr_2O_3 System Under the Mantle P–T Parameters

Phase relations and composition of the phases. Among the phases obtained in experiments on the $Mg_4Si_4O_{12}$–$MgCr_2O_4$ section there are: garnet (*Grt*) of the knorringite–majorite composition, anhydrous phase B (*anhB*), $Mg_2Cr_2O_5$ with modified ludwigite-type structure (*mLd*), Mg(Mg,Cr)(Mg,Si)O_4 phase with modified calcium titanate-type structure (*mCt*), bridgmanite (*Brd*), $MgCr_2O_4$ with the calcium titanate-type structure (*Ct*), and stishovite (*Sti*). Conditions of runs in the SiO_2–MgO–Cr_2O_3 system, phase assemblages and their compositions are reported in Table 3.3.

At 12 GPa, chromium-bearing majoritic garnet associates with anhydrous phase B and the phase with modified ludwigite-type structure. The texture of the samples is characterized by relatively large isometric crystals of garnet and phase B with sizes up to 50 μm and small, regularly distributed, often interstitial, segregations of *mLd*. The size of such segregations does not exceed 10 μm.

At the same starting composition, increase in pressure up to 16 GPa results in the formation of an association of knorringite–majorite garnet, *mLd*, and *mCt*. The texture of these samples shows a predomination of relatively large *mCt* crystals with

Table 3.3 Conditions, phase assemblages, and compositions of the phases produced in experiments in the section $Mg_4Si_4O_{12}$–$MgCr_2O_4$ at 10–24 GPa and 1600 °C

Run no. (sample)	*P* (GPa); *T* (°C)	Starting composition	Run products	Mean composition of the phases				
				Phase	MgO	SiO_2	Cr_2O_3	Total
2112-25	12; 1600	$Maj_{43}MChr_{57}$	*Grt* + *AnhB* + *mLd*	*Grt*	28.29 (0.72)	42.19 (1.12)	27.53 (0.92)	98.01
				AnhB	62.49	31.92	4.11	98.52
				mLd	34.04 (0.51)	0.49 (0.02)	64.38 (0.55)	98.91
2119-25	16; 1600	$Maj_{43}MChr_{57}$	*Grt* + *mCt* + *mLd*[a]	*Grt*	29.54 (0.13)	45.34 (0.36)	24.9 (0.87)	99.78
				mCt	36.48 (0.75)	19.43 (0.40)	41.47 (0.21)	97.38
3167-50	24; 1600	$Maj_{20}MChr_{80}$	*Ct* + *Brd* + *Sti*	*Ct*	26.01 (1.31)	4.84 (0.51)	69.75 (1.08)	100.6
				Brd	39.05 (0.84)	57.43 (0.92)	5.47 (0.89)	101.95
				Sti	0.02 (0)	98.13 (0.02)	1.04 (0.43)	99.19

[a]Because of the small grain size, composition of the phase was not analyzed

a size up to 60 μm; interstices between them are filled with small prismatic crystals of *mLd* with a size up to 10 μm and relatively small (<10 μm) isometric garnet grains (Fig. 3.24a).

At a pressure of 24 GPa, garnet-bearing associations are replaced with bridgmanite assemblages. Characteristically, chromium-bearing bridgmanite and $MgCr_2O_4$ phase associate with stishovite. The latter forms small anhedral grains with sizes up to 10 μm. $MgCr_2O_4$ in this association is represented by relatively large segregations with a size up to 50 μm (Fig. 3.24b).

General topology of the SiO_2–MgO–Cr_2O_3 model system. It may be derived using the results of experiments in the majorite–magnesiochromite section, as well as in the previously studied petrologically significant sections majorite–knorringite (Sirotkina et al. 2015) and forsterite–magnesiochromite (Sirotkina et al. 2018). The phase associations in the SiO_2–MgO–Cr_2O_3 system at different pressures, which account for the compositions of the different phases, are shown in Fig. 3.25.

At 12 GPa (Fig. 3.25a), most of the diagram is occupied by garnet of the knorringite–majorite composition associated with other high-pressure phases. The concentration of the knorringitic component in garnet ranges within 70–85 mol%, which is controlled by pressure and concentration of chromium in the bulk composition (Sirotkina et al. 2015). In the chromium-poor area of the diagram, garnet associates with pyroxene with the low chromium content. Increase in the magnesium concentration in the system results in the formation of chromium-bearing olivine and wadsleyite, as well as anhydrous phase B. The field of wadsleyite stability is relatively narrow, whereas significant part of the diagram is occupied by anhydrous phase B associated with garnet, *mLd*, and periclase.

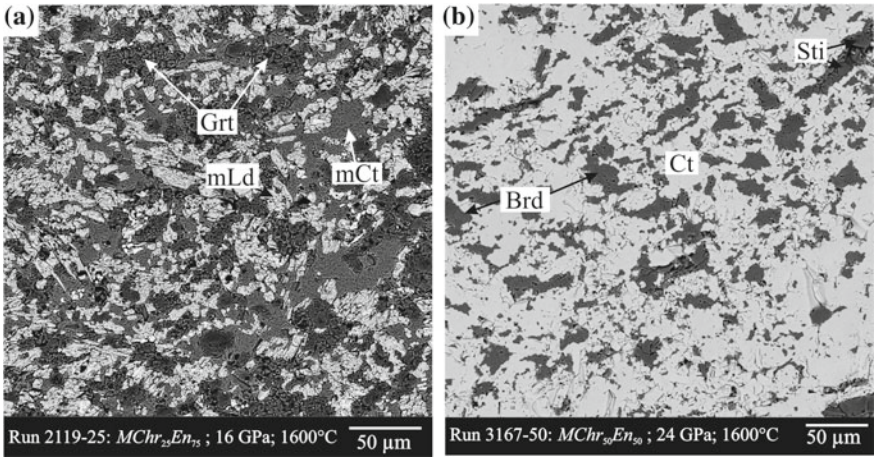

Fig. 3.24 BSE images of textural relationships and phase associations in run products in the section $Mg_4Si_4O_{12}$–$MgCr_2O_4$ at 10–24 GPa and 1600 °C: **a** large *mCt* crystals in the matrix composed of small prismatic crystals of $Mg_2Cr_2O_5$ (*mLd*) and isometric garnet grains; **b** aggregate of $MgSiO_3$ bridgmanite, $MgCr_2O_4$ (*Ct*), and stishovite

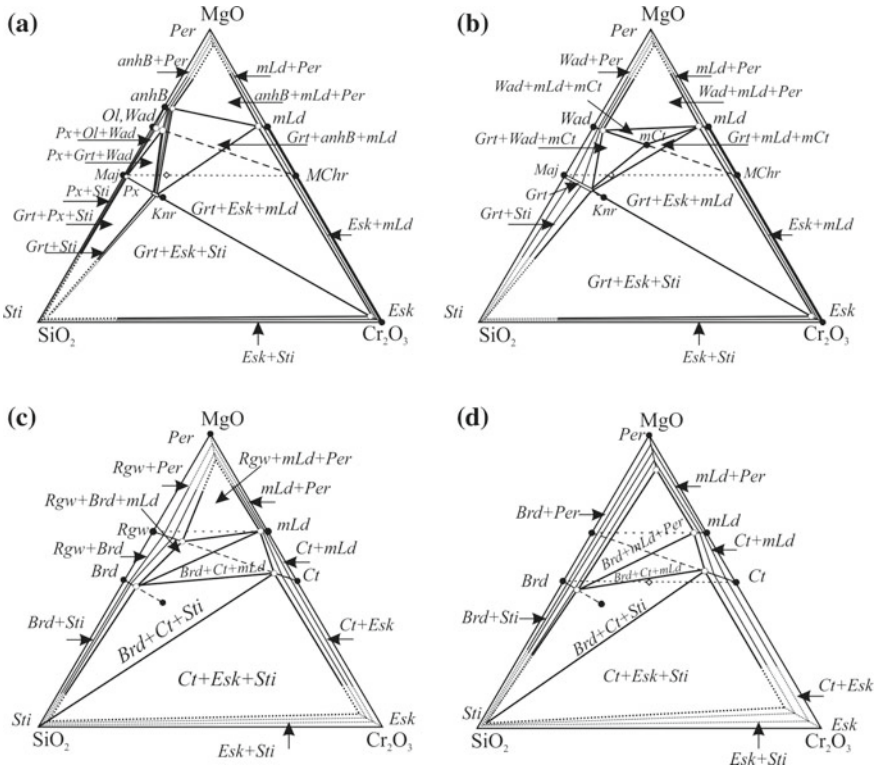

Fig. 3.25 General topology of the SiO_2–MgO–Cr_2O_3 model system and relative position of the phases at different pressures (Matrosova et al. 2018): **a** 12 GPa; **b** 16 GPa; **c** 22 GPa; **d** 24 GPa

Increase in pressure up to 16 GPa (Fig. 3.25b), corresponding to the uppermost part of the transition zone, results in the formation of the $Mg(Mg,Cr)(Mg,Si)O_4$ phase with modified calcium titanate-type structure (*mCt*) as a result of interaction between anhydrous phase B, components of garnet, and *mLd*:

$$Mg_{14}Si_5O_{24}(anhB) + 2Mg_3Cr_2Si_3O_{12}(Knr) + 4Mg_2Cr_2O_5(mLd) = 6MgCr_2O_4\,(mCt) + 11Mg_2SiO_4\,(mCt); \quad (3.13)$$

$$Mg_{14}Si_5O_{24}(anhB) + 2Mg_4Si_4O_{12}(Maj) + 4Mg_2Cr_2O_5(mLd) = 4MgCr_2O_4\,(mCt) + 13Mg_2SiO_4\,(mCt). \quad (3.14)$$

The phase diagram obtained may be divided into two fields corresponding to the stability of garnet and wadsleyite, which represent two most abundant phases in rocks of the uppermost transition zone of the Earth's mantle. The field of garnet stability is located in the Cr-richest part of the system. The composition of garnet varies from almost pure majorite to ~70 mol% of knorringitic component (Sirotkina et al. 2015),

which is evident from the phase diagram (Fig. 3.25b). Increase in the Mg content in the system promotes the formation of chromium-bearing wadsleyite.

Increase in pressure up to 22 GPa (Fig. 3.25c) allows us to simulate the phase associations typical of the lowermost transition zone of the Earth's mantle. This area is characterized by wide abundance of ringwoodite among the mantle phases, whereas the majoritic and knorringitic end-members of garnet become unstable. Because of this, the fields on the phase diagram (Fig. 3.25c) include parageneses with ringwoodite and bridgmanite due to the phase transitions *Wad* = *Rgw, Maj* = *Brd* and reaction of decomposition of the knorringitic component of garnet (Sirotkina et al. 2015). Ringwoodite is the major chromium-bearing phase in the part of the diagram depleted in chromium. The solubility of chromium in ringwoodite at 22 GPa is significantly higher than the maximal content of chromium in bridgmanite (Fig. 3.25c). We should note that the post-spinel $MgCr_2O_4$ phase with the calcium titanate-type structure is stable at pressures corresponding to the lowermost part of the transition zone. This phase occupies significant part of the diagram enriched in chromium.

Slight increase in pressure (by 2 GPa) results in significant changes of phase associations. A pressure of 24 GPa corresponds to the uppermost part of the lower mantle. The diagram of phase relations (Fig. 3.25d) shows the reaction of ringwoodite decomposition with the formation of bridgmanite and periclase that is typical of the boundary between the transition zone and lower mantle. Significant part of the phase diagram is occupied by bridgmanite, which is in accordance with the widest abundance of this compound among the lower-mantle phases. The chromium-rich part of the diagram is characterized by stability of the $MgCr_2O_4$ post-spinel phase with the calcium titanate-type structure.

3.4 Experimental Study of Multicomponent Systems with Cr-Bearing Phases at High P–T Parameters

3.4.1 Influence of Minor Al Concentrations on Crystallization of Garnet in the Majorite-Knorringite System

As it was shown by Zou and Irifune (2012) and Sirotkina et al. (2015), garnet is not formed in the SiO_2–MgO–Cr_2O_3 Al-free model system at $P < 8$ GPa. At the same time, analysis of some experimental data (Klemme 2004; Turkin and Sobolev 2009) shows that addition of aluminum to the starting compositions of this model system will result in crystallization of garnet of the majorite–knorringite–pyrope composition. Unfortunately, the experimental studies available do not report details on the Cr-rich part of the pyrope–knorringite system. To simulate crystallization of garnet with the low aluminum content and to understand the correlation between its composition, temperature, and bulk composition of the system, we performed a series

of experiments in the SiO_2–MgO–Cr_2O_3 system with addition of 5, 10, and 20 mol% of the pyrope component ($Mg_3Al_2Si_3O_{12}$) to the starting composition $Knr_{50}Maj_{50}$.

Experiments were performed at the Vernadsky Institute of Geochemistry and Analytical Chemistry (Moscow, Russia) on a toroidal "anvil-with-hole" apparatus at a pressure of 7 GPa and temperatures of 1500, 1600, and 1700 °C. The starting compositions included the following mixtures (mol%): Knr_{100}, $Prp_5Maj_{47.5}Knr_{47.5}$, $Prp_{10}Maj_{45}Knr_{45}$, and $Prp_{20}Maj_{40}Knr_{40}$ (Table 3.4).

The phase associations for the starting composition corresponding to pure knorringite contain chromium-bearing enstatite and eskolaite. Figure 3.26a shows a typical texture of the samples: relatively large (up to 100 μm) enstatite crystals and small (up to 10 μm) subhedral eskolaite segregations.

The phase associations for the aluminum-bearing starting compositions in all runs include garnet, enstatite, and eskolaite. The typical textures of the samples (Fig. 3.26b–d) are formed by small (up to 20 μm) prismatic crystals of enstatite, relatively large (up to 50 μm) isometric garnet crystals, and the smallest, often interstitial, eskolaite segregations (up to 10 μm).

The main feature of *pyroxenes* synthesized from the pure $Mg_3Cr_2Si_3O_{12}$ starting composition is the chromium admixture (Table 3.4), which increases to 3.2 wt% Cr_2O_3 with increasing temperature. In addition, all pyroxenes are characterized by a slight deficiency in Mg (relatively to 1 p.f.u.), which increases with increasing chromium content, whereas the concentration of Si in the formula (close to 1 p.f.u.) calculated for three oxygen atoms hardly depends on the chromium content. In all pyroxenes, Si > Mg, and this is controlled by Cr incorporation in the structure. The scheme of heterovalent isomorphism like $Mg^{2+} + Si^{4+} \rightarrow 2Cr^{3+}$, in which chromium enters the octahedral site, substituting Mg, as well as the tetrahedral site, substituting Si, by analogy with the ortho-corundum ($AlAlO_3$) component of pyroxene (Berman and Aranovich 1996), is unlikely. We suggest the following mechanism of substitution for chromium-bearing pyroxene: $1/2Mg^{M2} + Mg^{M1} = 1/2vac^{M2} + Cr^{M1}$ (eskolaite substitution) providing evidence for the presence of the $Mg_{0.5}CrSi_2O_6$ end member, similar to the Eskola molecule. According to this mechanism, the structural formula of the phase is the following: $Mg_xCr_{(1-x)}vac_{(1-x)/4}Mg_{(3+x)/4}SiO_3$. Chromium in the structure of this mineral substitutes for magnesium in the octahedra, whereas a vacancy appears on the place of magnesium in the 6- to 8-fold site.

Pyroxenes synthesized in the Al-bearing system are characterized by high concentrations of chromium (up to 2.9 wt% Cr_2O_3), whereas the concentration of Al_2O_3 does not exceed 1 wt%. The concentration of chromium in pyroxene increases with temperature, which is consistent with the results of experiments in the aluminum-free system.

The composition of *garnets* obtained in the MgO–Cr_2O_3–SiO_2 (±Al_2O_3) system at 7 GPa (Table 3.4) depends on the temperature, as well as on the starting composition. The concentration of chromium (knorringite end-member) in garnet increases significantly with temperature for the whole range of starting compositions (Fig. 3.27a, b). The highest concentration of *Knr* (70 mol%) was registered in garnet obtained at 1700 °C with addition of a minimal (5 mol%) portion of pyrope

Table 3.4 Conditions, phase assemblages, and compositions of the phases produced in experiments in the system SiO_2–MgO–Cr_2O_3 (+Al_2O_3) at 7 GPa and 1500–1700 °C

Run no. (sample)	*P* (GPa); *T* (°C)	Starting composition	Heating duration (minutes)	Run products	Mean composition of the phases					
					Phase	MgO	Al_2O_3	SiO_2	Cr_2O_3	Total
04-01	7; 1500	Knr_{100}	30	*Px* + *Esk*	*Px*	38.81 (0.51)	0.00	59.18 (0.31)	1.38 (0.19)	99.37
05-02	7; 1600	Knr_{100}	20	*Px* + *Esk*	*Px*	39.27 (0.16)	0.00	59.92 (0.42)	1.57 (0.12)	100.76
08-01	7; 1700	Knr_{100}	15	*Px* + *Esk*	*Px*	37.93 (0.21)	0.00	59.67 (0.21)	3.19 (0.13)	100.79
01	7; 1700	$Prp_5Knr_{47.5}Maj_{47.5}$	10	*Grt* [12] + *Px* + *Esk*	*Grt*	28.20 (0.04)	5.48 (0.06)	42.25 (0.17)	24.40 (0.09)	100.33
					Px	37.63 (0.03)	0.6 (0.02)	58.49 (0.04)	3.95 (0.03)	100.67
					Esk	0.00	0.00	0.14 (0.01)	98.97 (0.63)	99.11
02	7; 1600	$Prp_5Knr_{47.5}Maj_{47.5}$	20	*Grt* [8] + *Px* + *Esk*	*Grt*	28.32 (0.14)	10.07 (0.49)	42.56 (0.11)	18.74 (0.28)	98.08
					Px	38.56 (0.43)	0.65 (0.03)	59.29 (0.57)	2.47 (0.12)	100.61
					Esk	0.00	0.00	0.11 (0.01)	98.95 (0.03)	100.74
03	7; 1500	$Prp_5Knr_{47.5}Maj_{47.5}$	30	*Grt* [6] + *Px* + *Esk*	*Grt*	29.15 (0.23)	12.07 (0.13)	43.46 (0.08)	15.94 (0.31)	100.62
					Px	38.77 (0.31)	0.51 (0.02)	59.06 (0.06)	2.8 (0.03)	100.52

(continued)

Table 3.4 (continued)

Run no. (sample)	P (GPa); T (°C)	Starting composition	Heating duration (minutes)	Run products	Mean composition of the phases					
					Phase	MgO	Al_2O_3	SiO_2	Cr_2O_3	Total
					Esk	0.00	0.00	0.09 (0.03)	99.68 (0.18)	99.77
04	7; 1700	$Prp_{10}Knr_{45}Maj_{45}$	15	*Grt* [23] + *Px* + *Esk*	*Grt*	28.11 (0.10)	6.27 (0.13)	41.95 (0.15)	23.74 (0.44)	100.07
					Px	38.76 (0.14)	0.79 (0.18)	58.71 (0.43)	2.47 (0.15)	100.73
					Esk	0.00	0.00	0.07 (0.02)	98.98 (0.32)	99.05
05	7; 1600	$Prp_{10}Knr_{45}Maj_{45}$	20	*Grt* [18] + *Px* + *Esk*	*Grt*	28.77 (0.04)	10.68 (0.59)	43.20 (0.21)	17.39 (0.73)	100.04
					Px	38.65 (0.24)	0.79 (0.20)	58.81 (0.11)	2.27 (0.35)	100.73
					Esk	0.00	0.00	0.00	99.94 (0.35)	99.94
06	7; 1500	$Prp_{10}Knr_{45}Maj_{45}$	30	*Grt* [14] + *Px* + *Esk*	*Grt*	29.57 (0.18)	13.89 (0.62)	44.05 (0.17)	12.17 (0.24)	99.68
					Px	38.79 (0.30)	0.97 (0.15)	58.57 (0.28)	2.12 (0.19)	100.45
					Esk	0.00	0.00	0.11 (0.04)	99.45 (0.71)	99.56

(continued)

Table 3.4 (continued)

Run no. (sample)	*P* (GPa); *T* (°C)	Starting composition	Heating duration (minutes)	Run products	Mean composition of the phases					
					Phase	MgO	Al_2O_3	SiO_2	Cr_2O_3	Total
07	7; 1700	$Prp_{20}Knr_{40}Maj_{40}$	15	*Grt* [37] + *Px* + *Esk*	*Grt*	29.03 (0.53)	8.72 (0.74)	43.17 (0.80)	19.45 (0.99)	100.37
					Px	37.95 (0.46)	0.70 (0.03)	58.04 (0.30)	2.53 (0.18)	99.22
08	7; 1600	$Prp_{20}Knr_{40}Maj_{40}$	20	*Grt* [26] + *Px* + *Esk*	*Grt*	29.77 (0.22)	14.61 (0.62)	44.39 (0.38)	10.68 (0.19)	99.45
					Px	38.59 (0.24)	0.88 (0.04)	59.09 (0.21)	2.43 (0.09)	100.99
					Esk	0.00	0.00	0.15 (0.01)	98.42 (0.20)	98.57
09	7; 1500	$Prp_{20}Knr_{40}Maj_{40}$	30	*Grt* [22] + *Px* + *Esk*	*Grt*	29.63 (0.14)	16.51 (0.42)	44.15 (0.27)	9.59 (0.40)	99.88
					Px	38.34 (0.21)	0.82 (0.03)	58.31 (0.61)	2.45 (0.16)	99.92
					Esk	0.00	0.00	0.09 (0.04)	98.72 (0.24)	98.81

Note Modal proportions of garnet (vol %) in run products calculated using the CT-An software are shown in parentheses

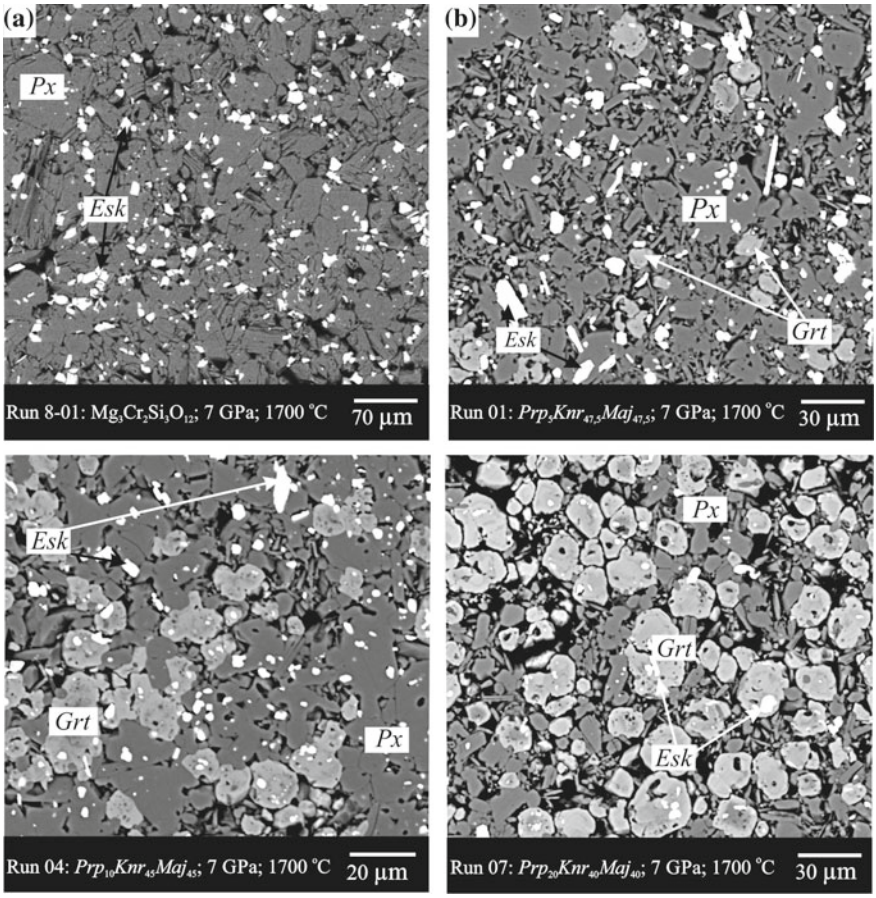

Fig. 3.26 BSE images of the samples obtained in the $MgO–Cr_2O_3–SiO_2$ ($\pm Al_2O_3$) system at 7 GPa and 1700 °C illustrating their textural peculiarities: **a** aggregate of small grains of chromium-bearing pyroxene with interstitial segregations of eskolaite; **b** minor isometric garnet crystals in the eskolaite–pyroxene matrix; **c** garnet–pyroxene aggregate with small eskolaite grains; **d** isometric garnet grains in the eskolaite–pyroxene matrix

(Sample 01). On the contrary, increase in the concentration of pyrope in the starting composition results in the decrease in the chromium content in garnet (Fig. 3.27c, d) and in the increase in the portion of garnet in the sample. All garnets are characterized by an excess of Si (>3 f.u.); i.e., they correspond to the majoritic type. The highest concentration of majorite in garnet reaches 13 mol% (3.13 f.u. Si).

It is characteristic that at such low aluminum contents in the system, high-chromium majoritic garnet crystallizes at given *P–T* parameters.

Of special attention is the fact that the modal concentration of garnet in experimental samples is always higher than the content of pyrope in the starting materials owing to the formation of the complex majorite–knorringite–pyrope series of solid

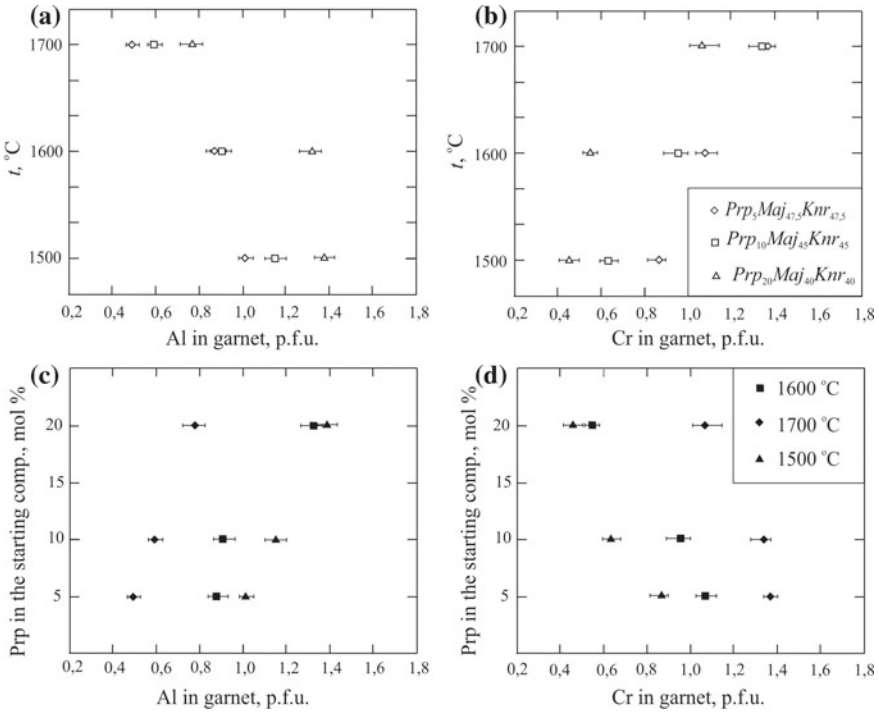

Fig. 3.27 Dependence of the chromium and aluminum concentrations in garnets on temperature (**a**, **b**) and starting compositions (**c**, **d**) (Sirotkina et al. 2016)

solutions. Thus, the portion of garnet is 6–12 vol.% with addition of 5 mol% of pyrope, 14–23 vol.% in the system with 10 mol% of pyrope, and 22–37 vol.% in the system with 20 mol% of pyrope. We should emphasize that the portion of garnet in the sample increases with temperature as well (Fig. 3.28). In this relation, we may assume that the increase in the chromium concentration in garnet with temperature may stabilize the structure.

It is necessary to mention that the composition of synthesized garnets is in good agreement with that of garnet inclusions in diamonds of the dunite–harzburgite paragenesis (Fig. 3.28a). Garnets obtained in the $MgO–Cr_2O_3–SiO_2$ ($\pm Al_2O_3$) system are characterized by quite high contents of the pyrope (from 23 to 80 mol%) and knorringite (from 22 to 70 mol%) components, which indicate their correspondence to the pyrope–knorringite solid solution on the Cr–Si diagram (Fig. 3.28b); garnets from inclusions in diamonds of moderate depth are related to this solid solution (Pokhilenko et al. 2004; Shatskii et al. 2010). The permanent silicon excess (>3 f.u.) increasing with decrease in the chromium concentration shows that the knorringite—majorite trend has a definite contribution to compositional variations of garnets.

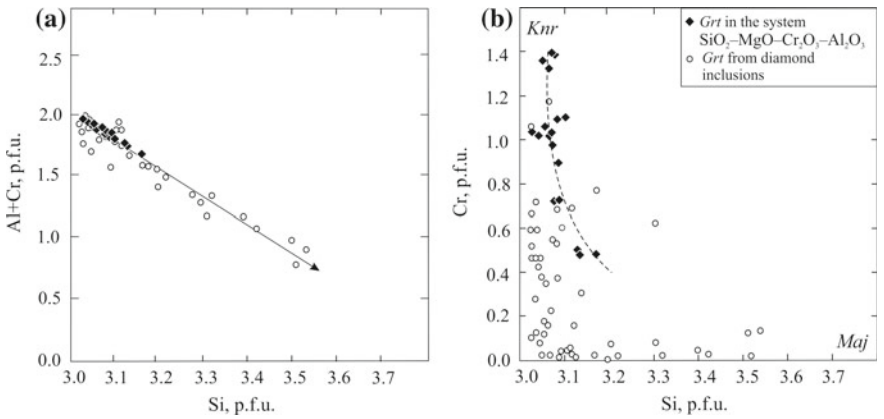

Fig. 3.28 Compositional peculiarities of chromium-bearing majoritic garnets synthesized in the $MgO–Cr_2O_3–SiO_2$ ($\pm Al_2O_3$) system, in comparison with the data on garnets from inclusions in natural diamonds (Sirotkina et al. 2016)

3.4.2 Crystallization of Knorringitic Garnet in the Pyrolite System

To establish the probability of crystallization of high-chromium garnet and to understand the relationship of its composition with the temperature and starting composition of the system, as well as to obtain new quantitative data on chromium component partitioning between restite and melt, we performed a series of runs simulating partial melting in the garnet (diamond) depth facies. The process of the formation of high-chromium protolith (restite) upon partial melting of model pyrolite was reconstructed in experiments within the spinel stability field at 2.5 GPa. To study the influence of the Cr/Al ratio in protolith (starting material) on the composition of garnet and to simulate crystallization of garnet from high-chromium restite formed upon partial melting, we performed experiments with the Cr-rich (3 wt% Cr_2O_3) starting material and with the Cr/Al values modeling the composition of restite produced in the run series at 2.5 GPa.

Experiments were performed at the Vernadsky Institute of Geochemistry and Analytical Chemistry (Moscow, Russia) on a toroidal "anvil-with-hole" apparatus at pressures of 7.0 and 2.5 GPa and temperatures of 1600–1800 °C. The starting composition was represented by the model pyrolite (wt%) (Ringwood 1966): 45.95 SiO_2, 3.56 Al_2O_3, 0.50 Cr_2O_3, 38.12 MgO, 8.13 FeO, 3.15 CaO, 0.58 Na_2O.

The textures and degree of crystallization of run products depend on temperature. All experimental samples show zoning (Fig. 3.29a) with clearly reflected area of the garnet–olivine composition (restite). This zone is characterized by the presence of euhedral garnet crystals with regular hexagonal outlines and euhedral olivine grains (Fig. 3.29b–d). The zone of melting is composed of large elongated (sometimes acicular) pyroxene grains with the fine-granular aggregate in the interstitials. The

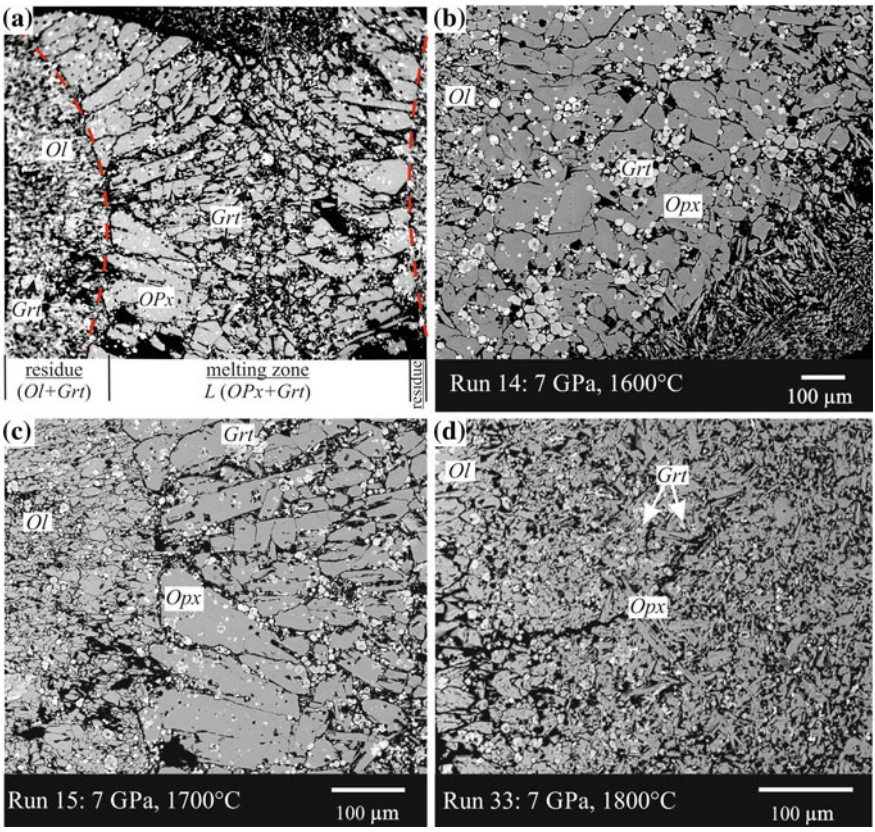

Fig. 3.29 BSE images of textural relationships and phase associations in run products produced upon partial melting of the model pyrolite within the garnet depth facies at 7 GPa and 1600–1800 °C: **a** zoned structure with clearly reflected zone of the garnet–olivine composition (restite) and area of melting; **b–c** fragments of the samples after runs

melt in run products was registered by the presence of microgranular quenched aggregates composed of tiny pyroxene and garnet crystals. Garnet forms clusters of isometric crystals with a size up to 50 μm in the quenched matrix.

Garnets obtained in all runs belong to the solid solution between the pyrope, knorringite, and majorite end-members. The major feature of garnets synthesized at 7 GPa is the presence of Si excess (>3.0 p.f.u.), which allows us to attribute these garnets to the majoritic type (Gasparik 2002). The highest concentration of majorite (7 mol%) is typical of garnets synthesized at 1600 °C. In addition, garnets from the restite zone contain a stable admixture of Cr_2O_3 (up to 4.3 wt%), which corresponds to 12 mol% of the knorringite component), whereas the composition of garnet from the quenched aggregate is significantly enriched in chromium (up to 8 wt% Cr_2O_3). The highest content of the knorringite end-member was registered in garnet from the zone of melting at a temperature of 1600 °C. An excess in Si (>3 p.f.u.) increasing

with decrease in the chromium content provides evidence for the contribution of the majorite–knorringite trend (Sirotkina et al. 2015) to the compositional variations of garnet. As a whole, it is evident that garnets from the restite area of the run products are characterized by quite low concentrations of Cr_2O_3, low concentrations of CaO and correspond to sub-calcium garnets of the dunite–harzburgite assemblage. The results of our runs show that the high-chromium garnets with the composition similar to that of mineral inclusions in diamonds of the dunite–harzburgite assemblage cannot be produced by partial melting of the model mantle pyrolite within the garnet depth facies.

To study the distribution of chromium between crystals and melts upon partial melting of mantle pyrolite, using our experimental data, we calculated the compositions of restite and melt. Our calculations show that an increase in temperature results in the redistribution of chromium into melt, whereas the concentration of this element in restite at 1800 °C becomes lower than its bulk concentration in the rock (Fig. 3.30).

Noteworthy, the process of partial melting in the mantle substrate within the garnet depth facies will not result in the formation of high-chromium restite, because garnet (restite) will accumulate not only chromium, but, to a higher degree, aluminum, with $D_{Cr/Al}{}^{restite/L} \approx 1$; this is consistent with assumptions made by Bulatov et al (1991) and Stachel et al. (1998).

To obtain high-chromium restite with Cr/Al more than five times higher than that in the starting pyrolite, we performed experiments on partial melting of pyrolite in the spinel depth facies at a pressure of 2.5 GPa and a temperature of 1400–1600 °C. Our runs show the opposite effect of chromium redistribution into restite under such conditions. At the highest run temperature of 1600 °C, the concentration of Cr_2O_3 in restite is ten times higher than that in the starting material; the concentration of Cr_2O_3 in melt does not exceed 0.2 wt%.

The results obtained allow us to conclude for the first time on a quantitative basis that the partial melting of the mantle pyrolite in the spinel depth facies can produce

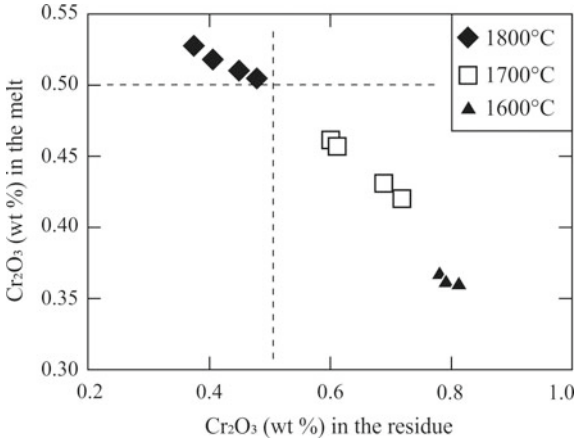

Fig. 3.30 Dependence of the bulk concentration of Cr_2O_3 in melt on the concentration of Cr_2O_3 in restite observed in experiments on partial melting of pyrolite at a temperature of 1600–1800 °C and pressure of 7 GPa. Dashed line shows the concentration of chromium in the starting material

a high-chromium restite with the chromium content more than 10 times higher than the bulk chromium concentration in pyrolite. Subduction of such chromium-rich protolith of oceanic crust to the garnet depth facies will result in the formation of essentially knorringitic garnets.

References

Akaogi M, Ito E, Navrotsky A (1989) The olivine-modified spinelspinel transitions in the system Mg_2SiO_4-Fe_2SiO_4: calorimetric measurements, thermochemical calculation, and geophysical application. J Geophys Res 94:15671–15685

Akaogi M, Akimoto A (1977) Pyroxene-garnet solid-solution equilibria in the system $Mg_4Si_4O_{12}$-$Mg_3Al_2Si_2O_{12}$ and $Fe_4Si_4O_{12}$-$Fe_3Al_2Si_3O_{12}$ at high pressures and temperatures. Phys Earth Planet Inter 111:90–106

Akaogi M, Akimoto A (1979) High pressure phase equilibria in a garnet lherzolite, with special reference to Mg^{2+}-Fe^{2+} partitioning among constituent minerals. Phys Earth Planet Inter 19:31–51

Babich YV (1980) A study of the stability of chromium-bearing pyrope–knorringite garnets at P = 3 GPa. In: Proceedings of 18th All-Union student conference "student and technological progress." Inst. Geol. Geophys., Novosibirsk, pp 57–65

Berman RG, Aranovich LY (1996) Optimized standard state and solution properties of minerals: I. Model calibration for olivine, orthopyroxene, cordierite, garnet, and ilmenite in the system FeO-MgO-CaO-Al_2O_3-TiO_2-SiO_2. Contrib Mineral Petrol 126:1–24

Bindi L, Sirotkina EA, Bobrov AV, Irifune T (2014a) Chromium solubility in $MgSiO_3$ ilmenite at high pressure. Phys Chem Miner 41:519–526

Bindi L, Sirotkina EA, Bobrov AV, Irifune T (2014b) Chromium solubility in perovskite at high pressure: the structure of $(Mg_{1-x}Cr_x)(Si_{1-x}Cr_x)O_3$ (with x = 0.07) synthesized at 23 GPa and 1600 °C. Am Mineral 99:866–869

Bindi L, Sirotkina EA, Bobrov AV, Irifune T (2014c) X-ray single-crystal structural characterization of $MgCr_2O_4$, a post-spinel phase synthesized at 23 GPa and 1600 °C. J Phys Chem Solids 75:638–641

Bindi L, Sirotkina EA, Bobrov AV, Irifune T (2015) Structural and chemical characterization of Mg[(Cr, Mg)(Si, Mg)]O4, a new post-spinel phase with six-fold coordinated silicon. Am Mineral 100:1633–1636

Bindi L, Sirotkina EA, Bobrov AV, Nestola F, Irifune T (2016) Chromium solubility in anhydrous phase B. Phys Chem Minerals 43:103–110

Binns RA (1970) $(Mg,Fe)_2SiO_4$ spinel in a meteorite. Phys Earth Planet Inter 3:156–160

Brey GP, Doroshev AM, Girnis AV, Turkin AI (1999) Garnet–spinel–olivine–orthopyroxene equilibria in the FeO–MgO–Al_2O_3–SiO_2–Cr_2O_3 system: I. Composition and molar volumes of minerals. Eur J Mineral 11(4):599–617

Bulanova GP, Barashkov YP, Tal'nikova SB, Smelova GB (1993) Natural diamond: genetic aspects. Nauka, Novosibirsk, 168 p

Bulatov V, Brey GP, Foley SF (1991) Origin of low-Ca, high-Cr garnets by recrystallization of low-pressure harzburgites. In: 5th international kimberlite conference, extended abstracts, CPRM, special publication, vol 91, pp 29–31

Bykova EA, Bobrov AV, Sirotkina EA, Bindi L, Ovsyannikov SV, Dubrovinsky LS, Litvin YuA (2014) X-ray single-crystal and Raman study of knorringite, $Mg_3(Cr_{1.58}Mg_{0.21}Si_{0.21})Si_3O_{12}$, synthesized at 16 GPa and 1600 °C. Phys Chem Miner 41(4):267–272

Chen M, Shu J, Xie X, Mao H (2003) Natural $CaTi_2O_4$-structured $FeCr_2O_4$ polymorph in the Suizhou meteorite and its significance in mantle mineralogy. Geochim Cosmochim Acta 67:3937–3942

Coes L (1955) High-pressure minerals. J. Am Ceram Soc 38:298

Dobrzhinetskaya L, Green HW, Wang S (1996) Alpe Arami: a peridotite massif from depths of more than 300 kilometers. Science 271:1841–1845

Doroshev AM, Brey GP, Girnis AV, Turkin AI, Kogarko LN (1997) Pyrope-knorringite garnets in the Earth's mantle: experiments in the MgO-Al_2O_3-SiO_2-Cr_2O_3 system. Rusian Geol Geophys 38:559–586

Gasparik T (2002) Experimentional investigations of the origin majoritic garnet inclusions in diamonds. Phys Chem Minerals 29:170–180

Girnis AV, Brey GP, Doroshev AM, Turkin AI, Simon N (2003) The system MgO-Al_2O_3-Cr_2O_3 revisited: reanalysis of Doroshev et al.'s (1997) experiments and new experiments. European J Miner 15(6):953–964

Gudfinnsson GH, Wood BJ (1998) The effect of trace elements on the olivine–wadsleyite transformation. Am Mineral 83:1037–1044

Harte B (2010) Diamond formation in the deep mantle: the record of mineral inclusions and their distribution in relation to mantle dehydration zones. Miner Mag 74(2):189–215

Herzberg CT, Gasparik T (1989) Melting experiments on chondrite at high pressures: stability of anhydrous phase B. EOS Trans AGU 70(15):484

Homan CG (1975) Phase diagram of Bi up to 140 kbars. J Phys Chem Solids 36:1249–1254

Irifune T (1987) An experimental investigation of the pyroxene–garnet transformation in a pyrolite composition and its bearing on the constitution of the mantle. Phys Earth Planet Inter 45:324–336

Irifune T, Fujino K, Ohtani E (1991) A new high-pressure form of $MgAl_2O_4$. Nature 349:409–411

Irifune T, Kurio A, Sakamoto S, Inoue T, Sumiya H, Funakoshi K (2004) Formation of pure polycrystalline diamond by direct conversion of graphite at high pressure and high temperature. Phys Earth Planet Inter 143:593–600

Irifune T, Ohtani E, Kumazawa M (1982) Stability field of knorringite $Mg_3Cr_2Si_3O_{12}$ at high pressure and its implication to the occurrence of Cr-rich pyrope in the upper mantle. Phys Earth Planet Inter 27:263–272

Ishii T, Kojitani H, Fujino K, Yusa H, Mori D, Inaguma Y, Matsushita Y, Yamaura K, Akaogi M (2015) High-pressure high-temperature transitions in $MgCr_2O_4$ and crystal structures of new $Mg_2Cr_2O_5$ and post-spinel $MgCr_2O_4$ phases with implications for ultra-high pressure chromitites in ophiolites. Am Mineral 100:59–65

Juhin A, Morin G, Elkaim E, Frost DJ, Fialin M, Juillot F, Calas G (2010) Structure refinement of a synthetic knorringite, $Mg_3(Cr_{0.8}Mg_{0.1}Si_{0.1})_2(SiO_4)_3$. Am Mineral 95:59–63

Kaminsky F (2012) Mineralogy of the lower mantle: a review of super-deep mineral inclusions in diamond. Earth Sci Rev 110:127–147

Katsura T, Ito E (1989) The system Mg_2SiO_4–Fe_2SiO_4 at high pressure and temperatures: precise determination of stabilities of olivine, modified spinel and spinel. J Geophys Res 94:15663–15670

Kawai N, Tachimori M, Ito E (1974) A high pressure hexagonal form of $MgSiO_3$. Proc Jpn Acad 50:378–380

Kennedy CS, Kennedy GC (1976) The equilibrium boundary between graphite and diamond. J Geophys Res 81(14):2467–2470

Klemme S (2004) The influence of Cr on the garnet–spinel transition in the Earth's mantle: experiments in the system MgO–Cr_2O_3–SiO_2 and thermodynamic modeling. Lithos 77:639–646

Kojitani H, Hisatomi R, Akaogi M (2007) High-pressure phase relations and crystal chemistry of calcium ferrite-type solid solutions in the system $MgAl_2O_4$–Mg_2SiO_4. Am Mineral 92:1112–1118

Litvin YA (1991) Physical and chemical studies of melting of materials from the deep Earth. Nauka

Liu L (1974) Silicate perovskite from phase transformations of pyrope-garnet at high pressure and temperature. Geophys Res Lett 1:277–280

MacGregor ID (1964) The reaction enstatite + spinel = forsterite + pyrope. In: Carnegie Institution Year Book 63. Carnegie Institute, Washington, p 157

Malinovskii IY, Doroshev AM, Ran EN (1975) The stability of chromium-bearing garnets pyrope: knorringite series. Experimental studies on the mineralogy (1974–1976). Institute of Geology and Geophysics of the Siberian Branch of AS USSR, Novosibirsk, pp 110–115

Matrosova EA, Bobrov AV, Bindi L, Irifune T (2018) Phase relations in the model system SiO_2–MgO–Cr_2O_3: evidence from the results of experiments in petrologically significant sections at 12–24 GPa and 1600 °C. Petrology 26(6):588–598

Nakatsuka A, Yoshiasa A, Yamanaka T, Ohtaka O, Katsura T, Ito E (1999) Symmetry change of majorite solid-solution in the system $Mg_3Al_2Si_3O_{12}$-$MgSiO_3$. Am Mineral 84:1135–1143

Ono S, Yasuda A (1996) Compositional change of majoritic garnet in a MORB composition from 7 to 17 GPa and 1400 to 1600 °C. Phys Earth Planet Inter 96:171–179

Ottonello G, Bokreta M, Sciuto PF (1996) Parameterization of energy an interactions in garnets: end-member properties. Am Mineral 81:429–447

Oxford Diffraction (2006) CrysAlis RED (Version 1.171.31.2) and ABSPACK in CrysAlis RED. Oxford diffraction Ltd., Abingdon

Parise J, Wang Y, Dwanmesia GD, Zhang J, Sinelnikov Y, Chmielowski J, Weidner DJ, Liebermann RC (1996) The symmetry of garnets on the pyrope ($Mg_3Al_2Si_3O_{12}$)—majoritc ($MgSiO_3$) join. Geophys Res Lett 23(25):3799–3802

Pokhilenko NP, Sobolev NV, Reutsky VN, Hall AE, Taylor LA (2004) Crystalline inclusions and C isotope rations in diamonds from the Snap Lake/King Lake kimberlite dyke system: evidence of ultradeep and enriched lithospheric mantle. Lithos 77:57–67

Price GD, Putnis A, Agrell SO, Smith DGW (1983) Wadsleyite, natural β-$(Mg, Fe)_2SiO_4$ from the Peace River meteorite. Canad Mineral 21:29–35

Ringwood AE (1966) The chemical composition and origin of the Earth. In: Adv Earth Sci 287–356

Ringwood AE (1977) Composition of the core and implications for origin of the Earth. Geochem J 11(3):111–135

Shatskii VS, Zedgenizov DA, Ragozin AL (2010). Majoritic garnets in diamonds from placers of the Northeastern Siberian Platform. Doklady Earth Sci 432(2):835–838)

Sirotkina EA, Bobrov AV, Bindi L, Irifune T (2015) Phase relations and formation of chromium-rich phases in the system $Mg_4Si_4O_{12}$–$Mg_3Cr_2Si_3O_{12}$ at 10–24 GPa and 1,600 °C. Contrib Miner Petrol 169:2

Sirotkina EA, Bobrov AV, Kargal'tsev AA, Ignat'ev YuA, Kadik AA (2016) The influence of low aluminum concentrations on the composition and conditions of crystallization of majorite–knorringite garnets: experiment at 7.0 GPa and 1500–1700 °C. Geochem Int 54(7):584–593

Sirotkina EA, Bobrov AV, Bindi L, Irifune T (2018) Chromium-bearing phases in the Earth's mantle: evidence from experiments in the Mg_2SiO_4–$MgCr_2O_4$ system at 10–24 GPa and 1600 °C. Am Mineral 103(1):151–160

Sobolev NV (1983) Diamond parageneses and the problem of deep-seated mineral formation. ZVMO 4:389–397

Sobolev NV (1974) Deep-seated inclusions in kimberlites and the problem of the Upper Mantle composition. Nauka 183 p

Spivak AV, Litvin YA (2004) Diamond syntheses in multicomponent carbonate–carbon melts of natural chemistry: elementary processes and properties. Diam Relat Mater 13(3):482–487

Stachel T, Harris JW (1997) Diamond precipitation and mantle metasomatism-evidence from the trace element chemistry of silicate inclusions in diamonds from Akwatia, Ghana. Contrib Mineral Petrol 129(2–3):143–154

Stachel T (2001) Diamonds from the asthenosphere and the transition zone. Eur J Mineral 13:883–892

Stachel T, Harris JW, Brey GP (1998) Rare and unusual mineral inclusions in diamonds from Mwadui, Tanzania. Contrib Mineral Petrol 132:34–47

Stixrude L, Lithgow-Bertelloni C (2007) Influence of phase transformations on lateral heterogeneity and dynamics in the Earth's mantle. Earth Planet Sci Lett 263:45–55

Taran MN, Langer K, Abs-Wurmbach I, Frost DJ, Platonov AN (2004) Local relaxation around $^{[6]}Cr^{3+}$ in synthetic pyrope–knorringite garnets, $^{[8]}Mg_3^{[6]}(Al_{(1-x)}Cr_x^{3+})_2^{[4]}Si_3O_{12}$, from electronic absorption spectra. Phys Chem Mineral 31(9):650–657

Taylor LA, Anand M (2004) Diamonds: time capsules from the Siberian Mantle. Chem Erde 64:1–74

Tschauner O, Ma C, Beckett JR, Prescher C, Prakapenka VB, Rossman GR (2014) Discovery of bridgmanite, the most abundant mineral in Earth, in a shocked meteorite. Science 346(6213):1100–1102

Turkin AI, Doroshev AM, Yu I (1983) Study of the phase composition of garnet-bearing associations of the system $MgO–Al_2O_3–SiO_2–Cr_2O_3$ system at high temperatures and pressures [in Russian]. Silicate systems under high pressure, Novosibirsk. p 5

Turkin AI, Sobolev NV (2009) Pyrope–knorringite garnets: overview of experimental data and natural parageneses. Russian Geol Geophys 50(12):1169–1182

Wang Z, O'Neill HSC, Lazor P, Saxena SK (2002) High pressure Raman spectroscopic study of spinel $MgCr_2O_4$. J Phys Chem Solids 63:2057–2061

Yu YG, Wu Z, Wentzcovitc RM (2008) $\alpha–\beta–\gamma$ transformations in Mg_2SiO_4 in Earth's transition zone. Earth Planet Sci Lett 273:115–122

Zou Y, Irifune T (2012) Phase relations in $Mg_3Cr_2Si_3O_{12}$ and formation of majoritic knorringite garnet at high pressure and high temperature. J Mineral Petrol Sci 107:197–205

Chapter 4
Structural Patterns of Cr-Bearing Phases and the Influence of Chromium on the Solid Solutions of the Major Mantle Minerals and Phase Transitions

4.1 Crystal Chemistry of Cr-Rich Mantle Phases

Crystals of chromium-rich phases of fair diffraction quality synthesized in experiments on the investigation of phase relations in the SiO_2–MgO–Cr_2O_3 system, have been studied by means of single-crystal X-ray diffraction. For the selected phases (majorite–knorringite garnet, akimotoite, bridgmanite, $MgCr_2O_4$ with calcium-titanate-type structure, $Mg(Mg,Si,Cr)_2O_4$ with distorted calcium-titanate structure, anhydrous phase B, olivine, wadsleyite and ringwoodite), we determined the unit-cell parameters, the space group, and the mechanism of chromium incorporation in their structures.

Garnet A crystal of majorite–knorringite garnet of fair diffraction quality was selected (Fig. 4.1) for the X-ray study from the sample H3420 synthesized at $P = 16$ GPa and $T = 1600$ °C (Bykova et al. 2014). The composition of garnet from this sample is $Mg_3(Cr_{1.58}Mg_{0.21}Si_{0.21})Si_3O_{12}$ which corresponds to $Knr_{79}Maj_{21}$.

Garnet was found to be cubic, space group $Ia\bar{3}d$, with unit cell parameters $a = 11.5718(1)$ Å, $V = 1549.54(2)$ Å^3 (Bykova et al. 2014).

It is important to note that garnet single crystals with such a high content of knorringite component were not synthesized previously. Indeed, the recently produced garnet with composition $Mg_3(Cr_{1.60}Mg_{0.20}Si_{0.20})Si_3O_{12}$ (Juhin et al. 2010) was only characterized by synchrotron X-ray powder diffraction, and the information about the structural features of knorringitic garnet were still based on the data of computer modelling for pure knorringite $Mg_3Cr_2Si_3O_{12}$ ($a = 11.6040$ Å) (Ottonello et al. 1996).

An extended series of solid solutions was obtained for the majorite–knorringite join in our runs. The general formula of studied garnets is $X_3Y_2Si_3O_{12}$ where X = Mg and Y = Mg, Cr, and Si. The X site is eightfold coordinated, the Y-site is octahedral and the Si site is tetrahedral. The studied garnets are characterized by the coupled substitution $Mg^{2+} + Si^{4+} = 2Cr^{3+}$, where Mg and Si replace Cr in the octahedral position, whereas the eightfold coordinated and tetrahedral sites are occupied by Mg

E. A. Matrosova et al., *Geochemistry of Chromium in the Earth's Mantle*,
Springer Geology, https://doi.org/10.1007/978-3-030-27018-6_4

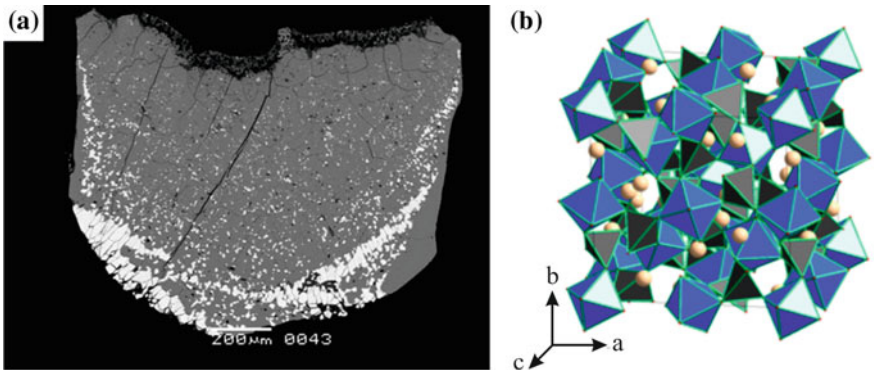

Fig. 4.1 **a** BSE image of an aggregate of euhedral knorringitic garnet crystals (gray) and small eskolaite (Cr_2O_3) grains (white) synthesized at $P = 16$ GPa and $T = 1600$ °C (Sample H3420); **b** the crystal structure of *Knr–Maj* garnet (Bykova et al. 2014)

and Si, respectively. This is supported by the clear negative correlation of chromium with magnesium and silicon (Fig. 3.11). Increase in Si content in the octahedral site with pressure is typical of high-pressure phases (e.g., Angel et al. 1989; Yang et al. 2007). The high concentration of Si (>3.03 p.f.u.; Gasparik 2002) indicates appearance of the majoritic ($Mg_4Si_4O_{12}$) component (Akaogi and Akimoto 1977).

Five relatively large (up to 100 μm) garnet crystals were selected for the X-ray single-crystal studies. The studied garnets belong to a wide compositional range from 3 to 90 mol% *Knr* (Table 3.1). As it was shown in the Sect. 3.1.2, garnet with the maximum chromium concentration (30.8 wt% Cr_2O_3), corresponding to ~90 mol% *Knr*, was obtained at 10 GPa. All garnets are characterized by cubic symmetry and space group $Ia\bar{3}d$. The cell parameter linearly decreases (Fig. 4.2) with increasing the majorite content from $a = 11.5879(2)$ Å ($Knr_{90}Maj_{10}$) to $a = 11.457$ Å (Knr_3Maj_{97}). The cell parameter of pure knorringite calculated by Ottonello et al. (1996) plots well at the end of our trend (Fig. 4.2). The cell parameter of garnet with the composition $Mg_3(Cr_{1.60}Mg_{0.20}Si_{0.20})Si_3O_{12}$ studied by X-ray powder diffraction (Juhin et al. 2010) plots at a considerable distance from our linear trend. The compositions and lattice parameters of garnets on the majorite–knorringite join are summarized in Table 4.1.

It is important to note that the cubic/tetragonal transition in garnet with high majorite content (~75–80 mol% Maj) registered along the majorite–pyrope join (Akaogi and Akimoto 1977; Parise et al. 1996) is not observed in the majorite–knorringite system. Essentially, majoritic garnet with low chromium content (3 mol% *Knr*, Sample 2425-5) does not show ordering of Mg and Cr being characterized by the cubic symmetry (space group $Ia\bar{3}d$) (Table 4.1). The shape of the high-θ reflections (e.g., 800) collected at $2\theta \approx 28.6°$ for garnets from samples 2425-5 with 3 mol% *Knr* and 2526–100 with 90 mol% *Knr* (Fig. 4.3) shows that there is no split of the 800 reflection induced by a twinning or tetragonal distortion. Our results (Sirotkina et al. 2015) are contrastingly different from the data on the majorite–pyrope join

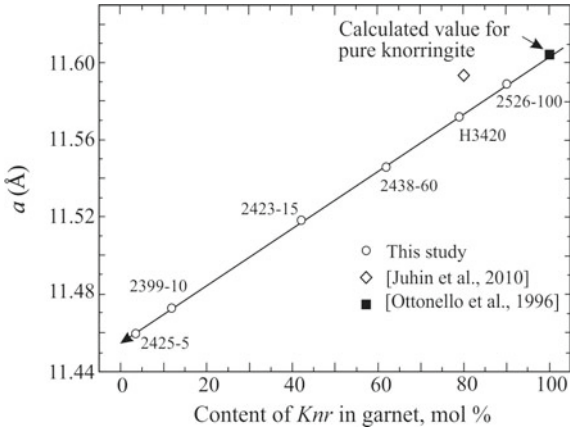

Fig. 4.2 Variations in unit cell parameters as a function of composition for knorringite–majorite garnets synthesized in the majorite ($Mg_4Si_4O_{12}$)–knorringite ($Mg_3Cr_2Si_3O_{12}$) system (Sirotkina et al. 2015). The calculated cell parameter (solid square) of pure knorringite (Ottonello et al. 1996) and unit cell parameter obtained by the powder X-ray diffraction (open rhomb) (Juhin et al. 2010) are shown for comparison. Sample H3420 is the synthetic garnet studied by Bykova et al. (2014)

Table 4.1 The lattice parameters of garnets in the majorite–knorringite join

Run number	Garnet composition	Lattice parameters (Å)	V (Å^3)	References
Knorringite	$Mg_3Cr_2Si_3O_{12}$	11.6040	1562.51	Ottonello et al. (1996)
2526-100	$Mg_{3.10}Cr_{1.80}Si_{3.10}O_{12}$	11.5879(2)	1556.02(3)	This study
H3420	$Mg_{3.21}Cr_{1.58}Si_{3.21}O_{12}$	11.5718(1)	1549.54(2)	This study
2438-60	$Mg_{3.38}Cr_{1.24}Si_{3.38}O_{12}$	11.5445(5)	1538.61(6)	This study
2423-15	$Mg_{3.58}Cr_{0.84}Si_{3.58}O_{12}$	11.5187(6)	1528.33(1)	This study
2399-10	$Mg_{3.88}Cr_{0.24}Si_{3.88}O_{12}$	11.4725(4)	1510.00(1)	This study
2425-5	$Mg_{3.97}Cr_{0.06}Si_{3.97}O_{12}$	11.457(3)	1503.99(5)	This study
Majorite	$Mg_4Si_4O_{12}$	11.5186(4)(a); 11.4204(4)(c)	1515.25	Heinemann et al. (1997)

reported by Heinemann et al. (1997), who showed splitting of the reflection (400) and explained this by ordering between Mg and Si in the octahedral sites, which is typical of reduction of symmetry to tetragonal. Thus, our data show that even a small concentration of chromium stabilizes the cubic symmetry of garnet.

Garnets of the knorringite–majorite series synthesized at 12 (Sample 2401-100), 14 (Sample 2403-100), and 16 GPa (Sample 2404-100) from the $Knr_{100}Maj_0$ starting composition were studied by Raman spectroscopy (Bykova et al. 2014). Figure 4.4 shows a comparison of the Raman spectra of crystals studied in our work with those collected on pure majorite and uvarovite. The main peak for majorite (near

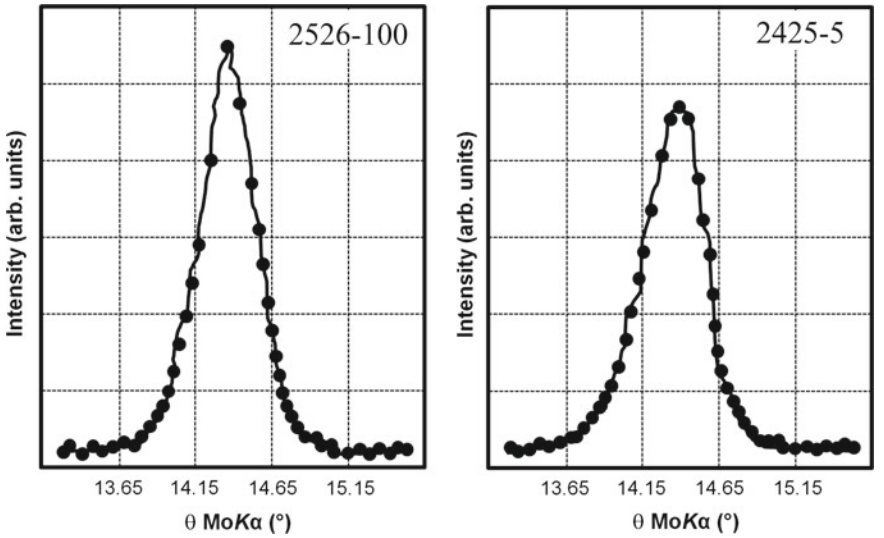

Fig. 4.3 Reflection (800) of the cubic structure of majoritic garnets collected at about $2\theta = 28.6°$ (Samples 2526-100 and 2425-5)

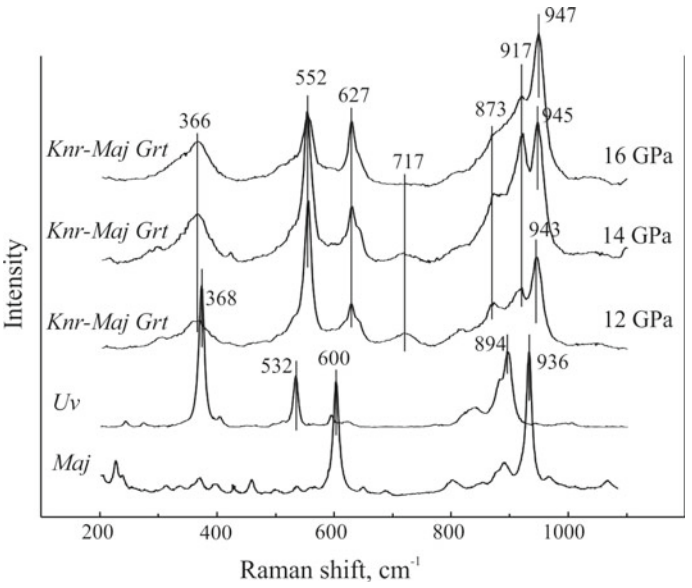

Fig. 4.4 Raman spectra of knorringite–majorite garnets (Samples 2404-100 (16 GPa), 2403-100 (14 GPa), 2401-100 (12 GPa), this study) in comparison with majorite (http://www.ens-lyon.fr/lST/raman/spectres/majorite.pdf) and uvarovite (Bykova et al. 2014)

600 cm^{-1}) has been addressed as a Si–O–Si bending vibration involving both the [SiO_4] tetrahedra and [SiO_6] octahedra also present in the structure of this high-pressure garnet (McMillan et al. 1989). During the formation of the *Knr–Maj* garnet solid solution, the Raman peak becomes more broad and weak. This peak splits into three peaks of lesser intensity defined in the range 550–720 cm^{-1}. It is important to note that the intensity of the peaks at 552 and 717 cm^{-1} decreases with pressure (with increasing content of the majorite component in the garnet composition), in contrast to the 627 cm^{-1} peak.

The well-defined sharp mode at 936 cm^{-1} is attributed to internal vibrations of the [SiO_4] units, similar to those in normal garnets. For uvarovite, the peak of this kind moves to the area of the lower Raman shift (894 cm^{-1}). Knorringite–majorite garnets are characterized by the formation of a broad stage that expands with decreasing majorite content in garnet (decreasing pressure). As a result, we can see the formation of some peaks within the Raman shift range from 850 to 950 cm^{-1}. Increase in the majorite content (with pressure) in garnet results in increase of intensity of 943–947 cm^{-1} peaks.

$MgSiO_3$ Akimotoite As it was noted above (Sect. 3.1.1), for Cr-poor bulk compositions (0–10 mol% *Knr* in the starting composition), a single-phase field represented by $MgSiO_3$ akimotoite opens up at pressures ≥~17 GPa. Chromium was found to substitute for both Mg at the octahedral X site and Si at the octahedral Y site, again consistent with a coupled Tschermak-style substitution $Mg^{2+} + Si^{4+} = 2Cr^{3+}$.

The ideal structural formula of the synthesized Cr-rich akimotoite may be presented as $(Mg_{1-x}Cr_x)(Si_{1-x}Cr_x)O_3$, where $x = 0.015$, 0.023, and 0.038. Akimotoite was found to have a trigonal symmetry with a space group $R\bar{3}$. The akimotoite crystal structure is based on an ordered derivative of the corundum structure, with Mg^{2+} and Si^{4+} ions occupying alternating layers perpendicular to the trigonal *c* axis (Fig. 4.5).

The unit-cell parameters of $MgSiO_3$ akimotoite are only slightly affected by the entry of Cr into the structure. We observed a general expansion of the unit cell, mainly related to the increase in the *a* parameter (by 4.5%) from pure $MgSiO_3$ (Horiuchi et al. 1982) to pure Cr_2O_3 (Ovsyannikov and Dubrovinsky 2011). The variation in the *c* parameter is more modest, increasing only by 2‰ (Bindi et al. 2014a). The studied crystals of Cr-akimotoite are characterized by the following compositions and cell parameters: $(Mg_{0.985}Cr_{0.015})(Si_{0.985}Cr_{0.015})O_3$, $a = 4.7336(1)$ Å, $c = 13.5596(2)$ (run 2530-5); $(Mg_{0.977}Cr_{0.023})(Si_{0.977}Cr_{0.023})O_3$, $a = 4.7348(1)$ Å, $c = 13.5603(2)$ (run 2415-10); $(Mg_{0.962}Cr_{0.038})(Si_{0.962}Cr_{0.038})O_3$, $a = 4.7380(1)$ Å, $c = 13.5611(2)$ (run 2410-30).

Further increase in pressure (>20 GPa) results in the formation of **chromium-rich bridgmanite**. The crystal structure and chemical composition of a crystal of $(Mg_{1-x}Cr_x)(Si_{1-x}Cr_x)O_3$ perovskite (with $x = 0.07$) have been studied by single-crystal X-ray diffraction. Chromium was found to substitute for both Mg at the dodecahedral X site (with a mean polyhedral distance of 2.187 Å) and Si at the octahedral Y site (mean: 1.814 Å), according to the scheme $Mg^{2+} + Si^{4+} = 2Cr^{3+}$. Such substitutions cause a shortening of the <X–O> and a lengthening of the <Y–O> distances with respect to the values typically observed for pure $MgSiO_3$ perovskite.

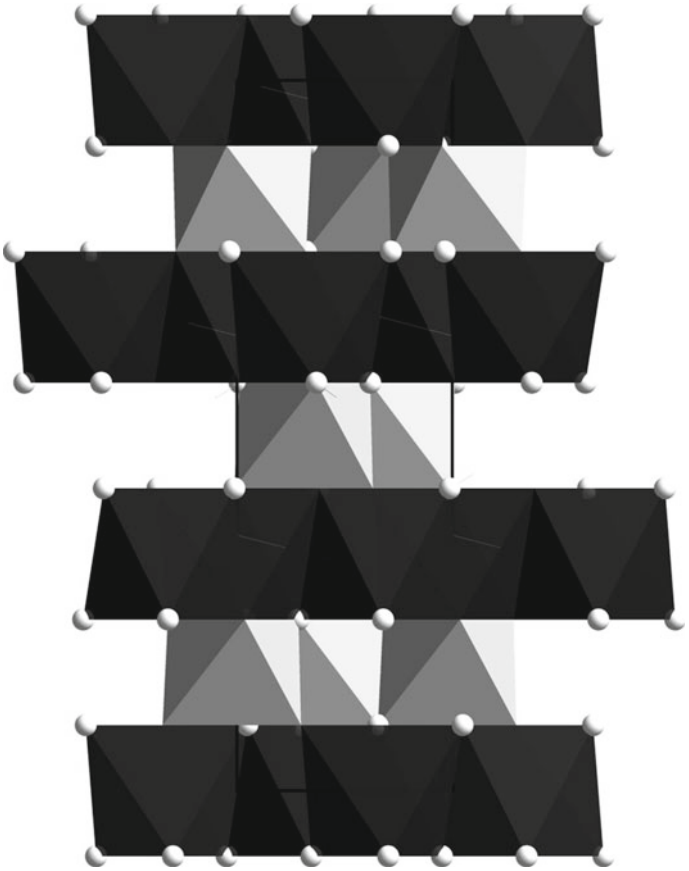

Fig. 4.5 Crystal structure of $MgSiO_3$ akimotoite projected down [010]. The vertical direction represents the c-axis. Mg- and Si-octahedra are depicted in dark and light gray, respectively. The unit cell is outlined (Bindi et al. 2014a)

The compound was found to be orthorhombic, space group *Pbnm*, with the following lattice parameters $a = 4.8213(5)$, $b = 4.9368(6)$, $c = 6.9132(8)$ Å, $V = 164.55(3)$ Å^3 (Bindi et al. 2014b). Chromium-bearing bridgmanite is characterized by the perovskite-type structure. However, the differences from the typical perovskite structure are very remarkable due to tilting of almost ideal Si octahedra (B site) and strong distortions of Mg polyhedra (A site), which change the coordination of an undersized A cation from 12 to 8. Here we can see the shortening of the <X–O> and a lengthening of the <Y–O> distances with respect to the values typically observed for pure $MgSiO_3$ perovskite (Horiuchi et al. 1987). In Cr-bridgmanite, Mg and Si atoms are specifically ordered in the dodecahedral and octahedral sites.

As it was shown above, all phases with the composition of Mg_2SiO_4 (olivine/wadsleyite/ringwoodite) synthesized in the *Fo–MChr* system contain chromium.

Chromium-bearing olivine with 3.2 wt% Cr_2O_3 was obtained at 10 GPa and 1600 °C (run 2632-30). The compound was found to be orthorhombic, space group *Pbnm*, with lattice parameters $a = 4.752(1)$, $b = 10.195(4)$, $c = 5.979(2)$ Å, $V = 289.98(9)$ Å^3.

Increase in pressure results in the formation of **chromium-rich wadsleyite**. A crystal of Cr-wadsleyite (run 2646-10, 14 GPa) of fair diffraction quality was selected for the refinement of structure from single-crystal X-ray diffraction. The orthorhombic unit-cell parameters are the following: $a = 5.6909(5)$ Å, $b = 11.4640(10)$ Å, $c = 8.2406(9)$ Å, $V = 537.62(9)$ Å^3, $Z = 8$, the space group *Imma* (Sirotkina et al. 2018b). The crystal structure of Cr-*Wad* is in a good agreement with previously reported structural data for chromium-rich wadsleyite (Zhang et al. 2016) and is similar to those of other wadsleyite-related compounds. The formula of wadsleyite obtained from the XRD refinement is: $^{M1}(Mg_{1.00})^{M2}(Mg_{0.95}Cr_{0.05})^{M3}(Mg_{0.95}Cr_{0.05})_2{}^{T}(Si_{0.93}Cr_{0.07})_2O_8$ ($Z = 4$), which corresponds to the simplified formula: $(Mg_{1.93}Cr^{3+}_{0.07})(Si_{0.93}Cr^{3+}_{0.07})O_4$ ($Z = 8$).

On the whole, the structural topology of chromium-rich wadsleyite is nearly identical to that of pure wadsleyite (Hazen et al. 2000). Zhang et al. (2016) pointed out that in Cr-bearing hydrous wadsleyite, Cr shows strong preferences for M3 over M1 and M2 sites and it also enters the tetrahedral site (T site); Mg1 does not host Cr in the structure of anhydrous wadsleyite, whereas Mg2 and Mg3 host the same amount of chromium. This crystal-chemical scenario is reflected in the bond distances: the <Mg1–O> bond distance (2.071 Å) is nearly identical to that observed in pure wadsleyite (2.069 Å; Hazen et al. 2000), whereas the <Mg2–O> and <Mg3–O> bond distances (2.081 and 2.085 Å, respectively) are shorter than the corresponding values in pure wadsleyite (2.085 and 2.089 Å; Hazen et al. 2000), due to the entry of the smaller Cr^{3+} cation. Noteworthy, the mean <Si–O> bond distance (1.654 Å) is unaffected by the Cr-for-Si substitution (<Si–O> bond distance for Cr-free Wad (Hazen et al. 2000) is 1.654 Å).

The unit cell parameters were determined by single-crystal X-ray diffraction for two wadsleyite crystals with different chromium contents. The studied Cr-Wad crystals are orthorhombic with space group *Imma* and lattice parameters $a = 5.690(1)$, $b = 11.456(4)$, $c = 8.250(2)$ Å, $V = 537.81(4)$ Å^3 (18 GPa, run 2639-10) for the composition $Mg_{1.95}Cr_{0.10}Si_{0.95}O_4$; $a = 5.686(2)$ Å, $b = 11.452(6)$, $c = 8.246(4)$, and $V = 537.02(1)$ Å^3 (19 GPa, run 2645-10) for the composition $Mg_{1.93}Cr_{0.14}Si_{0.93}O_4$.

Further increase in pressure results in the formation of **ringwoodite** with a higher chromium content. Cr-bearing *Rgw* (21 GPa, run 2649-10) with the composition $Mg_{1.98}Cr_{0.04}Si_{0.98}O_4$ is characterized by cubic symmetry, space group $Fd\bar{3}m$, and lattice parameters $a = 8.063(2)$, $V = 524.23(1)$ Å^3. This value is slightly lower than the a parameter observed for pure Mg_2SiO_4 *Rgw* (Hazen et al. 1993).

The mechanisms of Cr incorporation in *Wad* and *Rgw* are different. The substitution scheme for Cr^{3+} cannot be uniquely determined from the stoichiometry only.

We can identify the typical substitution mechanisms for wadsleyite using both the stoichiometry of wadsleyite and the original structural data. The possible substitution mechanisms for Cr^{3+} incorporation in wadsleyite were previously reported by Gudfinnsson and Wood (1998). These authors considered the following schemes: (1) $3Mg^{2+} = 2Cr^{3+} + vac$, where Cr replaces Mg in the octahedral sites, and the Si content should remain constant (2.0 p.f.u.); (2) $2\,^{VI}Cr^{3+} + {}^{IV}Mg^{2+} = 2\,^{VI}Mg^{2+} + {}^{IV}Si^{4+}$ suggesting the strong octahedral preference of Cr^{3+}, whereas Mg^{2+} replaces tetrahedral Si^{4+} leaving Cr^{3+} exclusively in octahedral sites; (3) $^{VI}Cr^{3+} + {}^{IV}Cr^{3+} = {}^{VI}Mg^{2+} + {}^{IV}Si^{4+}$, where Cr^{3+} enters both tetrahedral and octahedral sites replacing Si and Mg respectively. Considering the composition of the studied wadsleyite on a ternary Si–Mg–Cr diagram (Fig. 4.6), it is evident that the second and third substitution mechanisms illustrate the entry of the $MgCr_2O_4$ end-member to the wadsleyite structure. Hence, we can see that the composition of chromium-rich wadsleyite can be described by one of these two reactions.

The probable mechanism of Cr incorporation in *Wad* is also evident from the negative correlation between Cr and Si (Fig. 4.7) with an angular trend line coefficient of −0.5 observed for *Wad*. Thus, we deal with cation substitutions in both tetrahedral and octahedral sites. In the first mechanism, Mg replaces Si in the tetrahedral

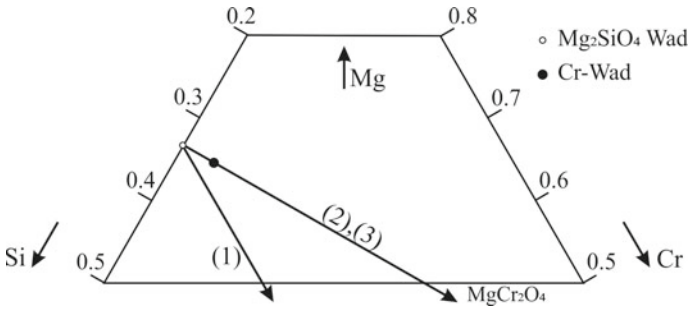

Fig. 4.6 Cr–Mg–Si diagram illustrating the possible mechanisms and trends of Cr incorporation in wadsleyite: (1) $3\,Mg^{2+} = 2Cr^{3+} + vac$, (2) $2\,^{VI}Cr^{3+} + {}^{IV}Mg^{2+} = 2\,^{VI}Mg^{2+} + {}^{IV}Si^{4+}$, and (3) $^{VI}Cr^{3+} + {}^{IV}Cr^{3+} = {}^{VI}Mg^{2+} + {}^{IV}Si^{4+}$ (Gudfinnsson and Wood 1998)

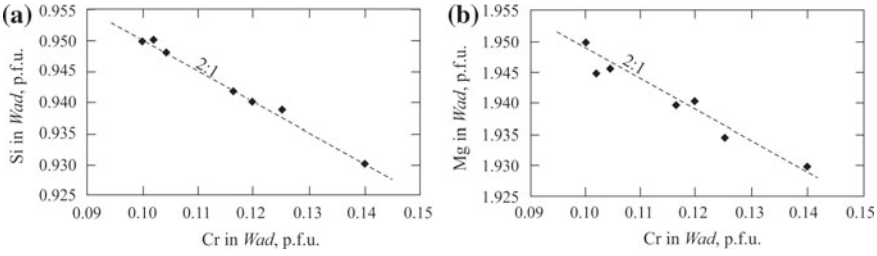

Fig. 4.7 Negative correlation between Cr and Si (**a**) and Cr and Mg (**b**) in wadsleyite synthesized in the system Mg_2SiO_4–$MgCr_2O_4$ at 12–19 GPa and 1600 °C

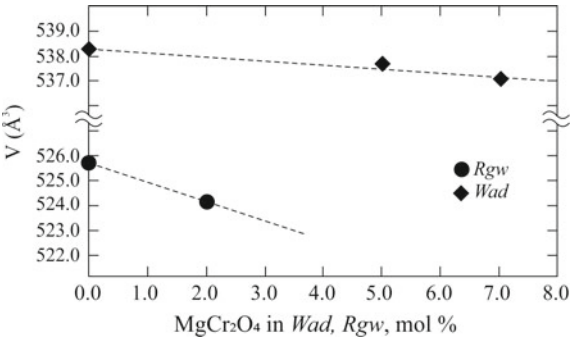

Fig. 4.8 Influence of Cr on cell volumes of wadsleyite and ringwoodite. The data for Mg_2SiO_4 *Wad*/*Rgw* are taken from Finger et al. (1993), Hazen et al. (1993)

site (inducing an increase in the size) and Cr substitutes for Mg in the octahedral sites (inducing a decrease in the size). The second mechanism has a similar effect, which is expressed in Cr substitution for both Si in the tetrahedral site (inducing an enlargement) and Mg in the octahedral site (inducing a decrease). It seems that lengthening of the T–O bond distances is perfectly counterbalanced by shortening of the M–O bond distances, thus provoking an almost unchanged unit-cell volume (Fig. 4.8). However, single-crystal X-ray observations show that the third substitution mechanism is preferable for wadsleyite.

Rgw is characterized by the negative correlation between Cr and Si with an angular coefficient of −0.5 (Fig. 4.7). *Rgw* has the spinel-type structure and, therefore, we suggest a different mechanism for Cr incorporation in this phase: Mg substitutes for Si in the tetrahedral site, whereas Cr fully enters Mg-octahedra by the following scheme: $2^{VI}Cr^{3+} + {}^{IV}Mg^{2+} = 2^{VI}Mg^{2+} + {}^{IV}Si^{4+}$. This substitution would be analogous to that observed in spinel $MgAl_2O_4$ with addition of the $MgCr_2O_4$ component. The unit-cell volume of *Rgw* decreases more significantly due the Mg-for-Cr and Si-for-Cr substitutions in comparison with *Wad* (Fig. 4.8).

XRD study of a Cr-bearing (Cr = 0.08 atoms per formula unit) ringwoodite crystal synthesized at 20 GPa and 1600 °C in the magnesiochromite (*MChr*)–forsterite (*Fo*) system showed that it had a completely inverted structure leading to the ideal formula $[MgSi]MgO_4$ (Bindi et al. 2018). Inverse ringwoodite (i*Rgw*) is associated with $Mg_2Cr_2O_5$ phase with modified ludwigite-type structure (m*Ld*), and garnet (*Grt*) (Fig. 4.9) and has the following composition: $[Mg_{1.96(5)}Si_{0.96(3)}Cr_{0.08(3)}]O_4$. The compound is cubic with space group $Fd\bar{3}m$ and the following unit-cell parameters: $a = 8.2364(2)$ Å, $V = 558.74(4)$ Å^3, and $Z = 8$. It is interesting, that the cubic unit-cell volume is 558.74(4) Å, 1.4(1)% less than that reported for the natural BWJ ringwoodite with inverse-spinel structure (Griffin et al. 2016) (566.8 Å), yet 5.9% greater than normal ringwoodite (Hazen et al. 1993) (525.7 Å). Mean bond distance of (Mg,Si)-octahedron (1.970(2) Å) of the synthesized phase is characterized by the intermediate position between the value of 2.072 Å observed for normal ringwoodite (Hazen et al. 1993) (with all Mg in the octahedral site) and 1.757 Å observed for stishovite (Hill et al. 1983). The Mg-tetrahedron shows a mean bond distance of 1.945(4) Å, slightly larger than the tetrahedral Mg in $Ca_2MgSi_2O_7$ akermanite

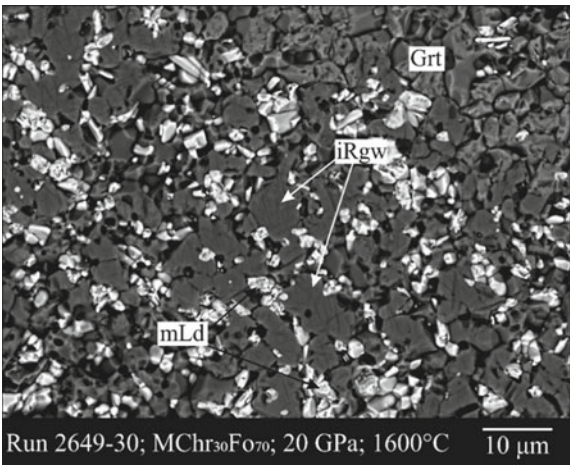

Fig. 4.9 SEM-BSE image of the experimental sample (run 2649-30) obtained at P = 20 GPa and T =1600 °C with the magnesiochromite (*MChr*)–forsterite (*Fo*) composition $MChr_{30}Fo_{70}$ (Bindi et al. 2018). Inverse ringwoodite (i*Rgw*) dominated the run products, accompanied by $Mg_2Cr_2O_5$ (m*Ld*) and garnet (*Grt*)

(1.92 Å) (Kimata and Ii 1981). Similar values were found for the B–O and A–O mean bond distances for the natural BWJ spinel (Griffin et al. 2016), i.e. 1.945 and 1.984 Å, respectively. Cr is totally concentrated in the octahedral site together with Mg and Si, consistent with the typical coordination of Cr^{3+} with oxygen. Likewise, in the BWJ phase (Griffin et al. 2016), the minor Fe and Al were found to be disordered at the octahedral site together with Mg and Si.

$MgCr_2O_4$ phase with the calcium titanate-type structure is stable at a pressure of >18 GPa for chromium-rich bulk compositions of the *Maj–Knr* and *Fo–MChr* systems. The compound was found to crystallize with the orthorhombic symmetry, space group *Bbmm*, and the following lattice parameters: $a = 9.468(1)$, $b = 9.670(1)$, $c = 2.845(1)$ Å, $V = 260.5(1)$ Å^3 (Bindi et al. 2014c). Magnesium was found to fully occupy the eightfold-coordinated A site (with a mean bond distance of 2.289 Å) and Cr, the octahedral B site (mean: 1.986 Å). The successful synthesis of $MgCr_2O_4$ with ($CaTi_2O_4$)-type structure and its structural characterization demonstrate the stability of the new post-spinel phase.

$Mg(Cr,Mg)(Si,Mg)O_4$ with a distorted orthorhombic calcium titanate ($CaTi_2O_4$)-type structure is stable in the pressure range of 12–18 GPa for Cr-poor bulk compositions in the Mg_2SiO_4–$MgCr_2O_4$ system. The compound was found to be orthorhombic, space group $Cmc2_1$, with lattice parameters $a = 2.8482(1)$, $b = 9.4592(5)$, $c = 9.6353(5)$ Å, $V = 259.59(1)$ Å^3, and $Z = 4$ (Bindi et al. 2015).

The difference from the classic *Cmcm* space group (Bindi et al. 2014c; Yamanaka et al. 2008) and the loss of the inversion center is due to the ordering of the octahedral cations, which is required to either account for the electron density at those sites or justify the variation of the octahedral bond distances. In detail, Cr (with minor Mg) is mainly hosted at the M1 site, Si (with minor Mg) is hosted at the M2 site, whereas the eightfold-coordinated site is fully occupied by Mg. The linkage among the octahedra is provided by edge and corner sharing. Such an ordered distribution induces a distortion thus provoking a change in coordination of Mg (Fig. 4.10), which

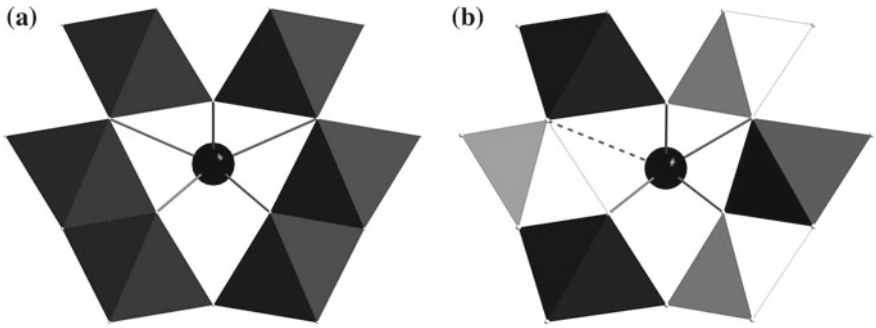

Fig. 4.10 Coordination environment of the Mg polyhedron in the crystal structure of $Mg(Cr,Mg)(Si,Mg)O_4$ (**a**) and in $MgCr_2O_4$ (**b**, Bindi et al. 2014c). M1 (Cr,Mg) and M2 (Si,Mg) cations are depicted as dark gray and white polyhedra, respectively, whereas the eightfold-coordinated Mg cations as black spheres. The long Mg-O1 bond distance in the structure of $Mg(Cr,Mg)(Si,Mg)O_4$ is indicated with a dashed line

becomes sevenfold-coordinated instead of the usual eightfold coordination observed in post-spinel phases (Yamanaka et al. 2008).

The crystal structure and chemical composition of a crystal of $(Mg_{14-x}Cr_x)(Si_{5-x}Cr_x)O_{24}$ ($x \approx 0.30$) anhydrous Phase B (*anhB*) synthesized in the model system $MgCr_2O_4$–Mg_2SiO_4 at 12 GPa and 1600 °C have been also investigated (Bindi et al. 2016). The compound was found to be orthorhombic, space group *Pmcb*, with the following lattice parameters: $a = 5.900(1)$, $b = 14.218(2)$, $c = 10.029(2)$ Å, $V = 841.3(2)$ Å^3 and $Z = 2$. Chromium was found to substitute for both Mg at the M3 site (with a mean bond distance of 2.145 Å) and Si at the octahedral Si1 site (mean bond distance: 1.856 Å), according to the reaction $Mg^{2+} + Si^{4+} = 2Cr^{3+}$. Such substitutions cause a reduction in the volume of the M3 site and an increase in the volume of the Si-dominant octahedron with respect to the values typically observed for pure *anhB* (Finger et al. 1989, 1991) and Fe^{2+}-bearing *anhB* (Hazen et al. 1992).

Some experimental samples obtained in the *Fo–MChr* system at 12–24 GPa contain a more chromium-rich $Mg_2Cr_2O_5$ (m*Ld*) high-pressure phase, which has been studied by Ishii et al. (2017) using single-crystal X-ray diffraction. The authors show that the **$Mg_2Cr_2O_5$ phase** has modified ludwigite (mLd)-type structure (space group: *Pbam*), and the lattice parameters are $a = 9.6091(2)$, $b = 12.4324(2)$, $c = 2.8498(1)$ Å, $V = 340.44(1)$ Å^3 ($Z = 4$). The *mLd* structure has four different $(Mg,Cr)O_6$ octahedral sites (M1–M4) with partially disordered Mg^{2+} and Cr^{3+} and a MgO_6 trigonal prism site (M5) in tunnel space formed by edge- and corner-shared M1–M4 sites.

4.2 Influence of Chromium on Structural Patterns of Mantle Phases and Phase Transitions

It is evident from some theoretical and experimental studies (e.g., Zhang and Weidner 1999; Panero et al. 2006; Andrault 2007) that even small concentrations of minor elements (for example Al and Cr) significantly influence the unit cell parameters, density and compressibility of major mantle minerals. In this regard, the use of pure $MgSiO_3$-akimotoite and $MgSiO_3$-bridgmanite for modelling the composition and properties of the transition zone and lower mantle can simplify and distort the real situation.

We believe that the most correct approach is to compare the influence of two minor elements (aluminum and chromium) on the unit-cell parameters of deep minerals (garnet, akimotoite and bridgmanite). This is due to the fact that the experimental works of recent years provided some quantitative information on the influence of these minor elements on structural features of deep mantle phases (Andrault 2007 and others), and very thoroughly evidenced their influence on the majorite-pyrope and knorringite-pyrope solid solutions.

Previously it was established that an increase in the content of majorite component in garnet along the majorite-pyrope join results in the gradual increase in cell parameters and, then, in the cubic/tetragonal transition (Akaogi and Akimoto, 1977; Parise et al. 1996). This transition occurs at a high majorite content (>80 mol% *Maj*) (Parise et al. 1996). Chromium-bearing majoritic garnet is characterized by decreasing the unit-cell parameters with increasing of majoritic component (Fig. 4.2) due to the coupled substitution $2Cr^{3+} = Mg^{2+} + Si^{4+}$ ($r(^{VI}Cr^{3+}) = 0.615$; $r(^{VI}Mg^{2+}) = 0.72$; $r(^{VI}Si^{4+}) = 0.40$). It is important to note that even a small concentration of chromium stabilizes the cubic symmetry of majoritic garnet (3 mol% *Knr*).

As it was shown above, incorporation of chromium in akimotoite results in the increase of the *a* parameter from pure $MgSiO_3$ (Horiuchi et al. 1982) to pure Cr_2O_3 (Ovsyannikov and Dubrovinsky 2011) with lesser variations in the *c* parameter (Bindi et al. 2014a). An opposite behaviour was observed for Al-bearing $MgSiO_3$ akimotoite (Fig. 4.11) (Akaogi et al. 2002). With increasing the Al content in the structure, indeed, a progressive decrease in the *c* parameter and a substantially unchanged *a* parameter was observed, which resulted in general reduction in the unit-cell the volume of akimotoite (Akaogi et al. 2002).

The unit-cell parameters of bridgmanite are strongly influenced by the entry of Cr into the structure (Bindi et al. 2014b), whereas the influence of aluminium is less significant. Incorporation of both chromium and aluminium in bridgmanite results in general increase of the cell volume (Fig. 4.11) in comparison with that of pure $MgSiO_3$ bridgmanite (Dobson and Jacobsen 2004). For Cr-rich bridgmanite, we observed an increase of all the values with the most affected being the *a* parameter, whereas the increase in the *b* and *c* parameters is insignificant (Bindi et al. 2014b). Al-bearing bridgmanite shows the opposite trend (Kojitani et al. 2007).

Thus, we can conclude that incorporation of chromium increases the unit-cell parameters of some high-pressure phases, such as bridgmanite and akimotoite,

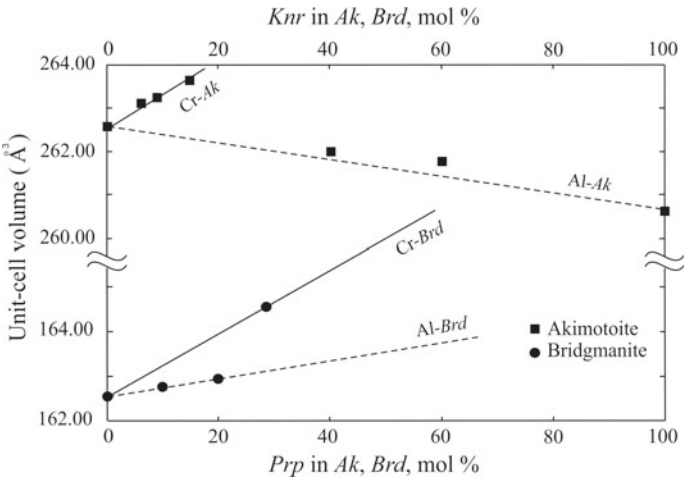

Fig. 4.11 Influence of chromium and aluminium on unit-cell volumes of akimotoite (Kojitani et al. 2007) and bridgmanite (Dobson and Jacobsen 2004)

whereas the influence of chromium on the wadsleyite and ringwoodite structures is less pronounced. As it is evident from natural and experimental data, bridgmanites are often characterized by significant aluminium contents, whereas the content of chromium in them is much lower. This fact can be explained by the different effects of Cr and Al on the increase of the cell volume of bridgmanite (Fig. 4.11). Incorporation of aluminum in high-pressure bridgmanite is more preferable than that of chromium due to less significant expansion of the unit cell of bridgmanite.

Figure 4.12 shows a comparison of the chromium and aluminium influence on the cell volume of garnet and bridgmanite. Bridgmanites are characterized by slightly different trends for Al and Cr incorporation (~3°), whereas entry of Cr and Al in garnet results in significant difference between cell volumes of knorringite- and pyrope-rich garnets (~37° between *Maj–Prp* and *Maj–Knr* trends). In contrast to the majorite–pyrope system with decrease of the cell volume with increasing pyrope content, the majorite–knorringite join shows an increase of the cell volume with increasing knorringite content (Figs. 4.2 and 4.12).

To understand the influence of chromium on the structure of the deep minerals, we used the octahedral angle variance (σ^2), which was proposed to describe the degree of distortion of coordination polyhedra (Robinson et al. 1971). Interestingly, the Cr-for-Mg substitution induces a regularization of the X octahedral site controlled by decrease in the octahedral angle variance σ^2 (Table 4.2), which changes from 143.43 in pure $MgSiO_3$ (Horiuchi et al. 1982) to 45.47 in Cr_2O_3 (Ovsyannikov and Dubrovinsky 2011). Such a decrease in distortion is also evident for the Cr-for-Si substitution which changes from 52.77 in pure $MgSiO_3$ (Horiuchi et al. 1982) to 45.47 in Cr_2O_3 (Ovsyannikov and Dubrovinsky 2011).

The opposite behaviour is typical of Cr-bridgmanite. The Cr-for-Si substitution also induces a distortion of the octahedral site quantifiable with an increase of the

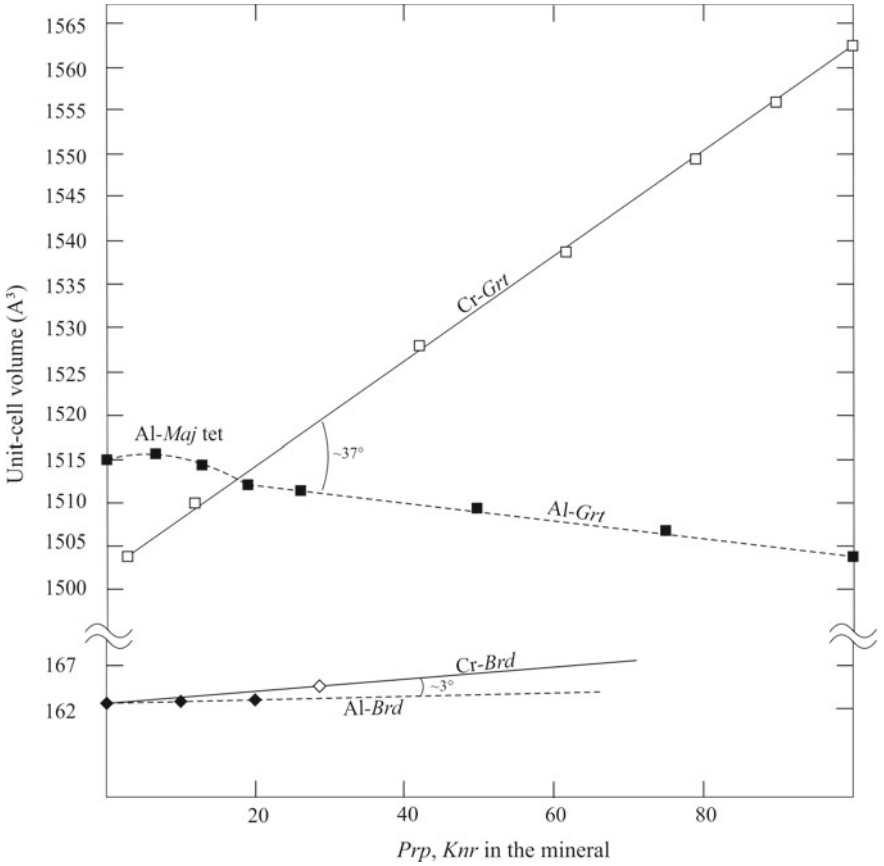

Fig. 4.12 Influence of chromium and aluminum on the unit-cell volumes of garnet and bridgmanite. The data for pure $MgSiO_3$ *Brd* are taken from Dobson and Jacobsen (2004); Al-*Brd* (Kojitani et al. 2007); Al-*Maj* and Al-*Grt* (Parise et al. 1996)

octahedral angle variance σ^2 (Robinson et al. 1971) from 1.56 in pure $MgSiO_3$ (Dobson and Jacobsen, 2004) to 7.48 in the studied crystal. A similar value (σ^2 = 7.63) can be calculated for $(Mg_{1-x}Al_x)(Si_{1-x}Al_x)O_3$ with x = 0.050 (Kojitani et al. 2007). Thus, substitution of a trivalent cation for Si in the perovskite structure increases the distortion of the almost ideal [SiO_6] octahedra.

We examined the effect of Al on chromium-rich high-pressure phases such as $Mg_2Cr_2O_5$ with modified ludwigite-type structure (Kojitani et al. 2010; Ishii et al. 2017) and $MgCr_2O_4$ with calcium titanate-type structure (Bindi et al. 2014c). High-pressure phase $Mg_2Al_2O_5$ is characterized by smaller lattice parameters and unit-cell volume ($V = 319.03(3)$ Å^3). The important factor for the stabilizing of the mLd-type structure is a high octahedral-preference of Cr^{3+} and Al^{3+}; thus, Mg^{2+} fully occupies the trigonal-prism site.

Table 4.2 Octahedral angle variance for akimotoite and bridgmanite depending on chromium content

Ak **$(Mg_{1-x}Cr_x)(Si_{1-x}Cr_x)O_3$**				
x = 0	x = 0.015	x = 0.023	x = 0.038	x = 1
σ^2 for MgO_6 octahedra				
143.43[a]	141.57	136.09	126.94	45.47[b]
σ^2 for SiO_6 octahedra				
52.77[a]	52.33	49.53	46.27	45.47[b]
Brd **$(Mg_{1-x}Cr_x)(Si_{1-x}Cr_x)O_3$**				
x = 0		x = 0.072		
σ^2 for SiO_6 octahedra				
1.56[c]		7.48		

[a]Horiuchi et al. (1982), [b]Ovsyannikov and Dubrovinsky (2011), [c]Dobson and Jacobsen (2004)

Kojitani et al. (2007) studied the $MgAl_2O_4$–Mg_2SiO_4 system up to 60 mol% $MgAl_2O_4$ at 20–27 GPa and 1600 °C. The authors showed that $MgAl_2O_4$ with calcium ferrite-type structure is stable at pressures above 23 GPa. The Si content in *Cf* phase decreases with pressure (Kojitani et al. 2007). An opposite behaviour was observed for $MgCr_2O_4$ with calcium titanate-type structure. We observed an increase in the Si content of this phase with pressure (Sirotkina et al. 2018a). Another important difference is observed for incorporation of Si in the structure of post-spinel phases. The highest solubility of Mg_2SiO_4 in *Cf* is 35 mol% at 24 GPa (Kojitani et al. 2007), whereas the *Fo* content in *Ct* does not exceed 20 mol% (Sirotkina et al. 2018a). However, it is important to note, that an increase in the Si content in the system results in the formation of a Si-rich new post-spinel phase Mg(Cr,Mg)(Si,Mg)O_4 with a distorted calcium-titanate ($CaTi_2O_4$) structure type (Bindi et al. 2015).

The influence of chromium on the phase relations in the $Mg(Cr,Al)_2O_4$ system is also significant. As is evident from our studies (Sirotkina et al. 2018a), $MgCr_2O_4$ (*MChr*) decomposes into $Mg_2Cr_2O_5$ + Cr_2O_3 phase assemblage at ~12 GPa and 1600 °C. This association changes to $MgCr_2O_4$ with calcium titanate-type (*Ct*) structure at ~18 GPa and 1600 °C. With increasing pressure, $MgAl_2O_4$ decomposes with the formation of MgO + Al_2O_3 phase assemblage at 1600 °C in the pressure range of 18–26 GPa (Kojitani et al. 2007, 2010). $MgAl_2O_4$ (*Sp*) dissociates into $Mg_2Al_2O_5$ + Al_2O_3 at ~20 GPa and 2000 °C. The formation of $MgAl_2O_4$ (*Cf*) occurs at a pressure of 26 GPa and 2000 °C (Kojitani et al. 2010). Comparison of the parameters of phase transitions for $MgAl_2O_4$ and $MgCr_2O_4$ suggests that with increasing chromium content in the system, the pressure and temperature of transition might slightly decrease. Thus, substitution of Al^{3+} with Cr^{3+} will expand the stability field of ($Mg_2(Cr,Al)_2O_5$ + $(Cr,Al)_2O_3$) to the lower pressure and temperature area.

Based on the results of our runs and previously published data (Sirotkina et al. 2015), we assume that even a small Cr admixture in deep minerals has a certain effect on the physical properties of deep minerals and local migration of the global seismic boundaries in the Earth's mantle. Likewise, Dymshits et al. (2014) showed that the

addition of ~20 mol% of *Knr* component to pyropic garnet (which corresponds to the actually measured concentrations in natural garnets from inclusions in diamonds) decreases the *P*- and *S*-velocities by 1.6% and the density of garnet increases by 1.7% compared to pure pyrope. These results show the importance of accounting for *Knr* end-member in accurate estimation of mantle garnet acoustic velocities.

Interpretation of the deep seismic boundaries is based on the different models of the mantle composition. The pyrolite model (Ringwood 1966) suggests the key role of the phase transformations of $(Mg,Fe)_2SiO_4$ ($\geq$57 vol% *Ol* in pyrolite) in the formation of global boundaries: *Ol* = *Wad* (~15 GPa, "410" km), *Wad* = *Rgw* (~20.5 GPa), *Rgw* = Prv + fPer (~23 GPa). Figure 4.13 shows the relative positions of the major phase transitions in the model systems $Mg_4Si_4O_{12}$–$Mg_3Cr_2Si_3O_{12}$ (Sirotkina et al. 2015) and Mg_2SiO_4–$MgCr_2O_4$ (Sirotkina et al. 2018a) depending on the bulk Cr concentrations. It is established that addition of Cr to the system moves the boundaries of phase transformations *Ol/Wad* and *Wad/Rgw* to the lower pressure area. Increase in the Cr concentration results in expansion of the area of *Ol/Wad* and *Wad/Rgw* phase transitions at the expense of appearance of divariant fields (*Ol* + *Wad*, *Wad* + *Rgw*), which may explain the gradual character of the "410" and "520" boundaries in some local areas of the mantle (Van der Maijde et al. 2003).

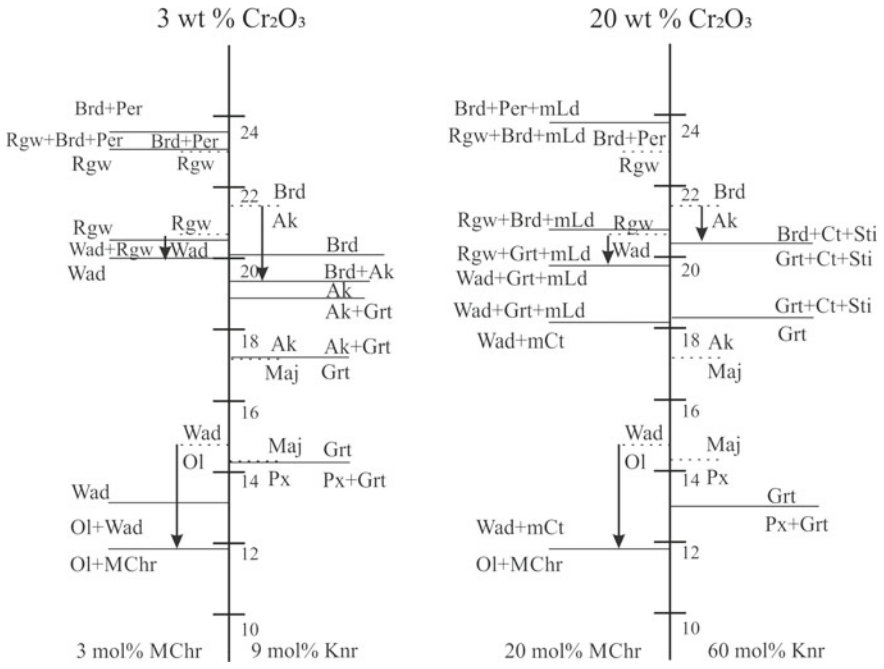

Fig. 4.13 Generalized diagram of phase assemblages of Cr-bearing minerals in the Earth's mantle based on the results of experiments in the Mg_2SiO_4–$MgCr_2O_4$ (Sirotkina et al. 2018a) and $Mg_4Si_4O_{12}$–$Mg_3Cr_2Si_3O_{12}$ (Sirotkina et al. 2015) at 10–24 GPa and 1600 °C

These seismic boundaries may be explained by other phase transitions as well. For example, the formation of the "410", "520", and "660" boundaries is interpreted by transitions in the (Mg,Fe)SiO_3 constituent of the pyrolytic mantle: *Maj* (garnet-type structure)–*Ak* (ilmenite-type structure)–*Brd* (perovskite-type structure) (Vacher et al. 1998). The results of some geophysical studies suggest local "splitting" of the "520" and "660" seismic boundaries (Deuss and Woodhouse 2001). In addition, all three boundaries are heterogeneous by the depth and thickness.

With increasing pressure, Cr-bearing $MgSiO_3$ *Ak* becomes unstable and transforms to the perovskite-type phase (*Brd*) at ~19–21 GPa. Cr incorporation changes the cell volume of *Brd* significantly and increases the mineral density. An effect of Cr incorporation is mostly impacted on the decrease of pressure of bridgmanite formation from ~22 GPa for pure $MgSiO_3$ to ~19.5 for chromium-bearing *Brd* (Sirotkina et al. 2015). Thus, addition of Cr to the system results in migration of the *Ak*/*Brd* boundary to a lower pressure area in comparison to the Cr-free system (Fig. 4.13). One more effect of increasing Cr concentration may be reflected in the local gradual character of the sharp boundaries at the expense of appearance of the *Maj* + *Ak*, *Maj* + *Brd*, and *Ak* + *Brd* divariant fields.

References

Akaogi M, Akimoto A (1977) Pyroxene-garnet solid-solution equilibria in the system $Mg_4Si_4O_{12}$–$Mg_3Al_2Si_2O_{12}$ and $Fe_4Si_4O_{12}$–$Fe_3Al_2Si_3O_{12}$ at high pressures and temperatures. Phys Earth Planet Inter 111:90–106

Akaogi M, Tanaka A, Ito E (2002) Garnet–ilmenite–perovskite transitions in the system $Mg_4Si_4O_{12}$–$Mg_3Al_2Si_3O_{12}$ at high pressures and high temperatures: phase equilibria, calorimetry and implications for mantle structure. Phys Earth Planet Inter 132:303–324

Andrault D (2007) Properties of lower-mantle Al-(Mg,Fe)SiO_3 perovskite, vol 421 (Special papers). Geological Society of America, pp 15–36

Angel RJ, Finger LW, Hazen RM, Kanzaki M, Weidner DJ, Liebermann RC, Veblen DR (1989) Structure and twinning of single-crystal $MgSiO_3$ garnet synthesized at 17 GPa and 1800 °C. Am Mineral 74:509–512

Bindi L, Sirotkina EA, Bobrov AV, Irifune T (2014a) Chromium solubility in $MgSiO_3$ ilmenite at high pressure. Phys Chem Miner 41:519–526

Bindi L, Sirotkina EA, Bobrov AV, Irifune T (2014b) Chromium solubility in perovskite at high pressure: the structure of $(Mg_{1-x}Cr_x)(Si_{1-x}Cr_x)O_3$ (with x = 0.07) synthesized at 23 GPa and 1600 °C. Am Mineral 99:866–869

Bindi L, Sirotkina EA, Bobrov AV, Irifune T (2014c) X-ray single-crystal structural characterization of $MgCr_2O_4$, a post-spinel phase synthesized at 23 GPa and 1600 °C. J Phys Chem Solids 75:638–641

Bindi L, Sirotkina EA, Bobrov AV, Irifune T (2015) Structural and chemical characterization of $Mg[(Cr,Mg)(Si,Mg)]O_4$, a new post-spinel phase with six-fold coordinated silicon. Am Mineral 100:1633–1636

Bindi L, Sirotkina EA, Bobrov AV, Nestola F, Irifune T (2016) Chromium solubility in anhydrous phase B. Phys Chem Miner 43:103–110

Bindi L, Griffin WL, Panero WR, Sirotkina E, Bobrov A, Irifune T (2018) Synthesis of inverse ringwoodite sheds light on the subduction history of Tibetan ophiolites. Sci Rep 8:5457. https://doi.org/10.1038/s41598-018-23790-9

Bykova EA, Bobrov AV, Sirotkina EA, Bindi L, Ovsyannikov SV, Dubrovinsky LS, Litvin YuA (2014) X-ray single-crystal and Raman study of knorringite, $Mg_3(Cr_{1.58}Mg_{0.21}Si_{0.21})Si_3O_{12}$, synthesized at 16 GPa and 1600 °C. Phys Chem Miner 41(4):267–272

Deuss A, Woodhouse J (2001) Seismic observations of splitting of the mid-transition zone discontinuity in the Earth's mantle. Science 294:354–357

Dobson DP, Jacobsen SD (2004) The flux growth of magnesium silicate perovskite single crystals. Am Mineral 89:807–811

Dymshits AM, Litasov KD, Sharygin IS, Shatskiy A, Ohtani E, Suzuki A, Funakoshi K (2014) Thermal equation of state of majoritic knorringite and its significance for continental upper mantle. J Geophys Res Solid Earth 119(11):8034–8046

Finger LW, Ko J, Hazen RM, Gasparik T, Hemley RJ, Prewitt CT, Weidner DJ (1989) Crystal chemistry of phase B and an anhydrous analogue: implications for water storage in the upper mantle. Nature 341:140–142

Finger LW, Hazen RM, Prewitt CT (1991) Crystal structures of $Mg_{12}Si_4O_{19}(OH)_2$ (phase B) and $Mg_{14}Si_5O_{24}$ (phase AnhB). Am Mineral 76:1–7

Finger LW, Hazen RM, Zhang J, Ko J, Navrotsky A (1993) The effect of Fe on the crystal structure of wadsleyite β-$(Mg_{1-x}Fe_x)_2SiO_4$, $0.00 < x < 0.40$. Phys Chem Miner 19:361–368

Gasparik T (2002) Experimental investigation of the origin of majoritic garnet inclusions in diamonds. Phys Chem Miner 29(3):170–180

Griffin WL, Afonso JC, Belousova EA, Gain SE, Gong XH, Gonzalez-Jimenez JM, Satsukawa T (2016) Mantle recycling: transition zone metamorphism of Tibetan ophiolitic peridotites and its tectonic implications. J Petrol 57(4):655–684

Gudfinnsson GH, Wood BJ (1998) The effect of trace elements on the olivine–wadsleyite transformation. Am Mineral 83:1037–1044

Hazen RM, Finger LW, Ko J (1992) Crystal chemistry of Fe-bearing anhydrous phase B: implications for transition zone mineralogy. Am Mineral 77:217–220

Hazen RM, Downs RT, Finger LW (1993) Crystal chemistry of ferromagnesian silicate spinels: evidence for Mg–Si disorder. Am Mineral 78:1320–1323

Hazen RM, Weinberger MB, Yang H, Prewitt CT (2000) Comparative high-pressure crystal chemistry of wadsleyite, β-$(Mg_{1-x}Fe_x)_2SiO_4$, with $x = 0$ and 0.25. Am Mineral 85(5–6):770–777

Heinemann S, Sharp TG, Seifert F, Rubie DC (1997) The cubic-tetragonal phase transition in the system majorite ($Mg_4Si_4O_{12}$)–pyrope ($Mg_3Al_2Si_3O_{12}$), and garnet symmetry in the Earth's transition zone. Phys Chem Miner 24:206–221

Hill RJ, Newton MD, Gibbs GV (1983) A crystal chemical study of stishovite. J Solid State Chem 47:185–200

Horiuchi H, Hirano M, Ito E, Matsui Y (1982) $MgSiO_3$ (ilmenite-type): single crystal X-ray diffraction study. Am Mineral 67:788–793

Horiuchi H, Ito E, Weidner DJ (1987) $MgSiO_3$ (perovskite-type): single crystal X-ray diffraction study. Am Mineral 72:357–360

Ishii T, Tsujino N, Arii H, Fujino K, Miyajima N, Kojitani H, Kunimoto T, Akaogi M (2017) A shallow origin of so-called ultrahigh-pressure chromitites, based on single-crystal X-ray structure analysis of the high-pressure $Mg_2Cr_2O_5$ phase, with modified ludwigite-type structure. Am Mineral 102:2113–2118

Juhin A, Morin G, Elkaim E, Frost DJ, Fialin M, Juillot F, Calas G (2010) Structure refinement of a synthetic knorringite, $Mg_3(Cr_{0.8}Mg_{0.1}Si_{0.1})_2(SiO_4)_3$. Am Mineral 95:59–63

Kimata M, Ii N (1981) The crystal structure of synthetic åkermanite, $Ca_2MgSi_2O_7$. Neues Jahr Min Monat 144:254–267

Kojitani H, Hisatomi R, Akaogi M (2007) High-pressure phase relations and crystal chemistry of calcium ferrite-type solid solutions in the system $MgAl_2O_4$–Mg_2SiO_4. Am Mineral 92:1112–1118

Kojitani H, Enomoto A, Tsukamoto S, Akaogi M, Miura H, Yusa H (2010). High-pressure high-temperature phase relations in $MgAl_2O_4$. J Phys Conf Ser 215(1):012098 (IOP Publishing)

McMillan P, Akaogi M, Ohtani E, Williams Q, Nieman R, Sato R (1989) Cation disorder in garnets along the $Mg_3Al_2Si_3O_{12}$–$Mg_4Si_4O_{12}$ join: an infrared, Raman and NMR study. Phys Chem Miner 16(5):428–435

Ottonello G, Bokreta M, Sciuto PF (1996) Parameterization of energy and interactions in garnets: end-member properties, pp 429–447

Ovsyannikov S, Dubrovinsky L (2011) High-pressure high-temperature synthesis of Cr_2O_3 and Ga_2O_3. High Pres Res 31:23–29

Panero WR, Akber-Knutson S, Stixrude L (2006) Al_2O_3 incorporation in $MgSiO_3$ perovskite and ilmenite. Earth Planet Sci Lett 252:152–161

Parise J, Wang Y, Dwanmesia GD, Zhang J, Sinelnikov Y, Chmielowski J, Weidner DJ, Liebermann RC (1996) The symmetry of garnets on the pyrope ($Mg_3Al_2Si_3O_{12}$)–majoritic ($MgSiO_3$) join. Geophys Res Lett 23(25):3799–3802

Ringwood AE (1966) The chemical composition and origin of the Earth. In: Hurley PM (ed) Advances in Earth science. M.I.T. Press, Cambridge, pp 287–356

Robinson K, Gibbs GV, Ribbe PH (1971) Quadratic elongation: a quantitative measure of distortion in coordination polyhedra. Science 172(3983):567–570

Sirotkina EA, Bobrov AV, Bindi L, Irifune T (2015) Phase relations and formation of chromium-rich phases in the system $Mg_4Si_4O_{12}$–$Mg_3Cr_2Si_3O_{12}$ at 10–24 GPa and 1,600 °C. Contrib Mineral Petrol 169:2. https://doi.org/10.1007/s00410-014-1097-0

Sirotkina EA, Bobrov AV, Bindi L, Irifune T (2018a) Chromium-bearing phases in the Earth's mantle: evidence from experiments in the Mg_2SiO_4–$MgCr_2O_4$ system at 10–24 GPa and 1600 °C. Am Miner 103(1):151–160

Sirotkina EA, Bindi L, Bobrov AV, Aksenov SM, Irifune T (2018b) Synthesis and crystal structure of chromium-bearing anhydrous wadsleyite. Phys Chem Minerals 45(4):361–366. https://doi.org/10.1007/s00269-017-0926-x

Vacher P, Mocquet A, Sotin C (1998) Computations of seismic profiles from mineral physics: the importance of the non-olivine components for explaining the 660 km depth discontinuity. Phys Earth Planet Inter 106:275–298

Van der Maijde M, Marone F, Giardini D, van der Lee S (2003) Seismic evidence for water deep in Earth's upper mantle. Science 300:1556–1558

Yamanaka T, Uchida A, Nakamoto Y (2008) Structural transition of post-spinel phases $CaMn_2O_4$, $CaFe_2O_4$, and $CaTi_2O_4$ under high pressures up to 80 GPa. Am Mineral 93:1874–1881

Yang J-S, Dobrzhinetskaya L, Bai W-J, Fang Q-S, Robinson PT, Zhang J, Green HW (2007) Diamond- and coesite-bearing chromitites from the Luobusa ophiolite, Tibet. Geology 35:875–878

Zhang J, Weidner DJ (1999) Thermal equation of state of aluminum-enriched silicate perovskite. Science 284:782–784

Zhang L, Smyth JR, Allaz J, Kawazoe T, Jacobsen SD, Jin Z (2016) Transition metals in the transition zone: crystal chemistry of minor element substitution in wadsleyite. Am Miner 101:2322–2330

Chapter 5
Implication of Experimental Results to Geochemistry of Cr in the Earth's Mantle

The phase associations occurring at various depths of the Earth's mantle are widely abundant among inclusions in natural diamonds (Stachel 2001; Moore and Gurney 1985; Scott Smith et al. 1984; Harte et al. 1999; and others). The complex analysis of the *P–T* regime of the mantle allows us to define a series of phase transitions and chemical reactions along the adiabatic *P–T* gradient under the conditions of the asthenosphere (>200 km) and transition zone (410−660 km). From the point of view of the possibility of chromium accumulation, let us analyze the major high-pressure phases obtained in experiments and established in nature.

Figure 5.1 illustrates the modal composition and phase relations in the Earth's mantle (Harte 2010; Stixrude and Lithgow-Bertelloni 2007; Perrillat et al. 2006). As it is evident from the diagram, the *P–T* conditions of our experiments (10–24 GPa, 1600 °C) are in a good agreement with certain temperatures and pressures in the mantle. It is assumed that the upper mantle has the pyrolytic composition (Ringwood 1966). This hypothetical rock (pyrolite) is mostly composed of olivine, pyroxene, and garnet with the bulk proportions of 4:2:1. With increasing pressure, the phase composition changes towards the higher garnet content, so that garnet may compose up to 50 vol.% of the transition zone (Ringwood 1991). According to the model of Ringwood (1966), the concentration of Cr_2O_3 in pyrolite is ~0.42 wt%.

According to the results of experiments in the *Maj–Knr* and *Fo–MChr* systems, experimental data on the systems with more complex (multicomponent) composition (Irifune and Ringwood 1987; Hirose 2002; Irifune 1987), as well as the huge volume of information on inclusions in natural diamonds, there is a number of mantle minerals which may contain chromium.

Among the host phases for chromium **in the upper mantle** are chrome-spinel, chromium-bearing pyroxene, and knorringitic garnet. However, garnet is the major phase concentrating chromium, since the contents of Cr_2O_3 in garnets may be high within the whole range of garnet stability including the field of majoritic garnet.

As it was shown in Sect. 2.1.2, two high-pressure components are typical of mantle garnets: *majorite* and *knorringite*. Analysis of the natural material in combination with the results of experiments at high *P–T* provides unambiguous evidence for the mechanism of incorporation of the majorite end-member in garnet is $Cr^{3+} + Al^{3+} =$

E. A. Matrosova et al., *Geochemistry of Chromium in the Earth's Mantle*,
Springer Geology, https://doi.org/10.1007/978-3-030-27018-6_5

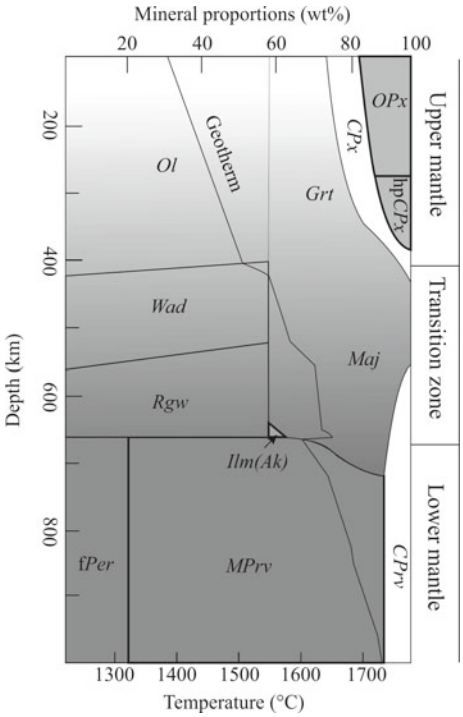

Fig. 5.1 Scheme illustrating change of phase associations with depth in the Earth's mantle, modified after Harte (2010), Stixrude and Lithgow-Bertelloni (2007), and Perrillat et al. (2006); the mantle geotherm is shown after Stixrude and Lithgow-Bertelloni (2007). Gray area shows the stability of the phases studied in our experiments

$Mg^{2+} + Si^{4+}$ (Ringwood and Major 1971). With increasing pressure, the concentration of both Cr and Al in garnet decreases (Akaogi and Akimoto 1977; Irifune 1987), whereas the contents of Si in the octahedral site, as well as divalent cations (Ca, Mg, and Fe) and Na progressively increase (Ono and Yasuda 1996), which results in the formation of garnet with >3 Si p.f.u. This is explained by dissolution of the pyroxene end-members (mainly (Mg, Fe)SiO_3) in garnet starting from a pressure of 7.5 GPa (Wang et al. 1998); with increasing pressure, the solubility of pyroxene in garnet increases reaching significant values at pressures of 10–15 GPa corresponding to the lowermost parts of the upper mantle and transition zone.

Incorporation of Cr in some majoritic garnets of the ultrabasic paragenesis illustrates the complex relationships between the composition of such garnets and pressure and for the concurring behavior of majorite and knorringite components in this mineral. The knorringite end-member may be found in the composition of garnet even at 3 GPa (beyond the diamond depth facies), whereas the content of chromium becomes significant (5–10 wt% Cr_2O_3 and higher) within the range of crystallization of most of the natural diamonds (4–7 GPa) (Malinovskii et al. 1975), which is an indicative feature of the diamond-bearing dunite–harzburgite paragenesis of the lithospheric mantle.

The different lowest pressures of knorringite- (3 GPa) and majorite-components (7.5 GPa) incorporation in natural garnets indicate that the relative saturation of garnet

with knorringite likely occurs in the lithospheric zone, whereas significant contents of the majoritic component (>5–10 mol%) are gained in the sub-lithospheric mantle only.

Thus, garnets of various compositions are the indicators of different depths of their formation. Indeed, in our experiments, we observed that with the increase of pressure from 10 to 18 GPa, the role of the majorite end-member increases and begins to replace the knorringitic component progressively (Fig. 3.11), even for the starting composition corresponding to pure knorringite $Mg_3Cr_2Si_3O_{12}$ (Fig. 3.12). In this case, appearance of garnet containing ~10 mol% majorite $Mg_4Si_4O_{12}$ was accompanied by crystallization of eskolaite (Cr_2O_3).

The characteristic compositional patterns of garnet, chrome-spinel, and pyroxene syngenetic to diamond allowed to distinguish the dunite–harzburgite paragenesis in the area of diamond stability. The minerals of this assemblage are characterized by the lower concentrations of Fe, Ca and higher contents of Cr in comparison with the known types of ultramafic rocks and diamond-bearing eclogite (Sobolev et al. 1973). Thus, the concentration of Cr_2O_3 in high-Cr and low-Ca garnets ranges within 3.00–20.60 wt% (Schulze 2003; Grütter et al. 2004; Stachel and Harris 1997) at a CaO content of 0.27–3.80 wt%.

Sobolev (1977, 1983) showed that incorporation of chromium in the form of the knorringite end-member reflects the high-pressure nature of garnets and may be considered as an indicator of the diamond-bearing assemblages. Later Grütter et al. (2006) suggested to apply the concentration of Cr_2O_3 in garnets from inclusions in garnets for quantitative estimation of the pressure of their formation. The results of experimental studies (Bulatov et al. 1991; Stachel et al. 1998; Grütter 2001) demonstrate that the high concentration of chromium in garnet is controlled by the high Cr/Al ratio in protolith rather than by the bulk chromium content in rock.

The concentration of chromium in garnets synthesized in our runs in the model pyrolite system (Sect. 3.4.2) is usually not fully consistent with the natural data. Among inclusions in diamond crystals, there are garnets with a substantial Cr_2O_3 content (>15 wt%) (Sobolev 1977; Taylor and Anand 2004; and others). In this regard, we face the problem of how such high-chromium garnets can be formed. In opinion of some authors (Kesson and Ringwood 1989; Canil and Wei 1992; Stachel et al. 1998), garnets with the high contents of the knorringite component may be formed in protolith with the high Cr/Al ratio only. Such a protolith may be formed as a residue from partial melting at low pressures, within the spinel depth facies, where spinel peridotite is stable and restite would be represented by olivine and chrome-spinel. In this process, $D^{Sp/L}_{Cr/Al} > 40$, where $D^{A/B}_{Cr/Al} = (Cr_2O_3/Al_2O_3)^A/(Cr_2O_3/Al_2O_3)^B$), so that restite would be characterized by the high Cr/Al ratios at a pressure of ~1–1.5 GPa (Bulatov et al. 1991). High-chromium garnets crystallize from this substrate upon its subduction into the garnet depth facies (Stachel et al. 1998). In particular, diamond-bearing garnet harzburgite with high-chromium low-calcium garnet was formed via this mechanism. At a pressure of 5–8 GPa (within the garnet depth facies), restite with high bulk chromium concentrations cannot be formed, since Cr will be redistributed into the melt with $D^{Grt/L}_{Cr/Al} \approx 1$.

Table 5.1 Comparison of the bulk concentration of Cr_2O_3 in pyrope peridotite xenoliths, Cr_2O_3 concentration in garnet, and modal content of garnet in xenoliths

Cr_2O_3 in mantle xenoliths (wt%)	Cr_2O_3 in garnet (wt%)	Content of garnet in xenoliths (vol. %)	References
1.7	4.24	40	Garanin et al. (2004)
1.29	11	12	van Achterbergh et al. (2001)
0.8	7.6	10	
0.77	9.8	7	Ionov et al. (2010)
0.68	7.06	9	Schulze (1995)
0.643	9.3	6	Ionov et al. (2010)
0.47	7.91	6	Schulze (1995)

Information on the high concentrations of chromium in mantle minerals and probably high bulk concentrations of this element in mantle rocks may be obtained from analysis of the data on inclusions in diamonds, as well as on mantle xenoliths of the peridotitic assemblage, especially garnet dunite and harzburgite with high-Cr low-Ca garnet. Thus, estimates of the bulk compositions of some xenoliths of mantle peridotite (Table 5.1) show that the concentration of Cr_2O_3 in these rocks reaches 1.7 wt% (Schulze 1995; van Achterbergh et al. 2001; Garanin et al. 2004; Ionov et al. 2010). This is 2–4 times higher than the concentration of chromium in the Earth's mantle (Ringwood 1966), whereas the concentration of Cr_2O_3 in garnets from these xenoliths reaches 11 wt%. It should be noted that the mentioned values of the bulk chromium concentration in the composition of mantle rocks are far from the maximum. For example Ivanic (2007) reported megacrysts of garnet (6.42 wt% Cr_2O_3) forming intergrowths with chrome-spinellides and single pyroxene crystals, for which the calculated bulk Cr_2O_3 concentration is 10.28 wt%.

In our study, the quantitative estimate of the influence of the Cr/Al ratio in protolith on the composition of garnet was obtained at 7 GPa in experiments on partial melting of high-chromium substrate (with addition of 3 wt% Cr_2O_3 to the starting composition) close to that produced in the experimental series at 2.5 and 3.0 GPa. According to the composition (up to 15 wt% Cr_2O_3 and higher), high-Cr low-Ca garnets synthesized in these runs are similar to garnets from inclusions in garnets of the dunite–harzburgite assemblage (Fig. 5.2).

Calculations of the compositions of restite and melt showed that, with increasing temperature, chromium is redistributed into melt (up to 2.95 wt% Cr_2O_3); however, for the given starting composition, the concentration of chromium in restite is higher than its bulk concentration in rock ($\geq$3.13 wt% Cr_2O_3) (Fig. 5.3). At the same time, it should be noted that $D_{Cr/Al}^{restite/L} \approx 1$ is consistent with experiments on partial melting of pyrolite at 7 GPa.

In addition to the temperature and pressure, the Cr/Al ratio in the bulk composition of rock is an important factor affecting the composition of garnet. The high concentration of chromium in garnet is controlled by the high Cr/Al ratio in protolith to a higher degree than by the bulk concentration of Cr_2O_3 in rock.

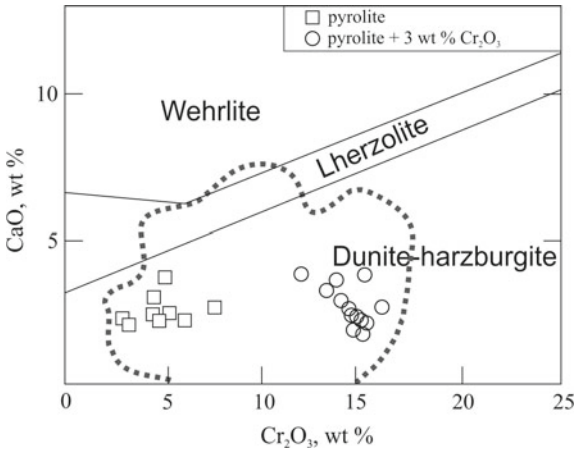

Fig. 5.2 Diagram of the composition of garnets (restite zone) synthesized in experiments on partial melting of model pyrolite at 7.0 GPa for two starting compositions with 0.5 and 3.0 wt% Cr_2O_3. Subdivision of garnets into the dunite–harzburgitic, lherzolitic, and wehrlitic types is given after Sobolev (1977). The field of garnet composition in diamonds of the ultrabasic assemblages in the different deposits worldwide is shown after Griffin et al. (1993)

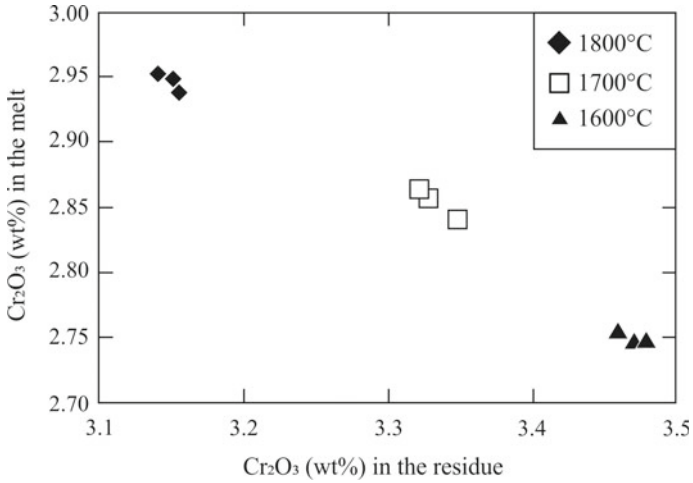

Fig. 5.3 Dependence of the concentration of Cr_2O_3 in melt on the concentration of Cr_2O_3 in restite in experiments on partial melting of pyrolite with addition of 3 wt% Cr_2O_3 at a temperature of 1600–1800 °C and pressure of 7 GPa

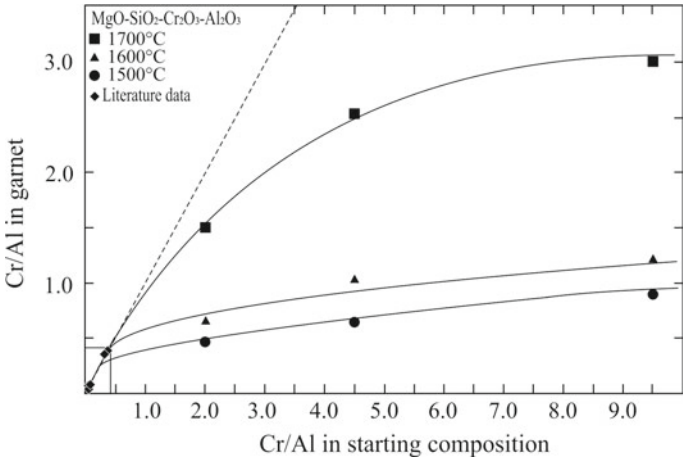

Fig. 5.4 Dependence of the composition of garnet on the Cr/Al ratio in the bulk/starting composition of rock, which accounts for the results of runs in the system $MgO–SiO_2–Cr_2O_3–Al_2O_3$ and other experimental data (Irifune and Ringwood 1987; Kato et al. 1988; Hirose 2002)

From this point, let us consider the compositions of garnets from experiments with different Cr/Al ratios in the starting composition. The studied $MgO–SiO_2–Cr_2O_3–Al_2O_3$ system (see Sect. 3.4.1) is supersaturated with chromium in relation to aluminum. With a certain degree of approximation, experiments in this system simulate the process of crystallization of garnet in high-chromium restite formed under the conditions of partial melting. As it is evident from the results of the runs described above, an increase in Cr/Al in the starting composition results in an increase in this ratio in the garnet composition. Characteristically, this dependence is not linear (Fig. 5.4), which is explained by the different influence of Cr and Al on changes in cell volume of garnet. Increase in Cr/Al ratio in the bulk composition of rock results in the increase in chromium content in garnet, which is accompanied by significant expansion of the cell volume of garnet, whereas increase in the Al content has an opposite effect (Fig. 5.5). Due to this, incorporation of aluminum in garnet under high-pressure conditions is more preferable than the entrance of chromium.

This important conclusion may be applied to the study of more complex natural systems. Experiments in the multicomponent systems with significant predomination of Al over Cr in the bulk composition of rock (Cr/Al <~0.5) show the formation of garnet with a Cr/Al ratio corresponding to that in the starting composition, i.e., garnets with significant content of pyrope and low concentrations of chromium. Thus, experiments in multicomponent natural systems simulate crystallization of garnet in rocks with low Cr/Al ratios in the bulk composition, which did not participate in the processes of partial melting within the spinel depth facies prior to subduction of rocks into the garnet depth facies. Judging from the natural data, most of garnets are low-chromium, so that the protolith of their host rocks was not subjected to partial

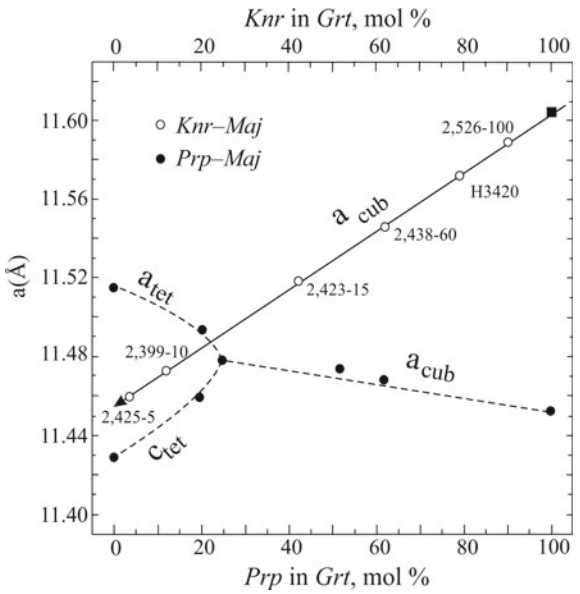

Fig. 5.5 Comparison of changes in cell parameters of members belonging to the majorite–knorringite join (Sirotkina et al. 2015) and those for the majorite–pyrope join (Parise et al. 1996)

melting, except for rocks with Cr-rich garnets (Cr-pyrope dunite and harzburgite, inclusions in diamonds of the dunite–harzburgite assemblage, etc.).

The actual material on mineralogy and geochemistry of the transition zone and the lower mantle cannot be compared in its entirety with the data on the upper mantle. Nevertheless, the data on high-pressure phase assemblages allow us to draw some conclusions about the composition of the transition zone and the lower mantle (Harte and Harris 1994; Harte et al. 1999, etc.). In the discussion on high-pressure phases, which can serve as potential chromium concentrators in the transition zone of the mantle, the key role should again be assigned to the knorringite-majorite garnet, which, with increasing pressure, is enriched by the majoritic component. With further increase in pressure up to ~17 GPa, it should be replaced with chromium-bearing akimitoite (Cr-*Ak*), which, however, is not found in mantle mineral associations.

Mg_2SiO_4 polymorphs (*Wad*, *Rgw*) are widely abundant in the transition zone as well. Figure 5.6 shows the ranges of the chromium concentrations in olivine, wadsleyite, and ringwoodite synthesized in the *Fo–MChr* system. According to the experimental data, the concentration of chromium in each of these phases is directly controlled by pressure, and the maximum Cr_2O_3 concentrations increase in the following row: *Ol* → *Wad* → *Rgw* (Table 3.2).

The results of our experiments are directly applicable to the origin of chromitite from the Luobusa ophiolitic complex (South Tibet, China). Some publications report the evidence for the UHP nature of rocks from this complex, which is not typical of most of podiform chromitites. Among these features is the presence of diamond (Robinson et al. 2004; Yang et al. 2007), coesite (Yang et al. 2007; Yamamoto et al. 2009), stishovite (Yang et al. 2007), and ringwoodite (Robinson et al. 2004; Bindi

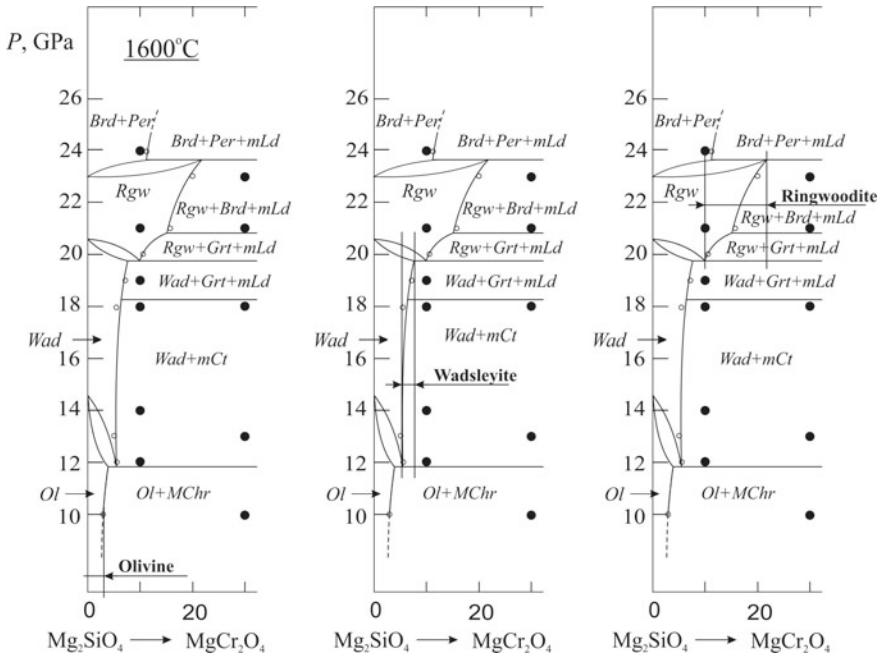

Fig. 5.6 Comparison of the ranges of chromium concentrations (shown by arrows) in Mg_2SiO_4 polymorphs based on the results of experiments in the *Fo–MChr* system at pressures of 10–24 GPa and a temperature of 1600 °C

et al. 2018). Recently, the data on the composition and mutual relationships between the chromium-bearing phases have been used to illustrate the high-pressure nature of the Luobusa chromitite (Ishii et al. 2015; Bindi et al. 2014, 2015, 2018; Sirotkina et al. 2018; Zhang et al. 2018).

As it was shown in Sect. 2.1.4, chrome-spinel from podiform chromitite in Tibet ophiolite contains exsolution textures of silicate phases (coesite, monoclinic, and orthorhombic pyroxenes) (Yamamoto et al. 2009). The highest concentration of SiO_2 typical of natural chromite does not exceed 0.6 wt% (~2 mol% Mg_2SiO_4).

Chromitite from Luobusa ophiolite contains olivines with extremely high concentrations of chromium. For example, the concentration of Cr_2O_3 in the studied olivine grains forming small (<100 μm) inclusions in chromite (Fig. 5.7) reaches 0.64 wt% (Table 5.2), which corresponds to ~0.6 mol% $MgCr_2O_4$.

The highest concentrations of chromium in olivine from Luobusa chromitite reach 1.5 wt% Cr_2O_3 (~1.6 mol% $MgCr_2O_4$) (Liang et al. 2014). Generally, such chromium contents are not typical of mantle olivines, but taking into account our experimental data, olivine may incorporate much higher concentrations of chromium (up to 3.2 wt% Cr_2O_3). Olivines from high-pressure complexes contain exsolution textures of chromium-rich phases, including chromite and Cr-bearing ilmenite (Dobrzhinetskaya et al. 1996; Yufeng et al. 2008).

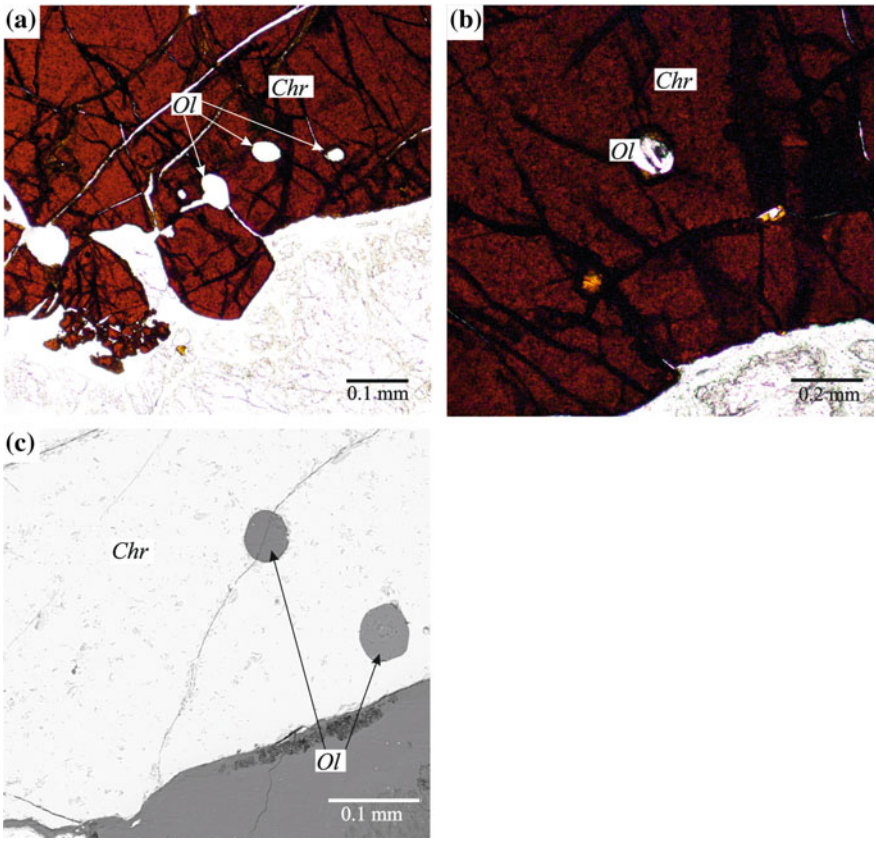

Fig. 5.7 Images in transmitting light (*a*, *b*) and BSE image (*c*) of chromite grains from Luobusa chromitite with inclusions of olivine (*Ol*)

Chrome-spinel in podiform chromitite from Tibet ophiolite contains exsolution textures of coesite, monoclinic and orthorhombic pyroxenes (Yamamoto et al. 2009). The presence of these lamellae in addition to microinclusions of monoclinic pyroxene in chrome-spinel requires a high solubility of SiO_2 and CaO in the chromite protophase in the form of $CaCr_2O_4$ (Kaminsky et al. 2015), $CaAl_2O_4$, and Mg_2SiO_4. In opinion of some authors (Yamamoto et al. 2009; Yang et al. 2007), exsolution textures of silicate phases in chromite are formed upon decompression from the high-pressure phase with the calcium ferrite ($CaFe_2O_4$)-type structure enriched in silicon and calcium and stable at a pressure of >12.5 GPa. The concentration of SiO_2 in natural $(Mg, Fe)(Cr, Al)_2O_4$ with the spinel-type structure does not exceed 0.6 wt%, whereas the concentration of CaO reaches several tens ppm (Arai and Yurimoto 1994).

The study of phase transitions in the simple $MgCr_2O_4$ and $FeCr_2O_4$ systems allowed Ishii et al. (2015) to conclude on the maximum pressure of the formation of

Table 5.2 Compositions of olivine and chromite from Luobusa chromitite, wt%

	SiO_2	Al_2O_3	FeO	MnO	MgO	CaO	NiO	Cr_2O_3	Total
Ol	41.89	0.00	2.36	0.00	54.45	0.00	0.89	0.64	100.23
Chr	0.07	10.16	13.89	0.35	14.44	0.04	0.11	59.75	98.81

Luobusa chromitite. These authors suggest that absence of the phase assemblage (Mg, Fe)$_2$Cr$_2$O$_5$ + Cr$_2$O$_3$ stable at 12–18 GPa provides evidence for the lower pressure origin of these rocks (<12 GPa).

In this discussion, the synthesis of a new phase Mg(Mg, Cr, Si)$_2$O$_4$ (*mCt*) with modified calcium titanate-type structure (Bindi et al. 2015) in the model *Fo–MChr* system (Sirotkina et al. 2018) is of great importance. As it is shown in the Sect. 3.3.2, this phase occurs in a wide pressure range (12–18 GPa) and covers a wide compositional range of starting materials. *mCt* occupies an intermediate position between Mg$_2$SiO$_4$ and MgCr$_2$O$_4$ and shows a quite narrow compositional range (58–63 mol% *Fo*). Our discovery of this phase supports the conclusion of Yamamoto et al. (2009) and, thus, limits minimum pressures of the formation of Luobusa chromitite to ~12 GPa. Moreover, the successful synthesis of inverse ringwoodite (i*Rgw*) with inverse-spinel structure (Bindi et al. 2018) and its recovery as natural mineral (Griffin et al. 2016) adds further constraints to the subduction history of the Luobusa peridotite. The new Mg(Mg, Cr, Si)$_2$O$_4$ post-spinel phase (Bindi et al. 2015), which contains significant amounts of the Mg$_2$SiO$_4$ component never reported before in a post-spinel phase, may be an intermediate product in the deep recycling of silicate-bearing UH*P* chromitites (Arai 2013) and the source of the recovered i*Rgw*, which might be formed during the inverse transformation from the new post-spinel phase Mg[(Cr, Mg)(Si, Mg)]O$_4$ to chromite during mantle upwelling.

Recently Zhang et al. (2018) reported on the synthesis of the MC-phase with an average composition of (Mg, Fe)$_3$[(Cr, Al)$_{2-2x-4/3y}$(Mg, Fe)$_x$Si$_{x+y}$]O$_6$ ($x \approx 0.2$, $y \approx 0.3$) and a cubic structure, space group of *Fd*3*m*. This phase was synthesized from the starting material of natural Luobusa chromitite and has an idealized stoichiometry of Mg$_3$Cr$_2$O$_6$. The stability field of the MC-phase associated with garnet, chromite, and eskolaite corresponds roughly to the top of the MTZ at pressures in the ~ 14–17 GPa range and temperatures in the 1400–1600 °C range, so that this phase may be considered as another probable precursor for the phases formed below 12 GPa.

In general, the formation of exsolution textures of chromium-bearing phases in olivine (Dobrzhinetskaya et al. 1996; Yufeng et al. 2008) and silicates in chromite (Yamamoto et al. 2009) may be explained using the *P–X* phase diagram of the *Fo–MChr* pseudobinary system (Fig. 3.23). An association of low-chromium olivine and magnesiochromite with the low Cr$_2$O$_3$ concentrations is stable at a pressure of <12 GPa. With increasing pressure, the contents of the "forsterite" component in chromite and "magnesiochromite" component in olivine increase (Figs. 3.23 and 5.6). Decompression would result in decomposition of silica-rich chromite or chromium-rich olivine with the formation of exsolution textures.

It is suggested that the lower mantle substrate is predominantly composed of magnesiowüstite (ferropericlase) (Mg, Fe)O, CaSiO$_3$ with the perovskite-type structure and MgSiO$_3$ bridgmanite; the latter is formed from MgSiO$_3$ *Ak* at a pressure of ~21 GPa (Figs. 3.15 and 3.25). The contents of other phases in the lower mantle is negligible, since the elements of pyrolite may be expressed by the composition of three major phases (Ringwood and Irifune 1988). The characteristic feature of

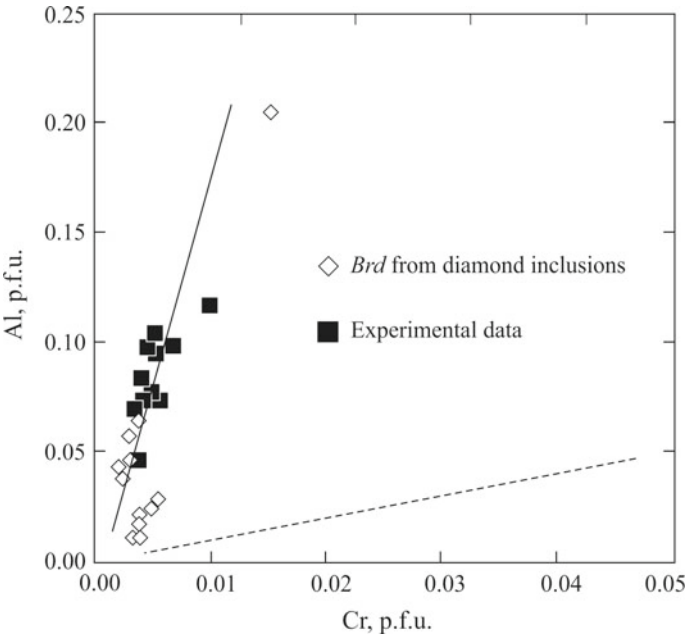

Fig. 5.8 Dependence of the concentration of chromium on the aluminum content in assumed bridgmanites from inclusions in diamonds (Stachel et al. 2000; Harte et al. 1999; Kaminsky et al. 2001; Hayman et al. 2005; Davies et al. 2004) and in bridgmanites from experiments (Irifune and Ringwood 1987; Kato et al. 1988; Hirose 2002). The dashed line shows equal distribution

$MgSiO_3$ bridgmanite is incorporation of trivalent cations by the mechanism $Mg^{2+} + Si^{4+} = 2Me^3$ (Andrault 2003; Irifune 1994).

Lower mantle bridgmanites are characterized by high aluminum concentrations. $MgSiO_3$ *Brd* usually contains 1–2.7 wt% Al_2O_3 (Wilding 1990; Kaminsky et al. 2001; Davies et al. 2004), whereas the concentration of Al_2O_3 in a group of diamonds from the Sao Luis placer in Brazil is 8.3–12.6 wt%. This is in agreement with the experimental data, according to which the garnet/bridgmanite transition in the pyrope–majorite system occurs at a higher pressure with increasing alumina content (Irifune et al. 1996; Wood 2000). Therefore, the concentration of Al_2O_3 in $MgSiO_3$ bridgmanite may be applied as a qualitative barometer for the lower-mantle mineral associations. Therefore, UHP diamonds from the São Luiz placer containing the lower mantle phase associations are among the deepest ones.

It is necessary to emphasize that an increase in the alumina content often results in an increase in the concentration of chromium, the second important minor element in the composition of bridgmanite (Fig. 5.8), and iron (McCammon 1997; Frost and Langenhorst 2002). The concentration of Cr_2O_3 in the lower-mantle bridgmanites ranges from 0.1 to 0.36 wt% (Kaminsky et al. 2001; Davies et al. 2004), and the most high-chromium bridgmanites were reported as inclusions in diamonds in the area of the São Luiz River, Brazil (Wilding 1990; Harte et al. 1999; Zedgenizov et al. 2015).

The concentrations of Cr_2O_3 in them vary from 0.1 to 1.33 wt%, which is almost three times higher than the assumed average chromium content in the Earth's mantle.

References

Akaogi M, Akimoto A (1977) Pyroxene-garnet solid-solution equilibria in the system $Mg_4Si_4O_{12}$-$Mg_3Al_2Si_2O_{12}$ and $Fe_4Si_4O_{12}$-$Fe_3Al_2Si_3O_{12}$ at high pressures and temperatures. Phys Earth Planet Inter 111:90–106

Andrault D (2003) Cationic substitution in $MgSiO_3$ perovskite. Phys Chem Minerals 4200:1–12

Arai S (2013) Conversion of low-pressure chromitites to ultrahigh-pressure chromitites by deep recycling: a good inference. Earth Planet Sci Lett 379:81–87

Arai S, Yurimoto H (1994) Podiform chromitites of the Tari-Misaka ultramafic complex, southwestern Japan, as mantle–melt interaction products. Econ Geol 89:1279–1288

Bindi L, Griffin WL, Panero WR, Sirotkina EA, Bobrov AV, Irifune T (2018) Synthesis of inverse ringwoodite sheds light on the subduction history of Tibetan ophiolites. Sci Rep 8:5457

Bindi L, Sirotkina EA, Bobrov AV, Irifune T (2014) X-ray single-crystal structural characterization of $MgCr_2O_4$, a post-spinel phase synthesized at 23 GPa and 1600 °C. J Phys Chem Solids 75:638–641

Bindi L, Sirotkina EA, Bobrov AV, Irifune T (2015) Structural and chemical characterization of $Mg[(Cr, Mg)(Si, Mg)]O_4$, a new post-spinel phase with six-fold coordinated silicon. Am Mineral 100:1633–1636

Bulatov V, Brey GP, Foley SF (1991) Origin of low-Ca, high-Cr garnets by recrystallization of low-pressure harzburgites. In: 5th Int kimberlite conf extended abstracts 91:29–31

Canil D, Wei KJ (1992) Constraints on the origin of mantle-derived low Ca garnets. Contrib Mineral Petrol 109:421–430

Davies RM, Griffin WL, O'Reilly SY, McCandless TE (2004) Inclusions in diamond from the K14 and K10 kimberlites, Buffalo Hills, Alberta, Canada: diamond growth in a plume. Lithos 77:99–111

Dobrzhinetskaya L, Green HW, Wang S (1996) Alpe Arami: a peridotite massif from depths of more than 300 kilometers. Science 271:1841–1845

Frost DJ, Langenhorst F (2002) The effect of Al_2O_3 on Fe-Mg partitioning between magnesiowüstite and magnesium silicate perovskite. Earth Planet Sci Lett 199:227–241

Griffin WL, Sobolev NV, Ryan CG, Pokhilenko NP, Win TT, Yefimova ES (1993) Trace elements in garnets and chromites: diamond formation in the Siberian lithosphere. Lithosphere 29:235–256

Grütter H, Latti D, Menzies A (2006) Cr-saturation arrays in concentrate garnet compositions from kimberlite and their use in mantle barometry. J Petrol 47:801–820

Grütter HS (2001) The genesis of high Cr/Al garnet peridotite, with implications for cratonic crust: mantle architecture. The Slave-Kaapvaal workshop, Merrickville

Grütter HS, Gurney JJ, Menzies AH, Winter F (2004) An updated classification scheme for mantle-derived garnet, for use by diamond explorers. Lithos 77:841–857

Garanin VK, Garanin KV, Vasilieva ER, Verichev EM, Kostrovitsky SI, Kudriavtseva GP, Pisarev PA (2004) Mineralogy of mantle xenoliths from diamondiferous V. Grib kimberlite pipe (Arkhangelsk Province, Russia). Izv Vuzov. Geol Razv 6:26–30 In Russian

Griffin WL, Afonso JC, Belousova EA, Gain SE, Gong XH, Gonzalez-Jimenez JM, Satsukawa T (2016) Mantle recycling: transition zone metamorphism of Tibetan ophiolitic peridotites and its tectonic implications. J Petrol 57(4):655–684

Harte B (2010) Diamond formation in the deep mantle: the record of mineral inclusions and their distribution in relation to mantle dehydration zones. Min Mag 74(2):189–215

Harte B, Harris JW (1994) Lower mantle mineral association preserved in diamonds. Min Mag 58A:384–385

Harte B, Harris JW, Hutchison MT, Watt GR, Wilding MC (1999) Lower mantle mineral associations in diamonds from Sao Luiz, Brazil. Mantle Petrol: field observations and high pressure experimentation: a tribute to Francis R (Joe) Boyd (The Geochemical Society, Houston) 6:125–153

Hirose K (2002) Phase transitions in pyrolitic mantle around 670-km depth: Implications for upwelling of plumes from the lower mantle. J Geophys Res, vol 107

Hayman PC, Kopylova MG, Kaminsky FV (2005) Lower mantle diamonds from Rio Soriso (Juina area, Mato Grosso, Brazil). Contrib Mineral Petrol 149(4):430–445

Ionov DA, Doucet LS, Ashchepkov IV (2010) Composition of the lithospheric mantle in the siberian craton: new constraints from fresh peridotites in the Udachnaya-East Kimberlite. J Petrol 51:2177–2210

Irifune T (1994) Absence of an aluminous phase in the upper part of the Earth's lower mantle. Nature 370:131–133

Irifune T (1987) An experimental investigation of the pyroxene–garnet transformation in a pyrolite composition and its bearing on the constitution of the mantle. Phys Earth Planet Inter 45:324–336

Irifune T, Koizumi T, Ando JI (1996) An experimental study of the garnet-perovskite transformation in the system $MgSiO_3$-$Mg_3Al_2Si_3O_{12}$. Phys Earth Planet Inter 96:147–157

Irifune T, Ringwood AE (1987) Phase transformations in a harzburgite composition to 26 GPa: implications for dynamical behaviour of the subducting slab. Earth Planet Sci Lett 86:365–376

Ishii T, Kojitani H, Fujino K, Yusa H, Mori D, Inaguma Y, Matsushita Y, Yamaura K, Akaogi M (2015) High-pressure high-temperature transitions in $MgCr_2O_4$ and crystal structures of new $Mg_2Cr_2O_5$ and post-spinel $MgCr_2O_4$ phases with implications for ultra-high pressure chromitites in ophiolites. Am Mineral 100:59–65

Ivanic TJ (2007) The chromite–garnet peridotite assemblages and their role in the evolution of the mantle lithosphere. Ph.D. Thesis, University of Edinburgh, Edinburgh

Kaminsky FV, Wirth R, Schreiber A (2015) A microinclusion of lower-mantle rock and other mineral and nitrogen lower-mantle inclusions in a diamond. Canadian Mineralogist 53(1):83–104

Kaminsky FV, Zakharchenko OD, Davies R, Griffin WL, Khachatryan-Blinova GK, Shiryaev AA (2001) Superdeep diamonds from the Juina area, Mato Grosso State, Brazil. Contrib Mineral Petrol 140:734–753

Kato T, Ringwood AE, Irifune T (1988) Experimental determination of element partitioning between silicate perovskites, garnets and liquids: constraints on early differentiation of the mantle. Earth Planet Sci Lett 89:123–145

Kesson SE, Ringwood AE (1989) Slab-mantle interactions: 1. Sheared and refertilised garnet peridotite xenoliths—samples of Wadati-Benioff zones? Chemical Geology 78(2):83–96

Liang F, Yang J, Xu Z, Zhao J (2014) Moissanite and chromium-rich olivine in the Luobusa mantle peridotite and chromitite, Tibet: deep mantle origin implication. J Himalayan Earth Sci (Special Volume) 103

Malinovskii IY, Doroshev AM, Ran EN (1975) The stability of chromium-bearing garnets pyrope—knorringite series. In: Experimental studies on the mineralogy (1974–1976), Institute of Geology and Geophysics of the Siberian Branch of AS USSR, Novosibirsk, pp 110–115. [in Russian]

McCammon CA (1997) Perovskite as a possible sink for ferric iron in the lower mantle. Nature 387:694–696

Moore RO, Gurney JJ (1985) Pyroxene solid solution in garnets included in diamond. Nature 318:553–555

Ono S, Yasuda A (1996) Compositional change of majoritic garnet in a MORB composition from 7 to 17 GPa and 1400 to 1600 C. Phys Earth Planet Int 96(2–3):171–179

Parise J, Wang Y, Dwanmesia GD, Zhang J, Sinelnikov Y, Chmielowski J, Weidner DJ, Liebermann RC (1996) The symmetry of garnets on the pyrope ($Mg_3Al_2Si_3O_{12}$) – majoritc ($MgSiO_3$) join. Geophys Res Lett 23(25):3799–3802

Perillat J-P, Ricolleau A, Daniel I, Fiquet G, Mezouar M., Guignot N., Cardon H (2006) Phase transformations of subducted basaltic crust in the upmost lower mantle.// Phys Earth Planet Inter 157:139–149

Ringwood AE (1966) The chemical composition and origin of the Earth. In: Hurley PM (ed) Advances in Earth science. M.I.T. Press, Cambridge, pp 287–356
Ringwood AE (1991) Phase transformations and their bearing on the constitution and dynamics of the mantle. Geochim Cosmochim Acta 55(8):2083–2110
Ringwood AE, Irifune T (1988) Nature of the 650-km seismic discontinuity: implications for mantle dynamics and differentiation. Nature 331:131–136
Ringwood AE, Major A (1971) Synthesis of majorite and other high pressure garnets and perovskites. Earth Planet Sci Lett 12:411–418
Robinson PT, Bai W-J, Malpas J, Yang J-S, Zhou M-F, Fang Q-S, Hu X-F, Cameron S, Standigel H (2004) Ultra-high pressure minerals in the Luobusa Ophiolite, Tibet, and their tectonic implications. In: Malpas J, Fletcher CJN, Ali JR, Aitchison JC (eds) Aspects of the tectonic evolution of China, Geological Society of London, pp 247–271
Schulze DJ (2003) A classification scheme for mantle-derived garnets in kimberlite: a tool for investigating the mantle and exploring for diamonds. Lithos 71:195–213
Schulze DJ (1995) Low-Ca garnet harzburgites from Kimberley, South Africa: Abundance and bearing on the structure and evolution of the lithosphere. J Geophys Res Solid Earth 617:12513–12526
Scott Smith BH, Danchin RV, Harris JW, Stracke KJ (1984) Kimberlites near Orroroo, South Australia. Kimberlites I: Kimberlites and Related Rocks. Elsevier 1:121–142
Sirotkina EA, Bobrov AV, Bindi L, Irifune T (2015) Phase relations and formation of chromium-rich phases in the system Mg4Si4O12–Mg3Cr2Si3O12 at 10–24 GPa and 1,600 & #xB0;C. Contrib Mineral Petrol 169:2
Sirotkina EA, Bobrov AV, Bindi L, Irifune T (2018) Chromium-bearing phases in the Earth's mantle: evidence from experiments in the Mg_2SiO_4–$MgCr_2O_4$ system at 10–24 GPa and 1600C. Amer Mineral 103(1):151–160
Sobolev NV (1977) Deep-seated inclusions in kimberlites and the problem of the composition of the Upper Mantle. American Geophysical Union, Washington, DC, p 279
Sobolev NV (1983) Parageneses of diamond and the problem of deep mineral genesis. Zap VMO 112(4):389–396 In Russian
Sobolev NV, Lavrent'Ev YG, Pokhilenko NP, Usova LV (1973) Chrome-rich garnets from the kimberlites of Yakutia and their parageneses. Contrib Mineral Petrol 40(1):39–52
Stachel T (2001) Diamonds from the asthenosphere and the transition zone. Eur J Mineral 13(5):883–892
Stachel T, Harris JW (1997) Diamond precipitation and mantle metasomatism-evidence from the trace element chemistry of silicate inclusions in diamonds from Akwatia, Ghana. Contrib Mineral Petrol 129(2–3):143–154
Stachel T, Brey GP, Harris JW (2000) Kankan diamonds (Guinea) I: from the lithosphere down to the transition zone. Contib Mineral Petrol 140:1–15
Stachel T, Harris JW, Brey GP (1998) Rare and unusual mineral inclusions in diamonds from Mwadui, Tanzania. Contrib Mineral Petrol 132:34–47
Stixrude L, Lithgow-Bertelloni C (2007) Influence of phase transformations on lateral heterogeneity and dynamics in the Earth's mantle. Earth Planet Sci Lett 263:45–55
Taylor LA, Anand M (2004) Diamonds: time capsules from the Siberian Mantle. Chem Erde 64:1–74
Van Achterbergh E, Griffin WL, Stiefenhofer J (2001) Metasomatism in mantle xenoliths from the Letlhakane kimberlites: estimation of element fluxes. Contrib Mineral Petrol 141(4):397–414
Wang Y, Weidner DJ, Zhang J, Gwanrnesia GD, Liebermann RC (1998) Thermal equation of state of garnets along the pyrope-majorite join. Phys Earth Planet Inter 105:59–71
Wilding MC (1990) A study of diamonds with syngenetic inclusions. Unpublished Ph.D. Thesis, University of Edinburgh, UK, p 281
Wood BJ (2000) Phase transformations and partitioning relations in peridotite under lower mantle conditions. Earth Planet Sci Lett 174:341–354
Yamamoto S, Komiya T, Hirose K, Maruyama S (2009) Coesite and clinopyroxene exsolution lamellae in chromites: In-situ ultrahigh-pressure evidence from podiform chromitites in the Luobusa ophiolite, southern Tibet. Lithos 109:314–322

Yang J-S, Dobrzhinetskaya L, Bai W-J, Fang Q-S, Robinson PT, Zhang J, Green HW (2007) Diamond- and coesite-bearing chromitites from the Luobusa ophiolite Tibet. Geology 35:875–878

Yufeng R, Fangyuan C, Jingsui Y, Yuanhong G (2008) Exsolutions of diopside and magnetite in olivine from mantle dunite, Luobusa ophiolite, Tibet, China. Acta Geologica Sinica (English Edition) 82:377–384

Zedgenizov DA, Shatsky VS, Panin AV, Evtushenko OV, Ragozin AL, Kagi H (2015) Evidence for phase transitions in mineral inclusions in superdeep diamonds of the São Luiz deposit (Brazil). Russ Geol Geophys 56(1–2):296–305

Zhang Y, Wang C, Jin Z, Chen T, Wu X, Liu W, Wu Y (2018) High-pressure phase transitions of natural chromitite from Tibetan ophiolites. Lithos 320–321:20–27

Chapter 6
Conclusion

An extensive set of mineralogical, geophysical, and experimental information allows us to establish the physicochemical parameters of phase transitions, the mechanisms and conditions of isomorphism in terms of the major components for the mantle phases. At the same time, our new experimental data provide evidence for importance of study of the behavior of minor elements in the mantle mineral associations and, in particular, in order to establish the host phases accumulating these elements, and to evaluate their influence on the physicochemical parameters of the major mineral reactions in the Earth's mantle.

Analysis of the model system SiO_2–MgO–Cr_2O_3 allowed us to reveal the petrologically significant sections for experimental study in a wide pressure range (10–24 GPa) at a constant temperature (1600 °C). Experimental study of the simple model systems *Maj–Knr* and *Fo–MChr* provided the fundamentally new data on incorporation of chromium in deep minerals, such as olivine, wadsleyite, ringwoodite, akimotoite, and bridgmanite. Based on the results of single-crystal X-ray diffraction, the schemes of chromium incorporation in the structures of deep minerals were suggested.

In the discussion of high-pressure phases, which can be the likely hosts for chromium in the upper mantle and transition zone, the key role should be assigned to the knorringite–majorite garnet, which is characterized by significant chromium contents in the entire range of its stability, including the thermodynamic stability of majorite. The major compositional feature of garnet at the *P–T* parameters of the lowermost upper mantle and the transition zone is an excess of silicon (>3 p.f.u. Si), which determines its belonging to the majoritic type. The highest concentrations of Cr_2O_3 in garnet registered in experiments exceed 30 wt% (90 mol% *Knr*) and are observed at a pressure of 10 GPa and a temperature of 1600 °C. With increasing pressure, the concentration of chromium in garnet decreases, which indicates the more significant effect of pressure on the formation of majorite in comparison with the knorringite end-member. There is the negative correlation between the concentrations of chromium, magnesium, and silicon in synthetic garnets, which allows us to consider the scheme of heterovalent isomorphism like $2Cr^{3+} = Mg^{2+} + Si^{4+}$ for high-pressure garnets.

E. A. Matrosova et al., *Geochemistry of Chromium in the Earth's Mantle*,
Springer Geology, https://doi.org/10.1007/978-3-030-27018-6_6

Mg_2SiO_4 polymorphs (*Wad*, *Rgw*) with fundamentally different mechanisms of chromium incorporation are widely abundant in the transition zone of the Earth's mantle. Chromium enters wadsleyite by the scheme $^{VI}Mg^{2+} + {}^{IV}Si^{4+} = {}^{VI}Cr^{3+} + {}^{IV}Cr^{3+}$. The mechanism of isomorphism in ringwoodite is $2{}^{VI}Cr^{3+} + {}^{IV}Mg^{2+} = 2{}^{VI}Mg^{2+} + {}^{IV}Si^{4+}$.

Ferropericlase and $(Mg,Fe)SiO_3$ are the host phases accumulating chromium in the lower mantle of the Earth. The major feature of $MgSiO_3$ bridgmanite synthesized in our runs is that Cr enters its composition by the mechanism $Mg^{2+} + Si^{4+} = Cr^{3+}$. The highest concentration of Cr_2O_3 registered in synthetic bridgmanite exceeds 11 wt%. The concentration of chromium in periclase is even higher (>22 wt% Cr_2O_3).

Experimental study of the simple model systems *Maj–Knr* and *Fo–MChr* allowed us to consider the influence of chromium on crystallochemical patterns of deep phases. In particular, we detected significant changes in cell parameters with increase in chromium content and radically different reaction of akimotoite and bridgmanite polyhedra on Cr incorporation in their structures. In this relation, simulation of the composition and physical properties of the Earth's mantle should account for the influence of chromium on mantle phases, since even the low concentrations of this element may significantly change cell volumes and a number of physical properties, such as density and thermoelastic properties of deep minerals.

Experimental study of the system SiO_2–MgO–Cr_2O_3–Al_2O_3 showed that addition of even small concentration of aluminum (1 wt% Al_2O_3) expands the field of garnet stability to the low-pressure area. This results in crystallization of garnet of the pyrope–majorite–knorringite composition and in increase in the modal proportion of garnet in mantle phase associations.

Among the new priorities in the field of petrology of Cr-bearing associations of the Earth's mantle is an experimental study of model and multicomponent systems with participation of knorringitic garnet under the conditions of partial melting. The gradual complication of the composition of systems involving high-pressure Cr-bearing phases will provide a more complete pattern of the effect of other minor components on phase relationships under the conditions of the Earth's mantle.